

**STUDIES ON DEVELOPMENT OF A PULSED EDDY CURRENT  
SYSTEM FOR TESTING THICK STAINLESS STEEL COMPONENTS**

By

**SAMBASIVA RAO KAMBALA  
(Enrollment No: ENGG02201104038)**

**Indira Gandhi Centre for Atomic Research, Kalpakkam**

*A thesis submitted to the  
Board of Studies in Engineering Sciences*

*In partial fulfillment of requirements  
for the Degree of*

**DOCTOR OF PHILOSOPHY**

*of*

**HOMI BHABHA NATIONAL INSTITUTE**



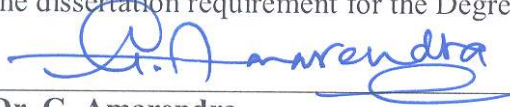
**June, 2017**



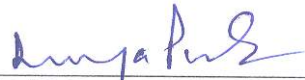
# Homi Bhabha National Institute

## Recommendations of the Viva Voce Committee

As members of the Viva Voce Board, we certify that we have read the dissertation prepared by **Sambasiva Rao Kambala** entitled “**Studies on development of a pulsed eddy current system for testing thick stainless steel components**” and recommend that it may be accepted as fulfilling the dissertation requirement for the Degree of Doctor of Philosophy.

  
Chairman-Dr. G. Amarendra Date: Jan 25, 2018

  
Guide / Convener-Dr. B. Purna Chandra Rao Date: 25/1/2018

  
Member 1-Dr. B.K. Panigrahi Date: 25/1/18

Member 2-Dr. V. S. Srinivasan Date: 25/1/2018  


Technology Adviser-Dr. S. Thirunavukkarasu Date: 25/01/18

  
External Examiner Prof. H. B. Nemade Date: 25-1-2018

Final approval and acceptance of this dissertation is contingent upon the candidate's submission of the final copies of the dissertation to HBNI.

I hereby certify that I have read this dissertation prepared under my direction and recommend that it may be accepted as fulfilling the dissertation requirement.

Date: 28/06/2017

Place: Kalpakkam

  
(Dr. B. Purna Chandra Rao)

Guide / Convener

**Homi Bhabha National Institute**  
**Recommendations of the Viva Voce Committee**

As members of the Viva Voce Board, we certify that we have read the dissertation prepared by **Sambasiva Rao Kambala** entitled “**Studies on development of a pulsed eddy current system for testing thick stainless steel components**” and recommend that it may be accepted as fulfilling the dissertation requirement for the Degree of Doctor of Philosophy.

---

Chairman-**Dr. G. Amarendra**

**Date:**

---

Guide / Convener-**Dr. B. Purna Chandra Rao**

**Date:**

---

Member 1-**Dr. B.K. Panigrahi**

**Date:**

---

Member 2-**Dr. V. S. Srinivasan**

**Date:**

---

Technology Adviser-**Dr. S. Thirunavukkarasu**

**Date:**

---

External Examiner

**Date:**

Final approval and acceptance of this dissertation is contingent upon the candidate's submission of the final copies of the dissertation to HBNI.

I hereby certify that I have read this dissertation prepared under my direction and recommend that it may be accepted as fulfilling the dissertation requirement.

Date:28/06/2017

Place: Kalpakkam

---

**(Dr. B. Purna Chandra Rao)**

Guide / Convener



## **STATEMENT BY GUIDE**

---

I hereby certify that I have read this dissertation prepared under my direction and recommend that it may be accepted as fulfilling the dissertation requirement.

Date: 28/6/2017

Place: Kalpakkam

---

**(Dr. B. Purna Chandra Rao)**

Guide / Convener



## **STATEMENT BY AUTHOR**

---

This dissertation has been submitted in partial fulfillment of requirements for an advanced degree at Homi Bhabha National Institute (HBNI) and is deposited in the library to be made available to borrowers under rules of the HBNI.

Brief quotations from this dissertation are allowable without special permission, provided that accurate acknowledgement of source is made. Requests for permission for extended quotation from or reproduction of this manuscript in whole or in part may be granted by the Competent Authority of HBNI when in his or her judgment the proposed use of the material is in the interests of scholarship. In all other instances, however, permission must be obtained from the author.

Date : 28/06/2017

Place : Kalpakkam

**(Sambasiva Rao Kambala)**



## **DECLARATION**

---

I, hereby declare that the investigation presented in the thesis entitled “**Studies on development of a pulsed eddy current system for testing thick stainless steel components**” submitted to Homi Bhabha National Institute (HBNI), Mumbai, India, for the award of **Doctor of Philosophy in Engineering Sciences**, is the record of work carried out by me under the guidance of **Dr. B. Purna Chandra Rao**, Head, Non-Destructive Evaluation Division, Metallurgy and Materials Group, Indira Gandhi Centre for Atomic Research, Kalpakkam. The work is original and has not been submitted earlier as a whole or in part for a degree / diploma at this or any other Institution/University.

Date : 28/06/2017

Place : Kalpakkam

**(Sambasiva Rao Kambala)**



## LIST OF PUBLICATIONS ARISING FROM THE THESIS

---

### JOURNALS

1. “A new approach to increase the flaw detection capability of pulsed eddy current technique”, K. Sambasiva Rao, S. Mahadevan, B. Purna Chandra Rao and S. Thirunavukkarasu, *Measurement*, **2016**(Under Review).
2. “Development of pulsed eddy current technique for testing thick stainless steel plates”, K. Sambasiva Rao, B. Purna Chandra Rao, S. Thirunavukkarasu and S. Mahadevan, *Studies in Applied Electromagnetics and Mechanics*,**2016**,*Vol. 42, 123-130*.
3. “Development of pulsed eddy current instrument and probe for detection of subsurface flaws in thick materials”, K. Sambasiva Rao, B. Purna Chandra Rao, and S. Thirunavukkarasu, *IETE Technical Review*, **2016**,*Vol. 34, 1-7*.
4. “Pulsed eddy current technique for testing of stainless steel plates”, K. Sambasiva Rao, T. Jayakumar, A. Chandra Sekhar and B. Purna Chandra Rao, *Studies in Applied Electromagnetics and Mechanics*,**2014**,*Vol. 39, 36-43*.

### CONFERENCE PRESENTATIONS

1. “Model based optimisation of Pulsed eddy current technique for detection of defects in stainless steel plates”, K. Sambasiva Rao, S. Thirunavukkarasu and B. Purna Chandra Rao, presented during the *25<sup>th</sup>National Seminar and Exhibition on Non-destructive Evaluation (NDE-2015)* –Hyderabad, December 2015.
2. “Study on the effect of excitation characteristics for subsurface defect detection sensitivity in pulsed eddy current technique”, K. Sambasiva Rao, V. Arjun, B. Sasi, B. Purna Chandra Rao and T. Jayakumar, presented during the *24<sup>th</sup>National Seminar and*

*Exhibition on Non-destructive Evaluation (NDE-2014)-Pune, December 2014.*

3. “Development of pulsed eddy current instrument for testing of stainless steel plates”, K. Sambasiva Rao, B. Purna Chandra Rao, B. Sasi, S. Thirunavukkarasu and T. Jayakumar, presented during the 38<sup>th</sup> *National Symposium on Instrumentation (NSI-38)-Hubli*, October 2013.

**(Sambasiva Rao Kambala)**

# DEDICATIONS

---

TO MY FAMILY MEMBERS AND

MENTORS



## ACKNOWLEDGEMENTS

---

This thesis would not have been possible without the support and encouragement of many people who contributed and extended their valuable co-operation in the completion of the research work. I feel short of words in expressing my appreciation for their help at various stages of this work.

First and foremost, I would like to express my sincere gratitude to my thesis advisor Dr. B. Purna Chandra Rao Head, Non-destructive Evaluation Division (NDED), Indira Gandhi Centre for Atomic Research (IGCAR) for his continuous support to my work, his patience, encouragement, enthusiasm and immense knowledge. His intellectual ideas and guidance helped me in my research work and writing this thesis. He has been always a source of motivation for me in difficult times during the research work. I express my deep sense of appreciation for his support and for energizing me to overcome all the hurdles.

I thank my doctoral committee members Dr. G. Amarendra, Dr. B. K. Panigrahi, Dr. V. S. Srinivasan and Dr. S. Thirunavukkarasu for their encouragement, insightful comments and suggestions during the course of the thesis work. I express my sincere gratitude to Dr. T. Jayakumar former Director, Metallurgy and Materials Group (MMG), IGCAR for his inspiration and encouragement. I extend my heartfelt thanks to the former directors of IGCAR, Shri S. C. Chetal, Dr. P. R. Vasudeva Rao and Dr. S.A.V. Satya Murthy and to the present Director, Dr. A.K. Bhaduri for permitting me to pursue research in this reputed centre. I wish to acknowledge Dr. C. K. Mukhopadhyay, Head EMSI Section, NDED, IGCAR, for providing his valuable suggestions at various occasions.

I express my gratitude to IGCAR colleagues, especially Dr. S. Mahadevan, Dr. B. Sasi, Dr. A. Chandra Sekar, Shri V. Arjun and Shri Saji Jacob George for their continuous help in learning the instrumentation and experimental techniques and providing me technical support

and for helping me in carrying out the experiments and for enriching my ideas. I thank my fellow colleagues Dr. W. Sharatchandra Singh, Dr. G. K. Sharma, Dr. Anil Kumar Soni, Dr. S. Shuaib Ahmed, Shri Chandan Kumar Bhagat, Ms. Vijayachandrika other NDED members and Research scholars for their timely help, useful technical discussions, suggestions, and moral support.

Apart from the intellectual support, an emotional support is always needed to conquer the hardships. For this, I would like to thank, from the bottom of my heart, Shri A. Viswanath, Shri G. V. K. Kishore, Shri G. M. S. K. Chaitanya, Shri Manoj Kumar Raja, Shri Satya Rajesh Medidi, Ms. Sravathi, Bava boys and all Enclavians for their warm friendship.

Last but not the least, my deepest gratitude is to my family for their support which brings belief and hope into my life; to my beloved parents Shri Rama Rao Kambala and Smt. Satyavathi Kambala, who have been so caring and supportive of me all the time. Immense love and affection of my brother K. Venkateswara Rao, sister K. Suneetha and brother-in-law Shri Gopal Krishna have been invaluable in the journey towards accomplishing my goal.

Apart from all the people mentioned in this acknowledgment, there are many others who have helped me in various ways during the course of this thesis work. My sincere thanks to all those I may have forgotten to mention.

**(Sambasiva Rao Kambala)**

# TABLE OF CONTENTS

---

<b>TABLE OF CONTENTS</b> .....	<b>i</b>
<b>Abstract</b> .....	<b>v</b>
<b>List of Figures</b> .....	<b>ix</b>
<b>List of Tables</b> .....	<b>xv</b>
<b>Nomenclature</b> .....	<b>xvii</b>
<b>1 Introduction</b> .....	<b>1</b>
1.1 NON-DESTRUCTIVE EVALUATION.....	1
1.2 EDDY CURRENT TECHNIQUE .....	4
1.3 PULSED EDDY CURRENT (PEC) TECHNIQUE .....	8
1.3.1 PEC governing equations.....	10
1.3.2 PEC signal interpretation .....	12
1.3.3 PEC techniqueadvantages.....	13
1.4 LITERATURE REVIEW .....	13
1.4.1 PEC instruments.....	14
1.4.2 PEC probes .....	17
1.4.3 PEC signal parameterextraction .....	21
1.5 MOTIVATION .....	25
1.6 OBJECTIVE OF THE RESEARCH.....	28
1.7 ORGANISATION OF THE THESIS.....	30
<b>2 Development of PEC instrument</b> .....	<b>32</b>
2.1 PREAMBLE .....	32
2.2 PEC INSTRUMENT .....	32
2.2.1 Excitation unit.....	33
2.2.2 Receiver unit.....	38
2.2.3 Signal processing unit.....	43
2.3 PERFORMANCE EVALUTION OF PEC INSTRUMENT .....	44
2.3.1 Test specimen.....	44

2.3.2	Pulse characteristics .....	45
2.3.3	Detection of flaws due to localised corrosion .....	50
2.4	SUMMARY .....	51
<b>3</b>	<b>Development of PEC probe.....</b>	<b>52</b>
3.1	PREAMBLE .....	52
3.2	FINITE ELEMENT (FE) MODELING.....	52
3.3	FE MODEL FOR PEC TESTING.....	53
3.3.1	Construction of model geometry.....	54
3.3.2	Meshing.....	55
3.3.3	Solving the model .....	56
3.4	OPTIMISATIONPEC PROBE .....	56
3.4.1	Position selection of pickup sensor in the probe .....	57
3.4.2	Selection of excitation coil configuration.....	59
3.4.3	Optimisation of outer diameter of the probe.....	67
3.4.4	Optimisation of height of the probe.....	68
3.5	FABRICATION OF THEPEC PROBE AND TESTING.....	73
3.6	TESTING OF THE PEC PROBE.....	74
3.7	SUMMARY .....	78
<b>4</b>	<b>Development of technique for detection of flaws due to localised corrosion .....</b>	<b>80</b>
4.1	PREAMBLE .....	80
4.2	DETECTION OF SUBSURFACE FLAWS.....	80
4.3	PROPOSED TECHNIQUE.....	82
4.4	EFFECT OF EXCITATION RISE TIME ON DETECTION OF FLAWS.....	86
<b>1</b>	<b>89</b>	
4.5	EXTRACTION OF CONVENTIONAL PEC PARAMETERS .....	94
4.6	DETECTION AND CLASSIFICATION OF FLAWS.....	98
4.6.1	Dimensional details of flaws.....	98
4.6.2	Detection of surface flaws .....	99

4.6.3	Detection of subsurface flaws .....	100
4.6.4	Classification flaws .....	101
4.7	SUMMARY .....	102
<b>5</b>	<b>Development of technique for estimation of thickness reduction due to uniform corrosion .....</b>	<b>104</b>
5.1	PREAMBLE .....	104
5.2	ESTIMATION OF THICKNESS REDUCTION.....	104
5.3	WAVELET BASED TECHNIQUE PROPOSED .....	109
5.4	PERFORMANCE EVALUATION OF THE PROPOSED TECHNIQUE .....	112
5.5	COMPARISON THE PROPOSED PARAMETERS.....	115
5.6	SUMMARY .....	116
<b>6</b>	<b>Conclusion and future work.....</b>	<b>118</b>
6.1	CONCLUSIONS .....	118
6.2	FUTURE WORKS .....	120
<b>7</b>	<b>References .....</b>	<b>123</b>



# ABSTRACT

---

Nondestructive evaluation (NDE) plays an important role in ensuring structural integrity of engineering components through detection and sizing of flaws. Many engineering components in nuclear industry are made of austenitic stainless steels of thickness from 8.0 mm to 12.0 mm, e.g. radioactive waste storage tanks. Due to the presence of hostile corrosive environment, these components undergo localised corrosion as well as uniform corrosion on the inner surface. Periodic inspection of such components is essential to ensure safety. For this application ultrasonic piezoelectric crystals are not useful as they are prone to coupling issues. Eddy current testing is an alternate nondestructive testing (NDT) technique. Detection of localised flaws and thickness reduction due to uniform corrosion located beyond 5.0 mm below the surface using eddy current technique from outer surface is challenging due to the presence of noise and lift-off variations.

This thesis focuses on the design and development of a pulsed eddy current (PEC) instrument and an optimal PEC probe for detection of flaws that occur due to localised corrosion as well as thickness reduction due to uniform corrosion in austenitic stainless steel (SS) components. The excitation unit in the PEC instrument is designed to deliver a variable current in the range from 0.2 A to 7.0 A based on MOSFET switching logic to generate strong primary magnetic fields. A variable high gain receiver unit (up to 60.0 dB) is specially designed along with a variable cut-off frequency low-pass filter to eliminate noise.

This thesis also focuses on the design and optimisation of a high-throughput PEC probe configuration using finite element model based studies. Three different types of probe configurations viz. air core (Probe-A), ferrite core (Probe-B) and ferrite core with outer shielding

(Probe-C) have been modeled. From the model predictions, induced eddy current density ( $J_\phi$ ) has been calculated at different locations inside the component. The  $J_\phi$  for the Probe-B has been found to be 47.0% while it is 30.0 % and 35.0% for Probe-A and Probe-C respectively. Ferrite cored probe has clearly shown enhanced flaw detection performance as compared to other two Probe configurations. Further, dimensional optimisation of the Probe-B configuration has been carried out. From the model predictions Probe-B with 20.0 mm outer diameter and 12.0 mm height has been found to be optimal for the chosen problem.

To detect flaws due to localised corrosion in an 8.0 mm thick SS component in the presence of noise, a new technique has been proposed based on the application of modified inductor current equation to the PEC signals. Two signal parameters viz. voltage ratio,  $V_r$  ( $V_1/V_0$ ) and time constant ( $\tau$ ) have been proposed. These two new signal parameters have been found to be very good for detection of flaws at deeper location (up to 6.0 mm). These parameters have also been found superior to the popularly used PEC signal parameters viz. peak amplitude and time-to-peak. The new parameters,  $V_r$  and  $\tau$  have shown a sensitivity of  $0.0029 \text{ mm}^{-1}$  and  $1.430 \mu\text{s}/\text{mm}$  respectively for detection of subsurface flaws and  $0.0016 \text{ mm}^{-1}$  and  $0.652 \mu\text{s}/\text{mm}$  for surface flaws.

This thesis also proposes a technique based on the application of continuous wavelet transform (CWT) to PEC signals for estimation of thickness reduction due to uniform corrosion in an 8.0 mm SS component. A new signal parameter called peak frequency ( $F_p$ ) has been derived from the CWT spectrogram. It has been found that this parameter is less influenced by lift-off variations.

The techniques presented in this thesis demonstrate that synergistic combination of PEC instrument, optimal probe configuration and new signal parameters ensure reliable detection of flaws due to localised corrosion and thickness reduction due to uniform corrosion in 8.0 mm thick austenitic stainless steel components. The studies establish a possible way to assess the structural integrity and safety of nuclear waste storage tanks made of austenitic stainless steels. The PEC instrument, probe and techniques developed in this thesis can also be applied to other components made of electrically conductive materials.



# LIST OF FIGURES

---

Figure 1.1. Generic NDE system. ....	2
Figure 1.2. <i>Skin-effect</i> phenomenon.....	4
Figure 1.3. Disruption of eddy currents around a flaw in a metallic object over which a coil is placed. ....	6
Figure 1.4. Different types of EC probes (a) absolute (b) send-receive with pickup coil (c) differential and (d) send-receive with magnetic sensor. ....	7
Figure 1.5. PEC time-domain parameters. ....	12
Figure 1.6. PEC system for testing covered plates [53]. ....	15
Figure 1.7. A new eddy current surface probe with minima lift-off noise that comprises tangential coils [64].....	19
Figure 1.8. Relation between PEC signal peak voltage and flaw depth. $u_1$ denotes the peak voltage of U-shape probe, while $u_2$ represents the peak voltage of three-core PEC probe. The dot lines are the linear curve fits [65]. ....	20
Figure 1.9. Schematic of two-layer structure specimen [69].....	22
Figure 1.10 Determining the location of (a) lift-off intersection point and (b) variation of lift-off intersection point with metal loss and gap [72].....	24
Figure 1.11. PEC measurements with lift-off variation (a) from Hall sensor and (b) normalized first order derivative of Hall sensor response [74]. ....	25
Figure 2.1. Schematic of the PEC instrument.....	32
Figure 2.2. Schematic of excitation unit.....	33
Figure 2.3. Internal circuit design of an excitation unit using MULTISIM software.....	36
Figure 2.4. Simulation results for current driving capability of the excitation unit.....	37
Figure 2.5. Simulation results for rise and fall time of the excitation current pulse.....	38
Figure 2.6. Schematic of receiver unit. ....	38
Figure 2.7. Internal circuit diagram of INA-129. ....	40

Figure 2.8. Frequency response of an instrumentation amplifier. ....	41
Figure 2.9. Off-set adjustment circuit. ....	41
Figure 2.10. The schematic of the 2 <sup>nd</sup> order low-pass filter. ....	42
Figure 2.11. Internal circuit diagram of the excitation and receiver unit.....	43
Figure 2.12. Photograph of the developed PEC instrument.....	44
Figure 2.13. Details of stainless steel plate with subsurface EDM notches.....	45
Figure 2.14. PEC signals for different excitation currents of (a) 0.5 A (b) 1.0 A (c) 2.0 A (d) 3.0 A and (e) peak amplitude with respect to current. ....	46
Figure 2.15. PEC signals for different pulse width of (a) 1.0 ms, (b) 2.0 ms, (c) 4.0 ms and (d) peak amplitude for different pulse widths.....	47
Figure 2.16. PEC signals for different pulse repetition frequencies of (a) 200 Hz (b) 300 Hz (c) 400 Hz and (d) peak amplitude variation with PRF. ....	48
Figure 2.17. PEC signals amplified by 20 dB and 30 dB for (a) flaw-free signal and (b) flaw signal. ....	49
Figure 2.18. PEC response for (a) subsurface flaws and (b) Peak amplitude vs. flaw location below the surface.....	50
Figure 3.1: PEC model geometry in 2D.....	54
Figure 3.2: PEC geometry with mesh. ....	55
Figure 3.3. Four different field components analyzed (a) $B_{zc}$ (b) $B_{rc}$ (c) $B_{za}$ and (d) $B_{ra}$ around the excitation coil. ....	58
Figure 3.4. (a) Different field components around the PEC probe and (b) differential PEC signals for an excitation coil placed over a SS plate. ....	59
Figure 3.5. Three PEC probe configurations considered (a) Probe-A (b) Probe-B and (c) Probe-C .....	60
Figure 3.6. Model predicted PEC signals for (a) Probe-A (b) Probe-B (c) Probe-C. The predicted (d) peak amplitude and (e) time-to peak as a function of flaw location below the surface.....	62

Figure 3.7. Model predicted contours of the induced current density for (a) Probe-A (b) Probe-B and (c) Probe-C placed over a SS plate of 8.0 mm thickness and having a flat bottom hole (5.0 mm diameter) 5.0 mm below the plate surface.....	63
Figure 3.8. 2D cut lines inside the SS plate at $z = -1.0$ (cut line-1) and $-5.0$ mm (cut line-2) for different $r=0.0$ to 6.0 mm.....	64
Figure 3.9. Radial distribution of induced eddy current at (a) $z= -1.0$ mm (cut line-1) and (b) $z= -5.0$ mm (cut line-2) inside the plate without flaw. ....	65
Figure 3.10. Cross-sectional view of the Probe-B for OD optimisation. ....	67
Figure 3.11. (a) PEC signals from a flaw-free region for different diameter of the probes and (b) the peak amplitude as function of flaw location below the surface.....	68
Figure 3.12. Optimisation of height of the Probe-B. ....	69
Figure 3.13. Model predicted contours of the induced eddy current density for an optimal probe dimensions (outer diameter = 20.0 mm and height = 12.0 mm) for the flaw located at 7.0 mm below the surface.....	70
Figure 3.14. PEC probe for detection of surface flaws. ....	71
Figure 3.15. Model predicted contours of the induced eddy current density for an optimal probe dimensions (outer diameter = 20.0 mm and height = 12.0 mm) for surface flaw depth of 1.0 mm.....	71
Figure 3.16. (a) PEC signals of surface flaws of different depths and (b) variation of peak amplitude and time-to-peak with surface flaw depth. ....	72
Figure 3.17. (a) PEC signals of subsurface flaws and (b) variation of $V_p$ and $T_p$ with flaw location below the surface. ....	73
Figure 3.18. Design of the optimal PEC probe, (b) photograph of the fabricated probe and (c) close up view of the probe. ....	74
Figure 3.19. Schematic of the thickness reduction of SS plate to simulate uniform corrosion. ....	75
Figure 3.20. PEC signals for (a) surface flaws and (b) peak amplitude vs. flaw depth. ....	75
Figure 3.21. (a) PEC signals for thickness reduction and (b) variation of peak amplitude with thickness reduction.....	77

Figure 3.22. PEC signals for subsurface flaws located at 3.0 mm and 6.0 mm below surface in an 8.0 mm thick SS plate. ....	78
Figure 4.1. (a) PEC difference signals (b) peak amplitude and time-to-peak with flaw location below the surface and (c) a close look at the PEC signal from a flaw-free region. ....	81
Figure 4.2. Flow chart of the proposed technique. ....	83
Figure 4.3. PEC response for probe in (a) air (b) noise signal with fit (c) for subsurface flaws and (d) the calibration graph in SS plate. ....	85
Figure 4.4. PEC signals from different excitation rise time. ....	87
Figure 4.5. $V_r$ for subsurface flaws $E_r$ values of (a) 0.25 ms, (b) 0.5 ms, (c) 0.7 ms, (d) 1.0 ms, and (e) 1.4 ms. ....	88
Figure 4.6. Linear fit for time constant with respect to flaw location below the surface for $E_r$ of (a) 0.25 ms, (b) 0.5 ms, (c) 0.7 ms, (d) 1.0 ms and (e) 1.4 ms. ....	91
Figure 4.7. Variation of sensitivity of time constant with respect to $E_r$ . ....	92
Figure 4.8. FFT amplitude for different excitation rise time pulses in the (a) 1 - 12 kHz range (b) 3 - 3.5 kHz in range (skin depth 7.6 to 8.2 mm) and (c) 10 -11 kHz in (skin depth 3.5 to 4.0 mm). ....	93
Figure 4.9. PEC differential signals for $E_r$ of (a) 0.25 ms, (b) 0.5 ms, (c) 0.7 ms, (d) 1.0 ms and (e) 1.4 ms. ....	95
Figure 4.10. Peak amplitude and time-to-peak for $E_r$ of (a) 0.25 ms, (b) 0.5 ms, (c) 0.7 ms, (d) 1.0 ms and (e) 1.4 ms as a function of location below the surface. ....	96
Figure 4.11. Comparison of time-to-peak parameter from (a) the conventional PEC technique and (b) the proposed technique. ....	97
Figure 4.12. Schematic of a SS plate having surface flaws of two different widths. ....	98
Figure 4.13. Variation of (a) $V_r$ and (b) $\tau$ with surface flaw depth (flaw width 1.0 and 3.0 mm). ....	99
Figure 4.14. Variation of (a) $V_r$ and (b) $\tau$ with flaw location below the surface for two different flaw widths (1.0 and 3.0 mm). ....	100

Figure 4.15. Classification of surface and subsurface flaws using a plot between $V_r$ and $\tau$ .....	102
Figure 5.1. Simulated thickness reduction ( $t_r$ ) from 0.0 to 3.0 mm in an 8.0 mm thick SS plate.....	105
Figure 5.2. PEC signals obtained from different thickness reduction locations of the test plate.....	106
Figure 5.3. Variation of fit parameters (a) voltage ratio and (b) time constant with thickness. ....	107
Figure 5.4. Simulated of the thickness reduction of the plate with lift-off (L). ....	108
Figure 5.5. Variation of (a) $V_r$ and (b) $\tau$ with thickness at different lift-off. ....	108
Figure 5.6. Flow chart of the proposed CWT based technique. ....	111
Figure 5.7. CWT of PEC signals from a 6.0 mm thick plate at lift-off of (a) 1.0 mm (b) 3.0 mm and (c) 5.0 mm. ....	112
Figure 5.8. CWT of PEC signals for a thickness reduction of (a) 1.0 mm (b) 2.0 mm and (c) 3.0 mm at a constant lift-off of 3.0 mm. ....	113
Figure 5.9. CWT results for (a) $F_p$ vs. lift-off for different thickness and (b) $F_p$ vs. thickness for two different lift-offs. ....	114



# LIST OF TABLES

---

Table 2.1. Details of the air core PEC send-receive type probe used for performance evaluation of the PEC instrument .....	45
Table 3.1. Details of the sub-domain parameters used in the FE modelling.....	55
Table 3.2. Dimensional details of the air core probe .....	57
Table 3.3. Variation of $J_{\phi}$ value with respect to subsurface flaw depth.....	66
Table 3.4. Dimensions of the fabricated PEC probe.....	73
Table 4.1. PEC signal parameters for subsurface flaws.....	86
Table 4.2. Measured $\tau$ for different $E_r$ and flaw depth below the surface .....	89
Table 4.3. Change in $\tau$ for different $E_r$ .....	90
Table 4.4. Variation of the fit parameters with flaws .....	101
Table 5.1. Experimental test parameters .....	106
Table 5.2. Comparison of the parameters at constant thickness (6.0 mm) for different lift-off.....	115



# NOMENCLATURE

---

## LIST OF SYMBOLS

kHz	Kilo Hertz
MHz	Mega Hertz
mm	millimeter
MSa/s	Mega samples per second
m/s	meter per second
$V_p$	Peak amplitude
$T_p$	Time-to-peak
$T_{zc}$	Time-to-zero crossing
$F_p$	Peak frequency
$E_r$	Excitation rise time
$t_r$	Rise time of the response pulse
$F_c$	Zero crossing frequency
$J_\phi$	Current density
$A$	Magnetic vector potential
$B$	Magnetic field vector
$\tau$	Time constant
$R$	Resistance
$L$	Inductance
$E$	Electric field
$\mu$	Magnetic permeability
$\mu_r$	Relative magnetic permeability
$\sigma$	Electrical conductivity
$R_c$	Correlation coefficient
$F$	Frequency
$Z$	Impedance
$\delta$	Standard depth of penetration
$\text{kA/m}^2$	Kilo ampere per meter square
$d$	Flaw location below the surface
$D$	Flaw depth
$A$	Ampere

V	Electric scalar potential or volts
<i>mA</i>	milli ampere
mV	milli volts
GND	Ground
dB	decibel

# LIST OF ABBREVIATIONS

AC	Alternating current
ADC	Analogue-to-digital converter
AISI	American Iron and Steel Institute
AMR	Anisotropic magnetoresistance
BJT	Bipolar Junction Transistor
CWT	Continuous wavelet transform
DC	Direct current
DAQ	Data acquisition
EC	Eddy current
ECT	Eddy current testing
EDM	Electric discharge machining
EM	Electromagnetic
ENDE	Electromagnetic non-destructive evaluation
FBH	Flat bottom holes
FEM	Finite element modelling
FFT	Fast Fourier Transform
GMR	Giant magnetoresistance
GUI	Graphical user interface
HPF	High pass filter
IACS	International Annealed Copper Standard
ICA	Independent component analysis
ID	Inner diameter
INA	Instrumentation amplifier
LOI	Lift-off intersection point
LOD	Limit of detection
LPF	Low pass filter
MOSFET	Metal-oxide semiconductor field-effect transistor
MPI	Magnetic particle inspection
NDE	Non-destructive evaluation
OD	Outer diameter
PCA	Principal components analysis

PDE	Partial differential equation
PEC	Pulsed eddy current
POD	Probability of detection
PRF	Pulse repetition frequency
PW	Pulse width
ROI	Region of interest
SNR	Signal-to-noise ratio
UT	Ultrasonic testing
TMR	Tunnel magnetoresistance

## Introduction

---

This chapter provides a brief introduction to non-destructive evaluation (NDE), eddy current and pulsed eddy current techniques for testing of electrically conductive materials. This chapter discusses the pulsed eddy current (PEC) signal important parameters to be considered for detection of surface flaws and subsurface flaws in thick austenitic stainless steel components. This chapter also identifies the gap areas which have helped in setting the motivation and in identifying the objectives of the research work.

### 1.1 Non-destructive evaluation

Nondestructive evaluation methods are used to test materials and components in such a way that they do not adversely affect their serviceability. It is essential to ensure quality, safety and reliability of engineering components. Ideally if such a testing is performed without damaging a component or shutting down of a plant, it enhances the profitability through higher plant availability factors [1,2]. This is important in nuclear, transportation, aerospace, petrochemical and other process industries. If a flaw is detected in a component, it may be necessary to repair or replace the component. Flaws in a component can arise due to any one of the following reasons [3]:

1. Presence of flaws in the raw material itself.
2. Improper manufacturing processes such as casting, welding, rolling, forging, machining and component assembly.
3. Environmental and loading conditions during transport, storage and service life e.g. stress corrosion cracking, fatigue, creep, wall thinning and hydrogen embrittlement.

Austenitic stainless steels (SS) are widely used in industries in view of their higher strength, corrosion resistance and ease of fabrication. Flaws occur in austenitic stainless steels components due to exposure to high temperatures, pressures, and hostile corrosive media. Hence, nondestructive detection of flaws in austenitic stainless steels is important. For this, NDE methods such as visual testing, dye penetrant, magnetic particle, ultrasonic testing, radiography and eddy current testing are used. None of these methods can be described as superior to another; they all have their own attractive features and limitations.

A schematic block diagram of a generic NDE system is shown in Figure 1.1. In general, an NDE system consists of three basic elements i.e. excitation source, reception unit and feature extraction unit. In the excitation unit, a particular form of energy is transferred into the object under test. The energy applied to the object is transformed depending on the material properties and presence of flaws in the object. The transformed energy is picked by the reception unit. Finally, the received signals are processed to extract information about the flaws present in the object under test [4].

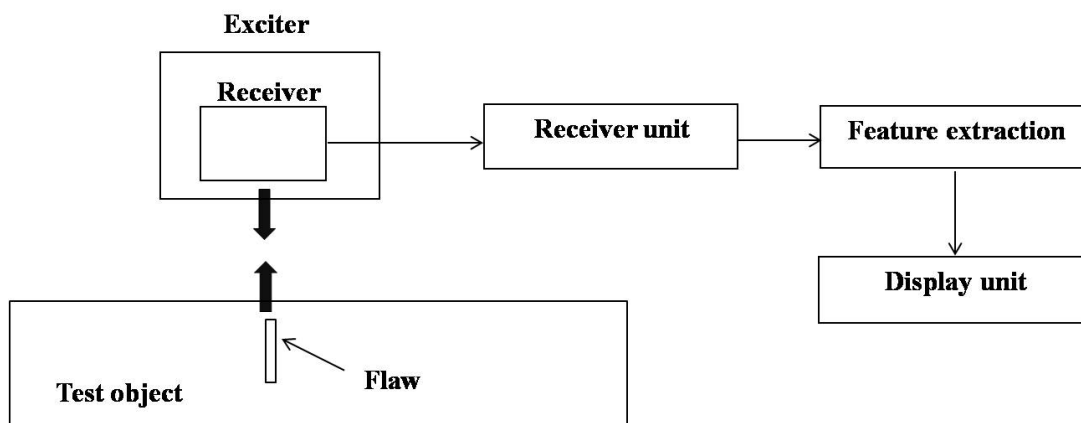


Figure 1.1. Generic NDE system.

NDE techniques can be broadly classified into two categories i.e. active and passive techniques. In an active technique, some form of energy is introduced into the object under test and the change in energy is monitored by the reception unit, if there is any flaw present in the test object.

Eddy current (EC), ultrasonic, and radiographic techniques are some of the active NDE techniques. In passive techniques, flaws are detected by response from the object without any excitation e.g. infrared thermography [5].

In visual technique the health of an object is assessed by using magnifying glasses, digital cameras and video equipments. Visual technique is not suitable for detection of subsurface flaws. Liquid penetrant technique is useful for detection of surface cracks in any kind of material, as long as it is non-porous. Magnetic particle technique is applicable for detection of surface and sub-surface flaws in ferromagnetic objects. Radiography technique is used for volumetric inspection of castings, welds and composite materials. This technique requires access from both sides and proper safety, precautions are required for inspection because of the use of X-rays or  $\gamma$ -rays. Ultrasonic technique is the most versatile NDE technique that uses high frequency (0.5 to 25 MHz) ultrasound energy for dimensional measurements, flaw detection and microstructure characterization. This technique always requires a coupling medium and ultrasonic probes are affected by couplant thickness variations. Acoustic emission and infrared thermography techniques are passive techniques that are used for detection of growing cracks and hot spots respectively.

EC technique is a widely used electromagnetic NDE (ENDE) technique for detection and sizing of surface as well as near subsurface flaws in electrically conducting materials. In this technique, flaws are detected by measuring changes in impedance of a coil excited with an alternating current or by measuring induced voltage in an adjacent receiver coil. This is a simple and portable NDE technique used for testing of components such as heat exchanger tubes, aircraft structures etc.

## 1.2 Eddy current technique

Eddy current technique (ECT) works on the principle of Oersted's law i.e. whenever a time varying current is passed through a coil, a time varying magnetic field is developed in and around the coil. If the coil is brought close to an electrically conducting object, eddy currents are induced in the material due to Faraday's law of electromagnetic induction. The eddy currents flow is influenced by the electrical conductivity and magnetic permeability of the material, object geometry and presence of flaws in the object. Generation of eddy currents in a test material is a diffusion process and eddy currents are induced in closed loops of circulating currents in planes perpendicular to the magnetic field [6]. They flow in opposite direction to the excitation current, following the Lenz's law. As the eddy currents diffuse into the material, their strength reduces exponentially following the *skin-effect* and they also lag in phase. As shown in Figure 1.2, maximum eddy currents concentrate near the surface of the object and they decay with depth from the surface. The eddy current density is maximum at the surface and becomes zero at the center of the coil and at distances far off from the surface.

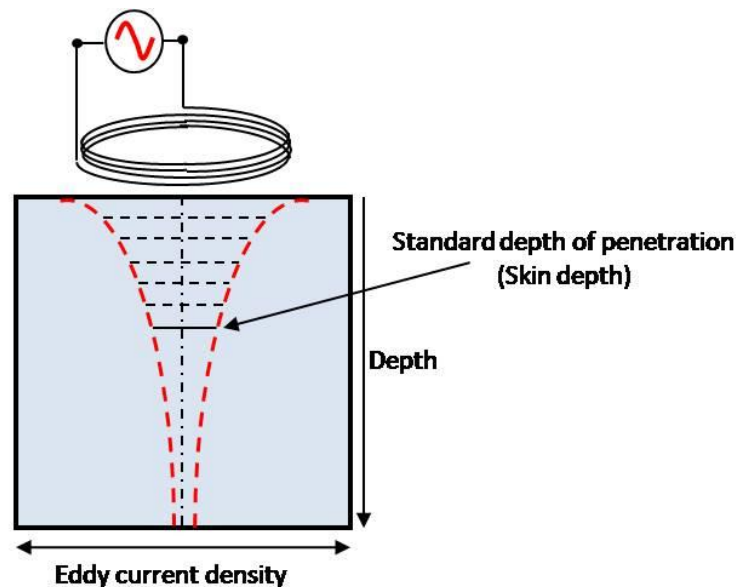


Figure 1.2. *Skin-effect* phenomenon.

Due to the flow of eddy currents in the object, secondary magnetic fields that oppose the primary excitation magnetic field are produced. The strength of eddy current density,  $J_x$  at any depth 'x' is

$$J_x = J_0 e^{-x/\delta} e^{-jx/\delta} \quad 1.1$$

$$\delta = \frac{1}{\sqrt{\pi\mu\sigma f}} \quad 1.2$$

where

$J_x$  is the eddy current density at x depth in  $A/m^2$

$J_0$  is the surface eddy current density in  $A/m^2$ ,

$\delta$  is the standard depth of penetration in m,

$\mu$  is the magnetic permeability of the material in H/m,

$\sigma$  is the electrical conductivity of the material in S/m and

f is the excitation frequency in Hz.

Increase in thickness of the object causes more induced eddy currents and hence, more opposing secondary magnetic fields that reduce the net magnetic field. Flaws in the material disrupt the flow of eddy currents as shown in Figure 1.3 and this causes change in secondary magnetic field and hence, coil impedance. Further, eddy currents attenuate and lag in phase with flaw depth or object thickness. Hence, phase angle of the eddy currents can be advantageously used to obtain information about the depth location of flaws.

From equation (1.2) it is evident that the depth of penetration of eddy currents depends on the frequency of the excitation current, the electrical conductivity and magnetic permeability of the material. Because of this, the excitation frequency for EC testing is selected based on the material properties and the expected location of the flaws below the surface. Lower excitation frequency is required for detection of deep subsurface flaws while higher frequencies are used for detection of surface flaws. For obtaining a detectable response from smaller flaws or deep subsurface

flaws, it must be ensured that the excitation coil induces large amount of eddy currents around the flaw [7].

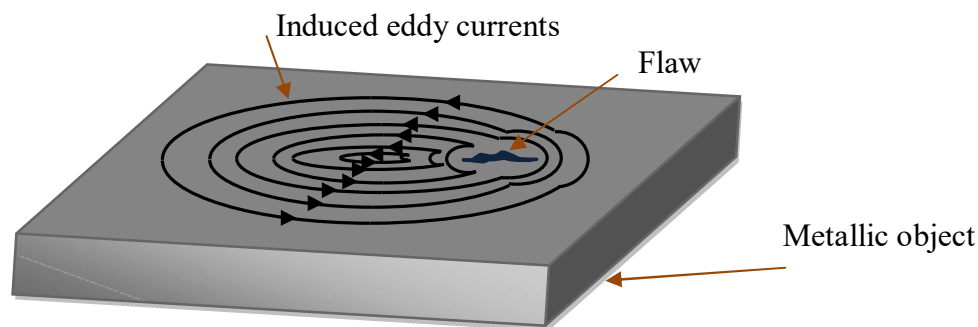


Figure 1.3. Disruption of eddy currents around a flaw in a metallic object over which a coil is placed.

The primary and secondary magnetic fields are detected by measuring the electromotive force (emf) across a pickup coil or by using a magnetic sensor such as Hall element [8]. There are different types of probe configurations reported in the literature and they are selected based on the geometry to be tested. Figure 1.4 shows the commonly used EC probe configurations for testing materials [3]. Figure 1.4 (a) shows a probe having only excitation coil, also called as absolute probe, in which the change in the impedance of the excitation coil itself is used for detection of flaws [9]. Absolute coils are useful for applications like measuring conductivity and thickness of materials. Figure 1.4 (b) is a send-receive type of probe having separate excitation and pickup coils. In this case, the induced voltage in the pickup coil is used for detection of flaws. This type of coil configuration is useful for detection of oriented cracks and to minimize noise due to lift-off variations [9]. Figure 1.4(c) shows a probe with two coils connected in opposition so that the net measured impedance or induced voltage is cancelled out when both coils experience identical conditions. These types of coils are highly sensitive to localised

material discontinuity as compared to absolute coils [6]. Figure 1.4 (d) shows probe with the solid state magnetic sensor to measure the magnetic field due to eddy currents for detection of deep surface flaws and far side corrosion. Such probes essentially operate in send-receive mode with solid state sensor in place of receiving coils. This type of integrated probe showed better detection sensitivity than the conventional EC probe as it can measure very low magnetic fields compared to coils [10].

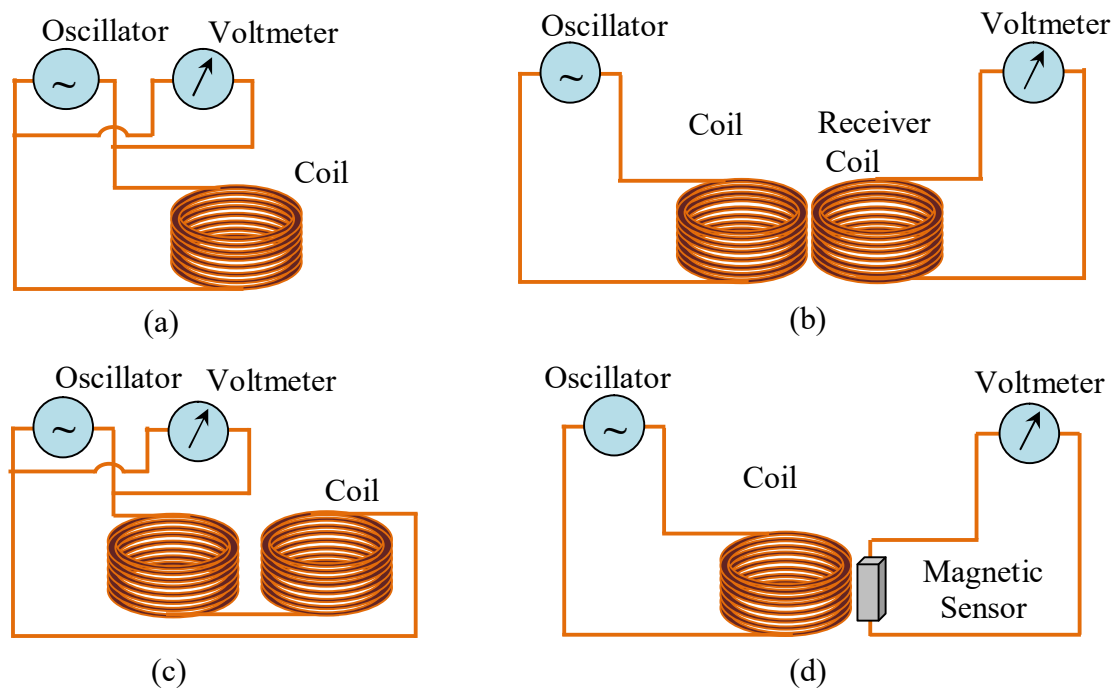


Figure 1.4. Different types of EC probes (a) absolute (b) send-receive with pickup coil (c) differential and (d) send-receive with magnetic sensor.

The conventional EC probes that use a pickup coil show poor sensitivity for detection of flaws particularly at low frequencies [11,12]. Recently, magnetic field sensors having wider bandwidth and higher sensitivity at low frequencies are replacing the traditional pickup coils [13,14]. Magnetic sensors produce an output voltage that is proportional to the magnetic field. These are extremely useful for detection of flaws located at deeper depths.

From the literature, it is observed that conventional EC testing technique is able to detect flaws located less than 4.0 mm below surface [15,16,17,18] and is sensitive to a variety of disturbing variables viz. lift-off, surface roughness, and conductivity variations that influence the flaw detection. Deeds and Dodd [19] showed that by using multiple frequencies, unwanted variables such as lift-off, support plate signals could be eliminated. The use of sweep or multi-frequency eddy current instruments sacrifices the measurement speed and adds to equipment cost [20]. Pulsed eddy current (PEC) technique is attractive.

### **1.3 Pulsed eddy current (PEC) technique**

Pulsed eddy current testing is a new emerging technology in electromagnetic nondestructive testing (NDT). It also works on the principle of Faraday's law of electromagnetic induction. Unlike continuous sinusoidal excitation in conventional eddy current testing, PEC technique uses a rectangular or square wave voltage pulses to excite the probe. The advantage of using a pulse voltage is that it contains a continuum of frequencies. As a result, the electromagnetic response from a range of depths due to several frequencies can be obtained at once. Perturbation occurs to the flow of eddy currents due to the presence of flaws in the test material and this generates secondary magnetic fields. As discussed in Section 1.2, the resultant magnetic fields can be measured as the induced emf across in a pickup coil or by using a magnetic sensor. Eddy currents are induced in the test material during the excitation pulse rise time and fall time. The induction process does not happen at other times of the excitation pulse [21]. Therefore, the PEC technique is also called a transient eddy current technique.

The rate of change of rising time of the current pulse is crucial as it determines the frequency components contained in it. The higher the rate of change, the more the high frequency components, as a result the lower the depth of penetration of eddy currents and surface diagnostic information extraction and vice versa [7]. As the pulse diffuses into the specimen, it is broadened

by dispersion and also influenced by flaws in the object. The flaws closer to the surface affect the eddy current response pulse earlier than those at deeper locations. Hence, there is a sweep of frequencies in a single pulse excitation in PEC technique [8]. A long duration pulse consists of a continuum of frequencies, and is especially rich in low frequency components, which are essential for subsurface flaw detection [22].

Use of PEC technique has been reported in nuclear, oil and petrochemical industries for detection of flaws in SS components [8]. In the last decade, significant progress in detection of flaws has taken place by incorporating the concurrent advances in instrumentation, signal processing etc.[23,24,25]. Its main successes are testing of thin metal tubes, sheets, cladding thickness measurement and sizing of flaws [26,27]. PEC technology has the potential to identify a large number of parameters, such as detection of flaws in thick materials, non-contact measurements at higher probe lift-off [28].

In most of the EC applications, coils are used for both magnetic field excitation and pickup. The amount of induced voltage in the pickup coil depends on the rate of change of magnetic flux ( $\phi$ ) and number of turns in the coil (N).

$$V = -N \frac{d\phi}{dt} \quad 1.3$$

Decrease in excitation signal frequency decreases the rate of change of the magnetic flux and consequently, decreases the induced voltage in the pickup coil[29]. Thus, at very low frequencies the response signal magnitude decreases to a level where signal-to-noise ratio (SNR) is too low for reliable detection. To improve the excitation coil sensitivity, increasing the flux through the excitation coil is a possibility. The magnetic flux ( $\Phi$ ) passing through a circular coil is given by:

$$\phi = B \pi r^2 \quad 1.4$$

where  $B$  is the magnetic flux density perpendicular to the surface of the test material,  $r$  is the radius of the excitation coil. Higher detection sensitivity can be achieved theoretically by building a larger excitation coil as it would allow a higher depth of penetration of the magnetic fields. On the other hand, if the same large size pickup coil is used for detection purpose, resolution and sensitivity would be compromised [30]. Use of a smaller diameter excitation coil would provide a better sensitivity and resolution but it would limit the eddy current penetration in the test object. Therefore, better solution would be to use a large diameter excitation coil and a small diameter pickup coil to achieve good resolution and better detection sensitivity. But these types of probes are less sensitive to low frequency electromagnetic fields. In this context, solid state semiconductor detectors such as Hall, GMR, AMR and SQUID etc. are attractive [31].

The magnetic sensors have advantages over the induction coils. Firstly, they measure the direct magnetic field itself instead of the rate of change of the magnetic field measured by the pickup coils and possess constant sensitivity down to zero frequency i.e. DC. Secondly, the size of the magnetic sensor is generally much smaller than excitation and receiver coils, and this contributes to higher spatial resolution. However, the magnetic sensor frequency response is limited by bandwidth. This allows the measurement of magnetic field intensity directly from DC to an upper frequency limit which depends on the chosen sensor, but it is in general in excess of 100 kHz [32]. They can be used as detectors in pulsed eddy current probes.

### 1.3.1 PEC governing equations

The governing partial differential equation of the pulsed eddy current technique can be derived from the following Maxwell's equations of electromagnetics:

$$\nabla \times E = -\frac{\partial B}{\partial t} \quad 1.5$$

$$\nabla \times B = \mu j \quad 1.6$$

where  $E$  is electric field intensity,  $B$  is magnetic flux density,  $\mu$  is the magnetic permeability of the material and  $J$  is current density. The magnetic flux density is expressed in terms of the vector potential  $A$  as given below.

$$B = \nabla \times A \quad 1.7$$

Upon combining equations (1.5) and (1.7), equation (1.8) is obtained as

$$E = -\nabla V - \frac{\partial B}{\partial t} \quad 1.8$$

where  $V$  is the electric scalar potential. The current density in equation (1.6) is a combination of applied excitation current density ( $J_s$ ) and the induced eddy current density ( $J_e$ ) in the material i.e.  $J = J_s + J_e$  where  $J_e = \sigma E$ , and  $\sigma$  is electrical conductivity of the material.

Substituting this equation in (1.7) results in

$$\nabla \times (\nabla \times A) = -\sigma \mu \frac{\partial B}{\partial t} - \sigma \mu \nabla V + \mu J_s \quad 1.9$$

Applying Coulomb gauge condition ( $\nabla \cdot A = 0$ ) equation (1.9) reduces

$$\nabla^2 A = \sigma \mu \frac{\partial B}{\partial t} + \sigma \mu \nabla V - \mu J_s \quad 1.10$$

Equation (1.10) is the governing partial differential equation to be solved for understanding the PEC technique. Analytical solution to equation (1.10) is difficult due to multiple interfaces and boundaries, especially in the presence of flaws. Finite element method based numerical techniques are extensively used due to their versatility as well as computational efficiency and they are attractive for solving equation (1.10)

### 1.3.2 PEC signal interpretation

A reference PEC signal is obtained by scanning the PEC probe over a flaw-free region on test object or by keeping the probe in air. APEC difference signal is obtained by subtracting the reference signal from that of a flaw signal. Thus, the PEC response appears zero until the probe is moved to a position where the geometry of the structure is changed or due to the presence of a flaw in the test object. Time domain parameters viz. Peak amplitude ( $V_p$ ), Time-to-peak( $T_p$ ) and Time-to-zero crossing ( $T_{zc}$ ) are obtained from the PEC difference signal and used for detection of a flaw and for determining its location [33]. Typical PEC signal and time domain parameters are shown in Figure 1.5. These parameters are also useful to classify flaws:

- The peak amplitude depends on the location and size of a flaw, in other words it is proportional to the amount of metal loss in the test object [34,35].
- Eddy currents are attenuated and dispersed as they travel deeper into the test material. Hence, the time-to-peak is related to the position of a flaw in the test object [36,37].

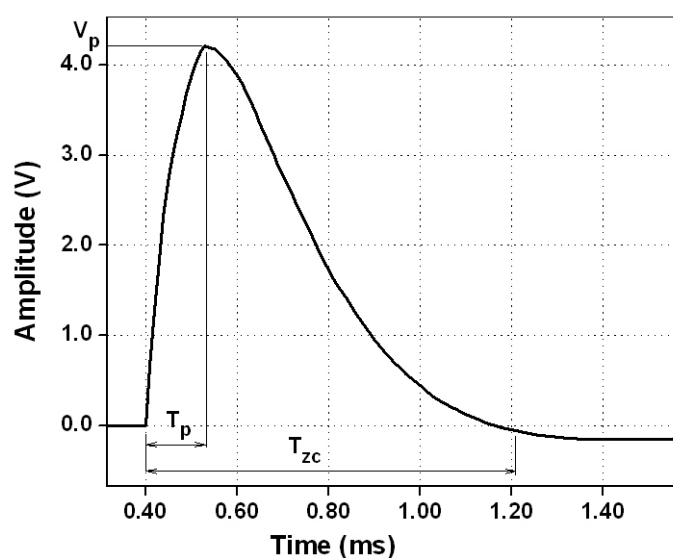


Figure 1.5. PEC time-domain parameters.

- c. In theory, there are several numbers of time-to-zero crossing points that are possible. However, only a few are visible in the measurements. Change in thickness of cladding alters the zero crossing point.  $T_{zc}$  is also related to the location of a flaw [38,39,40].

### 1.3.3 PEC technique advantages

Some of the attractive advantages of PEC technique [13,41] are:

- a. Pulse has a continuum of frequency components hence, multiple depth of investigation at once,
- b. Detection of flaws at deeper depth with improved sensitivity,
- c. Non-contact scanning large areas of a complex structure without the need for couplant,
- d. Ability to compensate for lift-off and edge effects and
- e. Less heating affects because of its low average power and pulsing

## 1.4 Literature Review

Research in pulsed eddy current technique was started in the early years of 1950 for detection of coating thickness and plate thickness of conducting plates [42,43]. Later, PEC technique has been used for inspection of pipes, vessels, aircraft structures and numerous other applications. Some of the established applications of the PEC technique are listed below:

- a. Detection of surface and subsurface flaws [15,44,45,46,47]
- b. Estimation of wall thickness loss due corrosion [48,49,50]
- c. Sorting of materials based on electrical conductivity [18,32,40]
- d. Detection of flaws due to corrosion in multilayer structures [13,41,51,52]
- e. Measurement of coating thickness [42,23,53]
- f. Measurement of stress in materials [35,54,55]

Most of the PEC applications encompass detection of wall thickness loss, coating thickness, surface as well near surface flaws. Several researchers attempted development of several approaches based on different PEC instruments, probe configurations and signal processing methods for the above applications.

#### 1.4.1 PEC instruments

Flaw detection depends on the sensitivity of the PEC instrument. The excitation parameters such as current, rise time, pulse width and pulse repetition frequency are important. The induced voltages in a pickup coil are in mV range and are influenced by external noise. The PEC instrument should be able to detect and amplify these feeble signals. Several researchers have reported development of PEC instruments for detection of flaws, wall loss and coating thickness variation.

Dodd *et al.* [56] designed a PEC instrument for inspection of thin wall of stainless steel tubes. The instrument transmits excitation pulses to the coil and detects the resultant fields using a receiver coil. A preamplifier was used to amplify the pickup coil response which was acquired by a 12-bit analog to digital conversion (ADC) card. The instrument and probe were able to detect wall thickness variation of 0.015 mm on inner as well as outer surfaces of 0.127 mm thick stainless steel tubes.

Xu *et al.* [57] studied the effect of PEC excitation parameters on detection of thickness loss due to corrosion in a magnetic steel plate. Based on the frequency analysis, the influences of the duty cycle and edge time on response signals were analyzed. They reported that for inspection of

specimen in the thickness range of 8.0 to 20.0 mm, a duty cycle of the order of 50 % to 1.0 % and edge time in the order of 1.0 ms to 10.0 ms were required.

Angani *et al.*[53] developed a PEC system for detection of wall thickness variation in a 5.0 mm thick SS plate covered with an 8.0 mm thick insulation. They used a cylindrical coil for excitation and Hall sensors connected in axial differential mode, as shown in Figure 1.6, for pickup. They used peak amplitude and time-to-zero of the PEC signals for thickness measurement and reported detection of thickness loss of 1.0 mm in the plate covered with an 8.0 mm thick insulation.

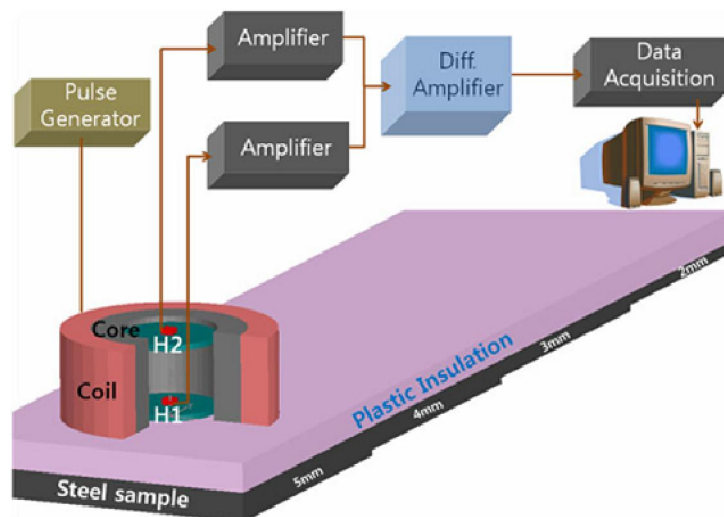


Figure 1.6. PEC system for testing covered plates [53].

Burke *et al.*[58] used a commercially available transient eddy-current system (TRECSCAN) for estimation of metal loss due to corrosion in multilayer structures. They used an air-core coil excited with current-controlled bipolar square-wave pulses and measured the normal component of the magnetic field on the axis of the coil using a Hall sensor. After suitable amplification and filtering, the signals were digitized using a 16-bit ADC card. The instrument was able to measure the wall thickness variation up to 3.6 mm in 4-multilayer structure interlayer gaps (2.5 mm) with a lift-off 2.5 mm.

He *et al*[59] used TRECSCAN instrument to detect atmospheric corrosion on 3.0 mm thick mild steel samples exposed for 1.0 to 10.0 months. The instrument operates in current excitation mode with an exponentially damped square wave of 50% duty cycle, repetition frequency of 200 Hz and time constant of 100  $\mu$ s. The response signals were low-pass filtered, amplified and acquired at a sampling rate of 500 kHz. They reported that with increase in exposure time there is an increase in peak amplitude value due to reduction in the average electrical conductivity and permeability of the material. The instrument was able to estimate thickness reduction of 0.04 to 0.110mm.

Bieber *et al*. [60,61] focused the research work on corrosion detection and characterisation in two layered (each one is of 1.5 mm thick) structures of 3.0 mm thickness. They used a time-gating method to determine the location of flaws whose diameter was 18.0 mm and depth varied from 10 % to 30 %. Using the time-gating method, peak arrival time corresponding to the flaw depth was investigated in a specified range of time. All peaks that occurred outside the range were neglected. They observed that the peak amplitude decreases and time-to-zero crossing increases with an increase in flaw location below the surface in multilayer structures.

Pulsed eddy current instruments available in the open market are generally aimed at specialized applications. For example, the PEC system, called RTD-Incotest, is useful for corrosion detection on insulated and coated pipelines [62]. However, details of general purpose PEC systems are not found in the open literature.

From the literature, it is inferred that the excitation parameters are important for strengthening the primary magnetic field to detect subsurface flaws. Hence, focussing research on high power variable current source is beneficial. The PEC signals from subsurface flaws are in the order of a

few mV and are affected by noise. In order to amplify such a low amplitude signals and extract PEC signal parameters, there is a definite need to develop a high sensitive receiving unit. A few researchers reported design and development of PEC instruments for detection of surface and near surface flaws in Aluminum and SS components. However, literature on PEC instruments which can detect flaws located 5.0 mm below the surface in thick SS materials is not found. Hence, there is a strong need to develop a sensitive general purpose PEC instrument which can detect flaws located beyond 5.0 mm below the surface in thick stainless steel components.

#### 1.4.2 PEC probes

It is important to study different types of probe configurations suitable for detection of subsurface flaws in thick components. In this context, there is a definite need to design and optimise PEC probe configuration. This can be accomplished either by experimentation or by numerical modelling. Various researchers have reported different types of probe configurations and for detection of localised flaws and thickness reduction due to uniform corrosion. In the literature, the most widely used probe configurations are[6]:

- ✓ Air core,
- ✓ Ferrite core,
- ✓ Double-D,
- ✓ Cup-core and
- ✓ Rectangular.

Beissner *et al.*[47] proposed a send-receive type PEC probe configuration for detection of surface flaws in a 1.5 mm thick titanium plate. Excitation coil was surrounded by a conducting shield to limit the spatial extent of the field incident on the specimen thus, improving the spatial

resolution. According to them, shielding also served to reduce the direct field coupling from the excitation coil to the pickup coil. The optimised PEC probe was able to detect 0.125mm deep surface flaws whose lengths in the range of 0.250 to 1.250mm.

Palanisamy *et al.*[51] studied the influence PEC coil with and without ferrite core using finite element model predictions on a 2.0 mm thick aluminium multilayer structure. They predicted the change in impedance of probe and distribution of induced eddy currents around a flaw in the second layer (1.27 mm below) of aluminium lap joint. They reported that the detection sensitivity of air core probe is higher for smaller radius coils while the detection sensitivity of ferrite core probe is higher for large radius coils. They also reported that ferrite core probe provides a better spatial resolution than that of air core probe, due to focused flux.

He *et al.*[63] proposed a rectangular excitation probe for identification of edge of the flaws of length (15.0 mm), depth (1.5 mm) and width (1.5 and 3.0 mm) in a 2.0 mm thick aluminium sample and for imaging of flaws. When the probe is scanned along the length of the flaws, PEC signal parameter ( $V_p$ ) showed a positive and negative maximum corresponding to the movement of the coil entering and leaving edge of the flaw, which are used to generate imaging of the flaws and therefore, evaluation of flaw length.

Hoshikawa *et al.*[64] designed a novel PEC probe to detect surface flaws of 15.0 mm length, (width, 0.5 mm) whose depth was varied from 0.5 to 1.5 mm in a 1.5 mm thick brass plate independent of lift-off variations as shown in Figure1.7.

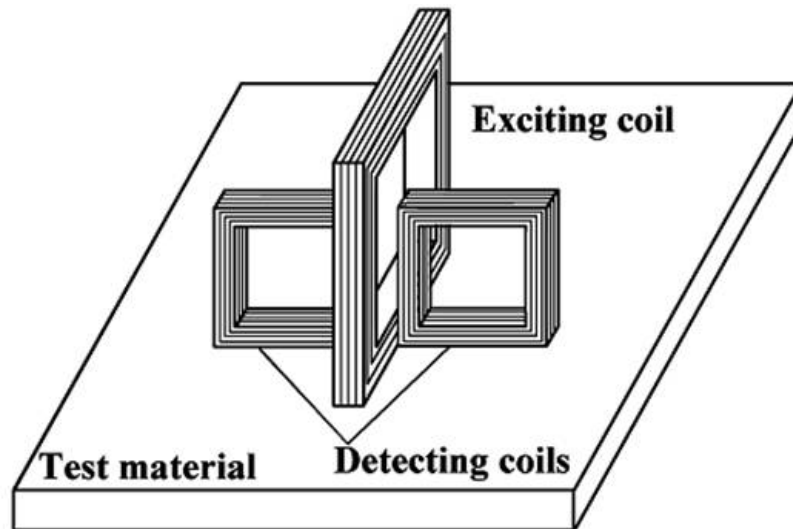


Figure1.7. A new eddy current surface probe with minima lift-off noise that comprises tangential coils [64].

The probe consists of a tangential excitation coil and two tangential detecting coils which are connected in differential mode. The probe was able to detect the flaws effectively independent of lift-off variations up to 1.05 mm whereas the conventional probe unable to detect.

Young *et al.*[48] studied the performance of different types of shielding in a send-receive type PEC probes for detection of wall thickness variation(from 1.08 to 4.5 mm) due to corrosion in a 10.0 mm thick copper material using FE modelling. From the model predictions they reported that the ferrite core shielding probe configuration showed improved sensitivity for wall thickness variation of 1.08 to 4.5 mm as compared to the conductive shielding.

Shu *et al.*[65] developed different types of differential probe configurations in the PEC testing for detection of surface flaws of 100.0 mm length, (width, 0.2 mm) with varying depth from 0.2 mm to 2.0 mm in a 15.0 mm thick iron specimen in the presence of noise, lift-off and probe tilt. They used  $V_p$  as a parameter for detection of flaws.

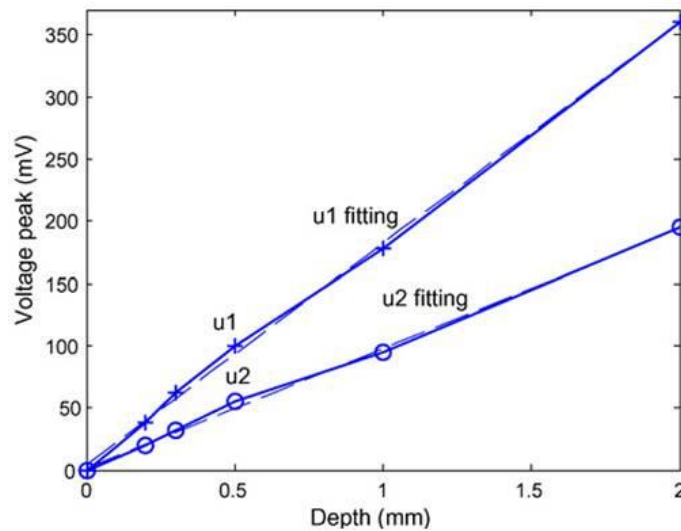


Figure 1.8. Relation between PEC signal peak voltage and flaw depth. u1 denotes the peak voltage of U-shape probe, while u2 represents the peak voltage of three-core PEC probe. The dot lines are the linear curve fits [65].

They observed that the flaw parameter ( $V_p$ ) increases with an increase in flaw depth. They reported that U-shaped differential probe design showed improved flaw detection response with respect to noise and lift-off variations, as compared to other probe configurations as shown in Figure 1.8.

It is observed from the literature that solid state sensors are useful to improve the detection sensitivity of subsurface flaws in thick materials. Angani *et al.*[66] designed a differential Hall sensor based ferrite core probe for detection of subsurface flaws in 6.0 mm thick SS plates. For the study, a 4.0 mm thick plastic sheet was placed over the plates to simulate the thermal insulation of the pipeline. They reported detection of flaws located at 5.0 mm below the surface with a lift-off of 4.0 mm.

From the literature it is noted that by using a cylindrical send-receive PEC probe configuration, effective depth of penetration can be increased in thick materials. Inspired by the enhanced

performance of ferrite core and send-receive types of probes, systematic studies can be focused to develop optimal send-receive type PEC probes for detection of deep subsurface flaws in thick stainless steel components.

### **1.4.3 PEC signal parameter extraction**

Detection and classification of flaws using pulsed eddy current technique is influenced by noise, lift-off etc. which mask the weak PEC signals from subsurface flaws and reduce the signal-to-noise ratio. In literature, different techniques were reported for detection and classification of flaws from the PEC signal parameters.

#### ***1.4.3.1 Detection and classification of flaws***

Xie *et al.*[67] applied averaging method to PEC signals over 100 cycles to reduce noise in the measurements. They reported estimation of thickness variation (from 2.0 to 8.0 mm) in a 10.0 mm thick austenitic stainless steel plate in the presence of noise with an accuracy of 1.0 mm.

He *et al.*[68] applied a wavelet transform based filtering technique to reduce noise in PEC measurements. This technique was able to detect both surface and subsurface flaws of 8.0 mm length (width, 0.8 mm) with depths of 1.0, 1.2 and 1.4 mm effectively in a 3.0 mm thick aluminium structure.

Mengchun *et al.*[69] used an approach based on fast Fourier transform (FFT) and principal component analysis (PCA) techniques for detection and classification of flaws in 3.0 mm thick two layer aircraft lap-joints. They reported detection and classification of flaws of 10.0 mm

length(depth,0.9 mm) and width of 2.9, 1.9 and 0.9 mm in the first-layer surface, first-layer subsurface, second-layer surface, and second layer subsurface as shown in Figure 1.9

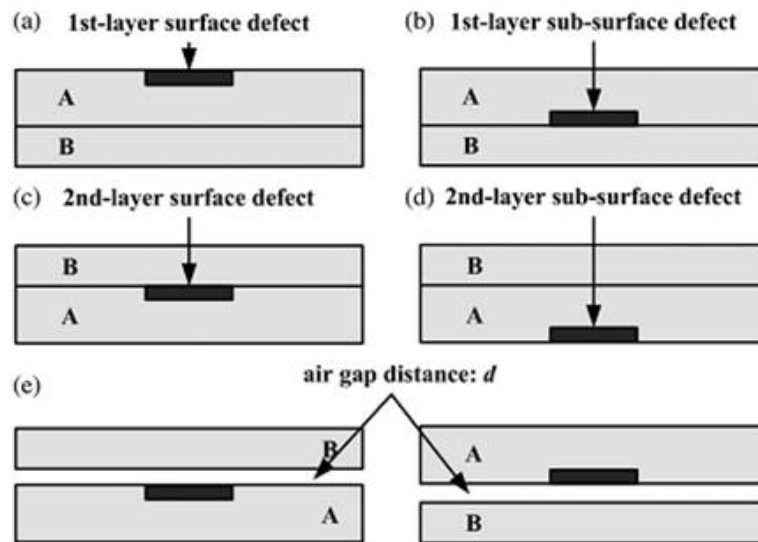


Figure 1.9. Schematic of two-layer structure specimen [69].

Hosseni *et al.*[70] applied short time Fourier transform (STFT) and PCA techniques to PEC signals for detection and classification of flaws in 2.0 mm thick aluminium multi-layer aircraft structures. They reported that with the principal components both metal loss (from 5 % to 25 %) and surface flaws (from 3 % to 25 %) are classified effectively.

Zhanget *al.*[71] identified a new parameter called sum of instantaneous frequency covariance (SCovIF) to separate surface flaws from subsurface flaws. They observed that the flaw classification could be improved significantly by combining the conventional time-domain parameters viz. rise time and time-to-peak with the SCovIF parameter.

Shin *et al.*[18] studied the effect of excitation coil time constant on estimation of thickness of materials such as Cu, Al, Ti, W and Inconel-600. The PEC parameters such as  $V_p$ ,  $T_p$  and  $T_{zc}$  were used for estimation of thickness. As the time constant gets shorter, peak values from thin

aluminum plates increase more than those from thick plates. They reported that larger time constant is required for testing of thick and highly conductive materials and vice versa.

From the literature, it is observed that electromagnetic interference and electromechanical noise are the major issues in the PEC measurements that affect the signal parameters leading to inaccuracies in the detection of subsurface flaws. It is essential to focus research towards exploring effective techniques for detection and classification of flaws in noisy environment.

It is also inferred from the literature that flaw detection sensitivity depends on the excitation pulse. The rate of change of the rising edge of the pulse is crucial as it determines the frequency components contained in it. In this context, it will be beneficial to focus research on rise time studies for exploring enhanced detection and classification of flaws.

#### ***1.4.3.2 Estimation of wall thickness***

Accurate estimation of thickness reduction due to uniform corrosion is desired for structural integrity assessment of critical engineering components. Lift-off, disturbs the PEC signals and leads to errors in thickness estimation.

Giguere *et al.* [72] observed a time-domain parameter called lift-off intersection (LOI) point when driver and pickup are inductive coils and its determination is shown in Figure 1.10. It is the point where all the lift-off signals intersect. The LOI point is independent of lift-off variation and varies with amount of wall loss. They reported that the proposed parameter was able to estimate thickness variation from 5 % to 25 % effectively, in a 2.0 mm thick Al plate at a lift-off up to 0.4 mm.

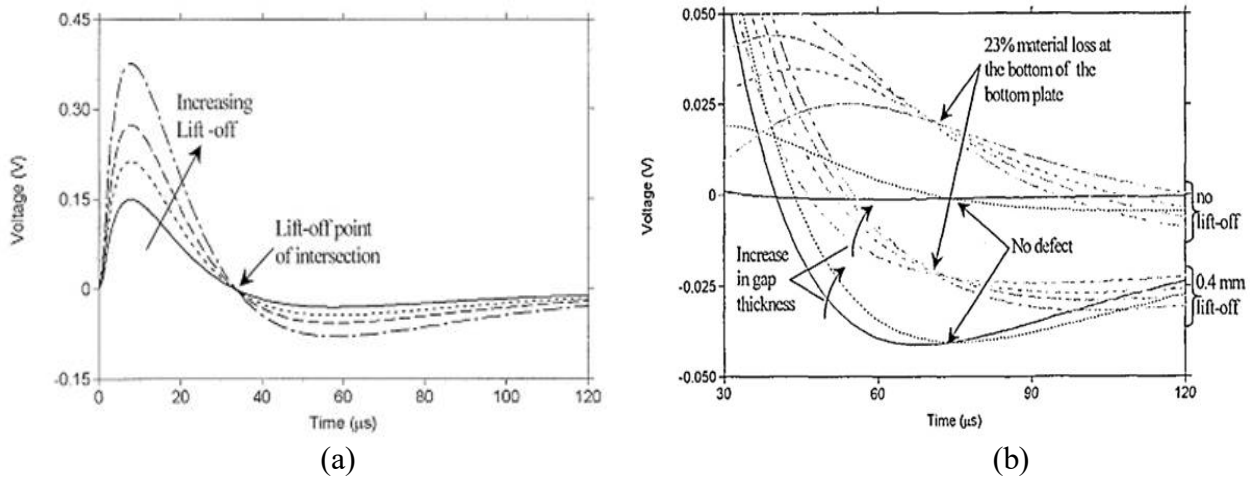


Figure 1.10 Determining the location of (a) lift-off intersection point and (b) variation of lift-off intersection point with metal loss and gap [72].

Shu *et al.*[73] reported novel PEC differential probe configurations to reduce the lift-off effect on PEC measurements. Among all, U-shaped differential probe showed improved flaw detection in the presence of lift-off variations. It was able to detect surface flaws of 10.0 mm length (width, 0.2 mm) and depth of 0.2, 0.3, 0.5, 1.0 and 1.5 mm effectively at a lift-off of up to 3.0 mm in a 15.0 mm thick SS plate.

Tian *et al.*[74] investigated LOI point characteristics when a Hall sensor was used for pickup. They observed that LOI point is not present with the Hall sensor as shown in Figure 1.11 (a). However, the LOI point can be observed by taking the first-order time derivative of the magnetic sensor signals which also is independent of lift-off as shown in Figure 1.11 (b). They further reported that the LOI point increases with an increase in conductivity of the materials.

Mengbao *et al.*[75] proposed a new approach based on calculation of phase value from the FFT of PEC signals. They validated this approach by both model predictions and experimental results.

They identified that at a particular frequency, the phase value is independent of the lift-off variations and changes with thickness and conductivity of the material.

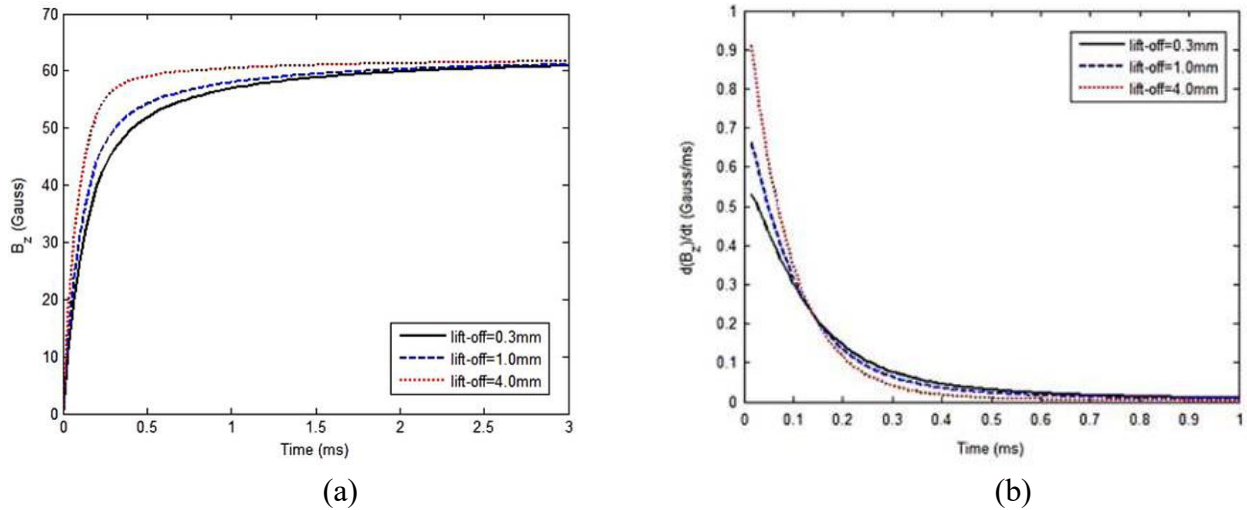


Figure 1.11. PEC measurements with lift-off variation (a) from Hall sensor and (b) normalized first order derivative of Hall sensor response [74].

From the literature, it is observed that estimation of the remaining wall thickness of components, especially that undergo corrosion damage, is a major challenge due to the disturbing influence of lift-off. Several parameters reported in the literature such as lift-off intersection point, use of a special kind probes and signal processing methods for wall thickness estimation independent of lift-off variations with a limited success. Hence, there is a need to focus research in this area and explore development of an efficient method for measuring the thickness reduction due to uniform corrosion at higher lift-offs.

## 1.5 Motivation

Austenitic stainless steel is one of the important structural materials used in nuclear, chemical and petrochemical industries. These steels undergo

- i. localised corrosion (flaws) and
- ii. uniform corrosion (thickness reduction).

It is important to detect these two forms of corrosion as they limit the remaining useful life of the components. Based on the corrosion rate, considering the factor of safety, higher thicknesses are preferred for prolonged life of the components. However, periodic monitoring of components using NDE techniques is essential for safe and reliable operation. Ultrasonic techniques are prone to large errors due to in appropriate coupling in inaccessible regions.

Eddy current technique is efficient in detecting surface as well as near sub-surface flaws reliably. Detection of deep sub-surface flaws in austenitic stainless steels by ECT technique is challenging due to loss of sensitivity at lower frequencies [76]. In order to obtain more information about the nature of the flaws embedded within a specimen, multi-frequency techniques are used. The limitations of multi-frequency techniques are complexity in hardware design and over-heating of the excitation coil when higher currents are used for detection of flaws at deeper location [77].

Pulsed eddy current appears potential technique for detection of subsurface as well as surface flaws and thickness reduction, because of the availability of a variety of frequency components in the excitation pulse. Researchers have reported design and development of PEC instruments and probes for detection of surface and near surface flaws. A few commercial PEC systems such as RTD-Incotest, PULSEC, EDDY PULSE and TRECSCAN are available for specific applications. However, details related to development of these instruments and optimisation of probe configurations are not available in the open literature [76,77]. However, detection of deep subsurface flaws in SS components by PEC technique is challenging. This is due to *skin-effect* i.e. the induced eddy currents attenuate exponentially and this limits the detection sensitivity to

within 5.0 mm below the surface. Therefore, it is worthy to focus research towards enhancing the detection sensitivity of deep subsurface flaws.

By designing a sensitive PEC instrument, probe and signal processing techniques, the detection sensitivity of PEC testing can be improved. From the literature, it is inferred that pickup signal amplitudes from flaws is feeble and hence, for enhancing these signals, development of a higher current driving source and a sensitive receiver units is attractive. There is a benefit if higher currents are used for driving the excitation coil which will also enhance the strength of secondary fields at deeper locations. Further, pulse characteristics such as rise time, pulse width and pulse repetition frequency (PRF) are to be systematically optimised depending upon the material properties and thickness, to detect flaws located at deeper locations.

From the literature, it is observed that the use of a send-receive type probe configurations with a field detection sensor as pickup is attractive for achieving better detection sensitivity. However, the existing literature does not adequately address the design of PEC probe configuration and probe dimensions for detection of deep subsurface flaws in thick metallic components, especially in thick stainless steels. Hence, focussing research on optimisation of PEC probe configuration and its dimensions for detection of deep subsurface flaws in thick components is expected to open new avenues for NDE of thick components, especially where ultrasonic technique cannot be applied.

From the literature, it is observed that noise affects the PEC signals leading to inaccuracies in the detection of flaws. It is interesting to note that the traditional time-domain parameters viz.  $V_p$ ,  $T_p$  can be used to determine the size and location of the flaws without signal processing. In this regard, development of time-domain techniques and identification of novel PEC signal

parameters can be explored for detection of flaws due to localised corrosion despite the presence of noise.

The rate of change of the rising edge of the excitation pulse is important as it determines the frequency components useful for detection of flaws. Hence, there is a clear benefit if research is focused on studying the effect of excitation rise time on detection of subsurface flaws due to localised corrosion in thick components.

Accurate estimation of thickness reduction in components is desired in the presence disturbing variables such as lift-off. Several techniques proposed in the literature such as lift-off intersection point, use of specialized probes and signal processing techniques are applied with a limited success. Thus, research on development of new techniques will enhance the capability of the PEC technique for practical non-contact test situations that involve higher lift-off.

## **1.6 Objective of the research**

The objective of this thesis is to develop a PEC system for detection of deep subsurface flaws due to localised corrosion and thickness reduction due to uniform corrosion in thick austenitic stainless steel components. Based on the inputs gained from the literature and the motivation, the following objectives are set:

- 1) To develop a pulsed eddy current instrument that can deliver higher excitation currents and variable pulse parameters for experimentation.

- 2) To design an optimal PEC probe configuration and determine its dimensions through finite element modeling for detection of deep subsurface flaws in 8.0 mm thick AISI 304L austenitic stainless steel components.
- 3) To develop techniques for detection of flaws due to localised corrosion in the presence of noise and for estimation of thickness reduction due to uniform corrosion despite lift-off variations.

The thesis mainly focuses on detection of subsurface flaws in the presence of noise and thickness reduction in an 8.0 mm thick SS components due to different types of corrosion under varying lift-off conditions. Highlights and novelty of the thesis are discussed below:

For detection of flaws at deeper location in thick components with increased sensitivity, a high current pulse source is required. The flaw detection sensitivity also depends on the pulse characteristics i.e. pulse width, rise time and pulse repetition rate and sensitivity of the receiver unit which includes amplification and filtering unit of the PEC instrument. In view of this, the thesis focuses on development of a PEC instrument which can meet the above requirements.

A high throughput PEC probe is required for ensuring deeper penetration of eddy currents into the test component. In view of this, the thesis focuses on optimisation of probe configuration and its dimensions through FEM software.

Noise limits the subsurface flaw detection sensitivity of the PEC technique. In this regard, development of time-domain technique and identification of novel PEC signal parameters can be explored for detection of flaws due to localised corrosion despite the presence of noise.

Lift-off affects the accurate estimation of thickness reduction of the components. In view of this, research on development of new techniques will enhance the capability of the PEC technique for practical non-contact test situations that involve higher lift-off.

## 1.7 Organisation of the thesis

The thesis is structured into four major working chapters addressing the studies carried out, towards developing a PEC system. It includes development of an instrument, design of an optimal probe configuration and selection of PEC signal parameters for detection of flaws due to localised corrosion and thickness reduction due to uniform corrosion:

**Chapter-2** explains the detailed design and development of a pulsed eddy current instrument for detection of subsurface flaws in thick components. It describes the detail design of excitation unit with variable pulse parameters, receiver unit with amplification and filters. It then discusses the performance evaluation of the developed instrument.

**Chapter-3** discusses the optimal design of PEC probe configuration and its dimensions using finite element (FE) modeling. It describes the three possible probe configurations considered for selection of an optimal one for detection of subsurface flaws in 8.0 mm thick SS components. This chapter also discusses the FE model studies carried out to identify the sensitive location of the pickup sensor in the exciter coil of the PEC probe.

**Chapter-4** discusses the influence of noise on PEC signal parameters for detection of deep subsurface flaws. Further, it describes a new technique proposed for enhanced detection of flaws due to localised corrosion in the presence of noise. It also discusses the effect of excitation rise

time and its optimisation for detection and classification of flaws (surface and subsurface) in an 8.0 mm thick SS plate.

**Chapter-5** discusses the technique based on wavelet transform for estimation of thickness reduction due to uniform corrosion despite lift-off variations where time-domain PEC parameters fail to detect.

**Chapter-6** summarizes the major conclusions drawn from the research work towards design and development of a PEC system for detection and classification of flaws due localised as well as uniform corrosion. This chapter also explains the scope for possible improvement of the PEC instrument, probe and data processing techniques.

## Development of PEC instrument

### 2.1 Preamble

The scope of this chapter is to present the design and development of a pulsed eddy current instrument for detection of flaws due to localised corrosion and uniform corrosion in thick metallic components. After a detailed discussion on the design considerations, this chapter also presents the performance evaluation of the PEC instrument through detection of subsurface flaws machined in an 8.0 mm thick stainless steel component.

### 2.2 PEC instrument

There are three modules that are to be considered while designing a PEC instrument viz. excitation unit, receiver unit and signal processing unit. The schematic of the PEC instrument is shown in Figure 2.1 and the details of the each module are explained in this section.

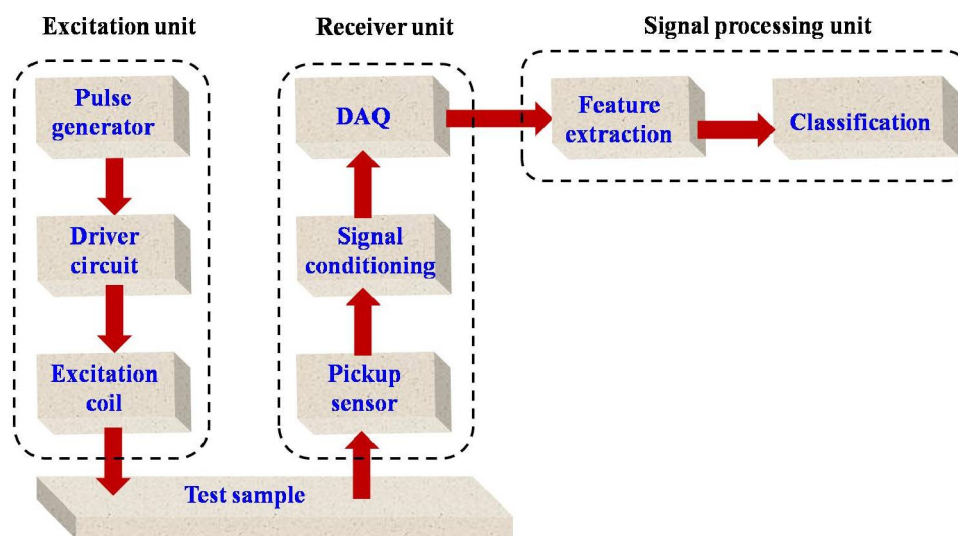


Figure 2.1. Schematic of the PEC instrument.

The PEC instrument works as follows; the pulse generator in the excitation unit produces a unipolar rectangular waveform having variable frequency and duty cycle. The waveform is fed to the driver circuit to pass higher current through the excitation coil for generating high intensity primary magnetic field. The pickup sensor detects the resultant magnetic field, which is the vector sum of the primary magnetic field and the opposing secondary magnetic field. The sensed voltage as a function of time i.e. the PEC signal is fed to the signal conditioning unit having a pre-amplifier with a variable gain. This circuit amplifies the PEC signal so that the dynamic range of the signal is improved. The analog-to-digital converter (ADC) card digitizes the PEC signal. The digitized signal is stored and processed in the personal computer to extract parameter for flaw detection and sizing.

### 2.2.1 Excitation unit

The essential aspects to be considered for designing the excitation unit of the PEC instrument are the peak current value and the transient characteristics of the rising edge of the current pulse. Higher the peak current, the higher the generated primary magnetic field strength and hence, the more the induced eddy currents in the test object. Figure 2.2 shows the schematic of the excitation unit. The magnetic field generated is proportional to the excitation coil inductance ( $L$ ), number of turns ( $N$ ) and current ( $I$ ) flowing through it. For an excitation coil, the  $L$  and  $N$  values are constant. Hence, in order to increase the primary magnetic field strength, excitation current has to be increased.

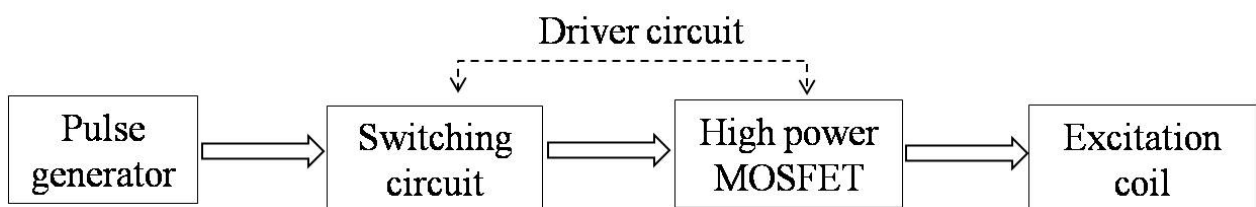


Figure 2.2. Schematic of excitation unit.

### ***2.2.1.1 Design considerations of the excitation unit***

The excitation unit should be capable of producing high current pulses to drive the excitation coil. However, too high current can cause overheating of the coil. This needs to be considered while choosing the excitation current range:

- i.* pulse amplitude,
- ii.* duty cycles,
- iii.* pulse repetition frequency (PRF) and
- iv.* pulse rise and fall times.

The other important parameters to be taken into consideration during the design of the excitation unit included the following. This is due to the fact that magnetic field produced by the probe is proportional to the time derivative of the coil currents. To maximize the magnetic field produced by the coil, it is desirable to change the coil current rapidly. In practice, the rate at which the current through a coil is limited by the rise time [57].

Higher pulse amplitude (current) is also desired for achieving deeper penetration of eddy currents with higher intensity and hence, for detection of flaws located at deeper location. For this purpose, a pulse source which can deliver current in the range of 0.2 A- 7.0 A is desired. Duty cycles of less than 50% are usually required for measuring the coil response for a given excitation current. Similarly, use of lower pulse duration results in better measured response and this also reduces heating of the excitation coil.

Selection of appropriate PRF in the range of 50 Hz to 1 kHz is also essential for meaningful and repeatable measurements. The rise time and time fall time of the pulse mainly depend on the time

constant of the coil and one does not have any control over them. Hence, a suitable circuit design is required for changing the rise time and fall time characteristics of the pulse independent of the coil dimensions so that a single coil can be used for detection of both surface and subsurface flaws. In addition to the above requirement, it is also essential to protect the excitation unit against any surge current or back EMF from the PEC probe during OFF time of the excitation pulses.

### ***2.2.1.2 Development of excitation unit circuit***

An excitation unit has been developed based on metal oxide semiconductor field effect transistor (MOSFET) switching logic to meet the design requirements. MOSFET the following advantages over the traditional bipolar junction transistors:

- ✓ High input impedance ( $G\Omega$ ),
- ✓ Low output impedance ( $m\Omega$ ),
- ✓ Fast switching speed (ns),
- ✓ Less noisy,
- ✓ Doesn't require input current and delivers higher currents to loads,
- ✓ Less power consumption (mW) and
- ✓ Doesn't have thermal runaway issues

A high power MOSFET has been chosen to deliver higher excitation current. The MOSFET is operated as an ON/OFF switch. When it is ON state, due to low drain to source resistance ( $R_{ds}$ ), a major proportion of the supply voltage drops across the coil and hence, increases the current based on supply voltage. When it is in OFF state, there is no closed path and current flows through the diode and coil. The circuit has been designed in MULTISIM software to optimise the circuit components and to verify the functionality of the excitation unit. The internal circuit diagram of the excitation unit is shown in Figure 2.3.

It consists of three modules, namely:

1. Pulse source
2. Switching circuit and
3. MOSFET with coil assembly

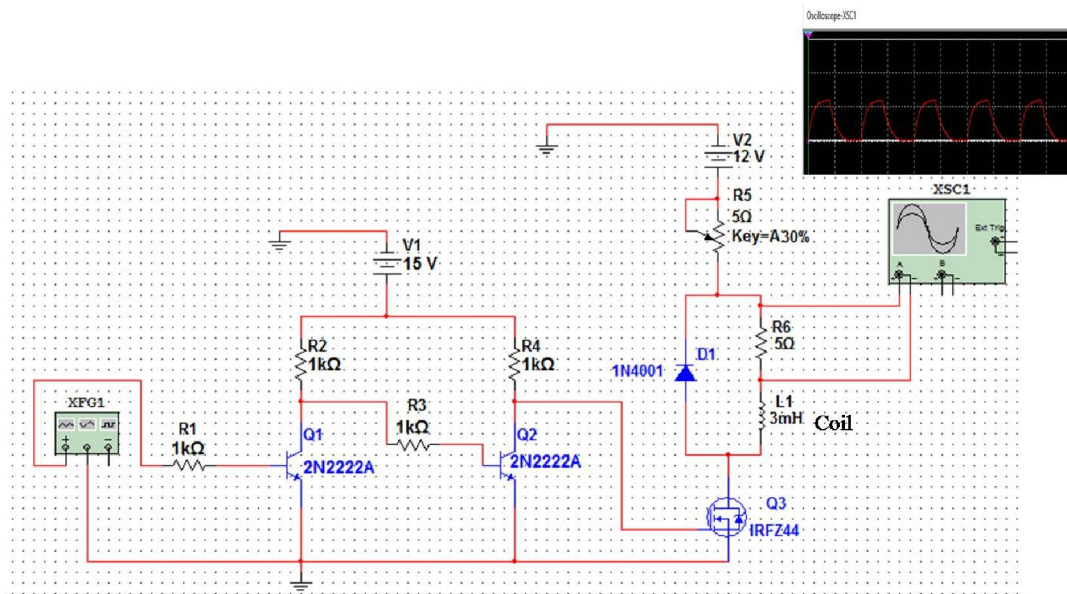


Figure 2.3. Internal circuit design of an excitation unit using MULTISIM software.

The pulse source produces a voltage pulse of 5V amplitude with a specified duty cycle and PRF. A programmable function generator is used for this purpose. The duty cycle and PRF of the pulse source can be programmed in the range of 20-70% and 10-1000 Hz respectively. The MOSFET is operated in transconductance mode i.e. it converts the input voltage pulses generated by the pulse source into an output current pulses which are used to drive the excitation coil. A switching circuit uses the voltage pulses from pulse source to toggle the MOSFET between ON and OFF states. General purpose transistors (Q1, Q2) and associated resistive networks form the switching circuit. The maximum current driving capability of the Q1 is only 500 mA. In order to meet the design requirement current rating of 0.2 to 7.0 A, a MOSFET (Q3) is used which can be switched ON and OFF by Q1& Q2 based on the input excitation pulse. The peak current flowing through

the excitation coil is measured by observing voltage drop across a known resistance (R6) which is connected in series as shown in Figure 2.3

To vary the current flowing through the excitation coil, the value of the potentiometer (R5) is varied. Typically two excitation currents of 0.4 A and 0.8 A which are measured across the R6 as shown in Figure 2.4. Therefore, by changing the resistance value of R5, the current flowing through the circuit is varied.

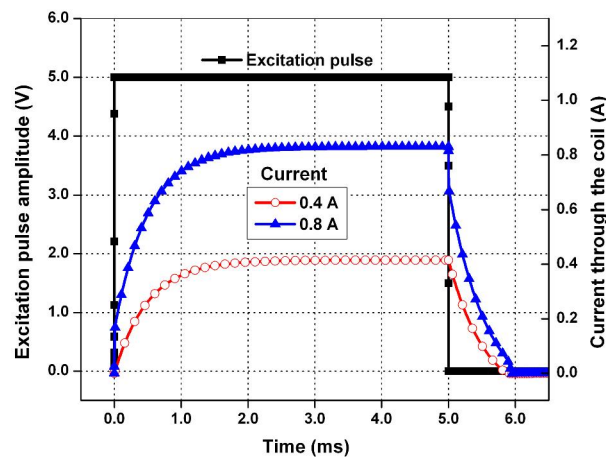


Figure 2.4. Simulation results for current driving capability of the excitation unit.

A "freewheeling diode" (D1) is placed parallel to the excitation coil to protect the MOSFET being damaged by the reverse current induced in the excitation coil. The diode does not conduct during the rise time ( $t_r$ ) and conducts during the fall time ( $t_f$ ) of the ON pulse. Since, the diode having ON resistance which is in series with the R6, the rise time of the excitation pulse is greater than the fall time as shown in Figure 2.5 that is obtained by simulation. This is due to fact that an increase in resistance of the circuit decreases the time constant ( $\tau$ ) and hence, the rise time of the response pulse.

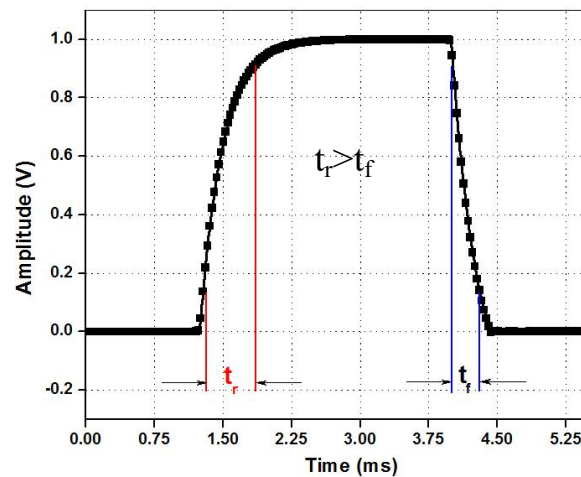


Figure 2.5. Simulation results for rise and fall time of the excitation current pulse.

### 2.2.2 Receiver unit

The receiver unit is required for PEC signal amplification, filtering and data acquisition. Typical pickup sensors used in PEC applications are coils, Hall, GMR, SQUID, AMR and TMR. Without the receiver unit, the pickup sensor amplitude is in the order of mV which gives rise to a non-optimum use of data acquisition. The schematic of the receiver unit is shown in Figure 2.6. The receiver unit consists of a pre-amplifier with variable gain, an off-set adjustment and a low-pass filtering circuit.

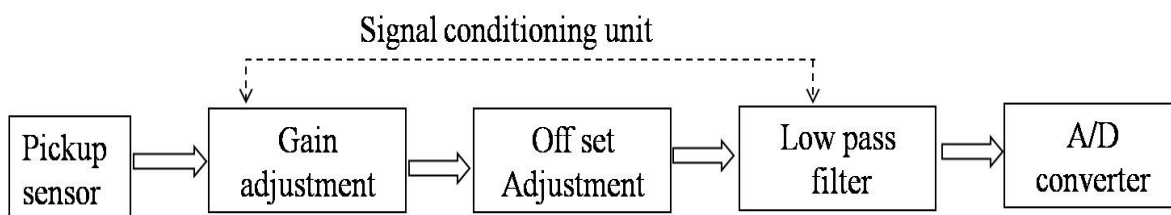


Figure 2.6. Schematic of receiver unit.

### ***2.2.2.1 Design considerations of the receiver unit***

The primary function of the receiver unit is to acquire the signal from the pickup sensor without degrading the SNR. The important parameters to be considered while designing the pre-amplifier circuit include:

- i. amplification gain,
- ii. common-mode rejection ratio and
- iii. frequency bandwidth

Typical sensor output signal amplitudes are in mV and the magnetic field intensity may vary significantly depending on the magnetic permeability, conductivity and excitation coil dimension. A non-ferromagnetic material with low magnetic permeability such as austenitic stainless steel produces low resultant voltage as compared to ferromagnetic materials that give out high voltage for same and constant parameters. Therefore, gain adjustment is required to amplify the output voltage levels appropriately for optimal use of the ADC card.

A pre-amplification stage with a minimum of 1000 x amplification is desired for amplification of low amplitude PEC signals likely from subsurface flaws. The pickup sensor output signals are affected by external noise; hence a filter circuit is to be included to reduce noise. Sampling frequency and number of bits are important parameters to be considered while selecting the ADC card. It is also essential to use a high resolution (higher number of bits) ADC to improve the dynamic range. The useful frequency components in PEC signals are around 100kHz. Hence, the sampling frequency should be at least 10 times higher to satisfy the Nyquist criteria.

### 2.2.2.2 Development of the receiver unit

The pre-amplifier circuit is implemented with an instrumentation amplifier (INA-129) which is having a user selectable gain up to 60 dB, 1 MHz bandwidth and high common-mode rejection of 120 dB. The INA-129 is a low power and general purpose amplifier that offers excellent gain. The internal circuit diagram of the INA-129 is shown in Figure 2.7 in which  $A_1$  and  $A_2$  form a high input impedance buffer amplifiers and  $A_3$  acts as a subtractor.

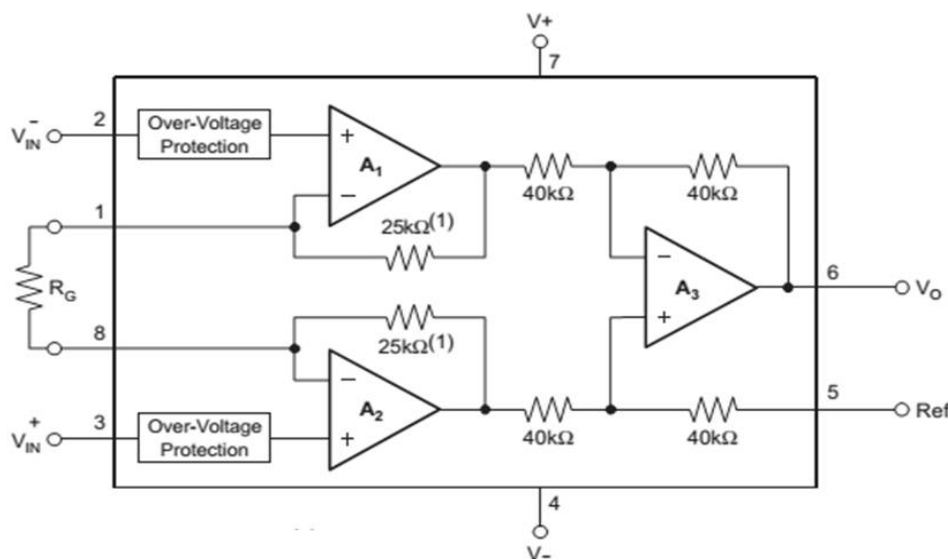


Figure 2.7. Internal circuit diagram of INA-129.

The gain of INA-129 can be varied with a potentiometer ( $R_G$ ) from 1 to 1,000 using:

$$G = 1 + \frac{49.4 \text{ K}\Omega}{R_G} \quad 2.1$$

where  $G$  is the gain of the amplifier and  $R_G$  is the external variable resistor. The circuit provides high input impedance so that the impedance of the sources will have a minimal effect on the common-mode rejection. The frequency response of the INA-129 is shown in Figure 2.8. As can be seen, the gain is different for different frequency ranges. It provides a constant gain ( $G=100$ ) for a wide bandwidth nearly 200 kHz and it is used to amplify PEC signals.

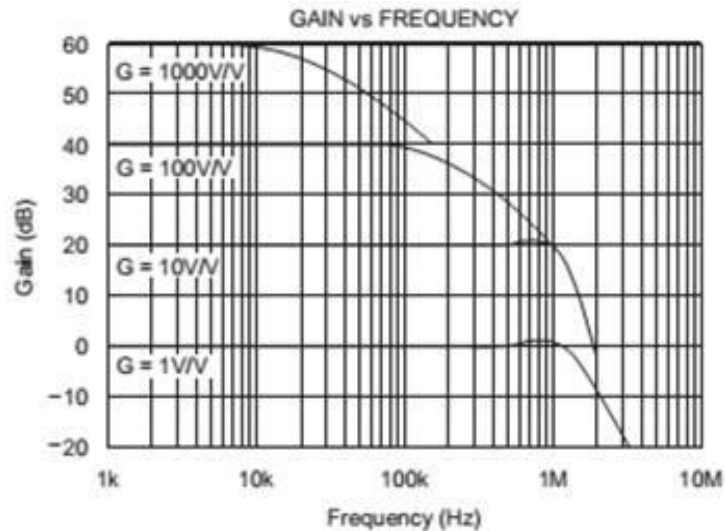


Figure 2.8. Frequency response of an instrumentation amplifier.

As no two magnetic sensors have same operating point, a DC shift always likely to be present in the sensor output. To compensate this, an off-set adjustment circuit has been designed using an operational amplifier with associated resistive components. The circuit diagram of the off-set adjustment circuit is shown in Figure 2.9, where the maximum off-set can be varied to  $\pm V_{cc}$ .

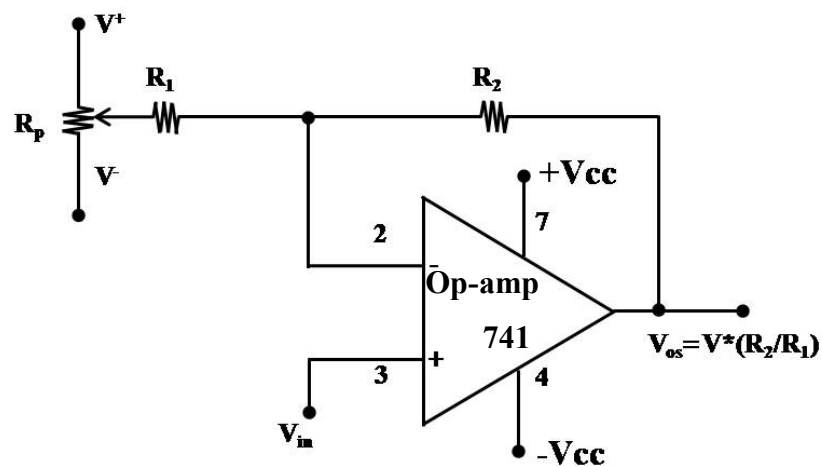


Figure 2.9. Off-set adjustment circuit.

A low-pass filter (LPF) is used to filter out the high-frequency noise signals due to electromagnetic interference. A second order Butter Worth filter is chosen, as it has fewer ripples in the pass band and fast roll-off in the stop band. A well-known Sallen key filter is selected and implemented with a general purpose op-amp 741. The circuit diagram of a LPF is shown in Figure 2.10.

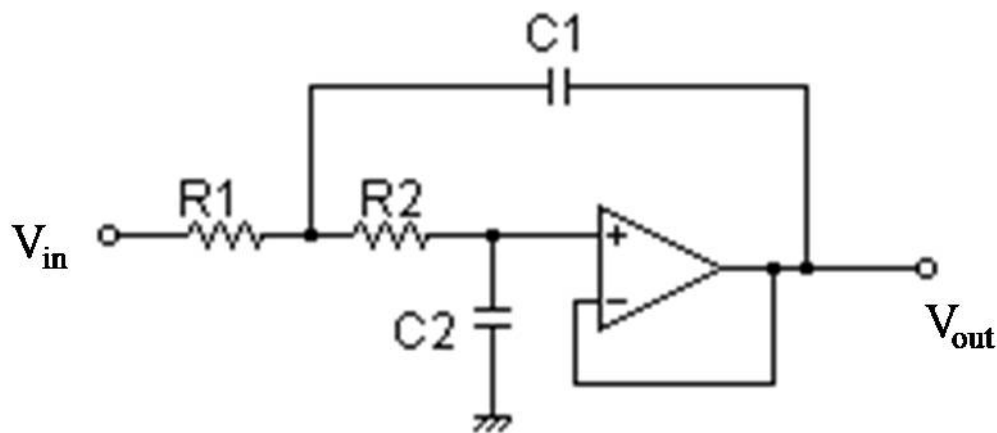


Figure 2.10. The schematic of the 2<sup>nd</sup> order low-pass filter.

The cut-off frequency of the LPF is varied by changing the R and C values. If  $C_1$  and  $C_2$  are set to C and  $R_1$  and  $R_2$  are set to R, then the cut-off frequency of the filter becomes

$$f = \frac{1}{2\pi RC} \quad 2.2$$

The accuracy of the PEC measurements depends on the bit resolution and sampling frequency of the ADC card. The receiver unit has a high dynamic range (24-bit) ADC card to acquire signals at a sampling rate of 1.25 MSa/s which gives higher voltage precision of 6  $\mu$ V in  $\pm$  3V peak-to-peak value. The internal circuit diagram of the excitation and receiver unit is shown in Figure 2.11.

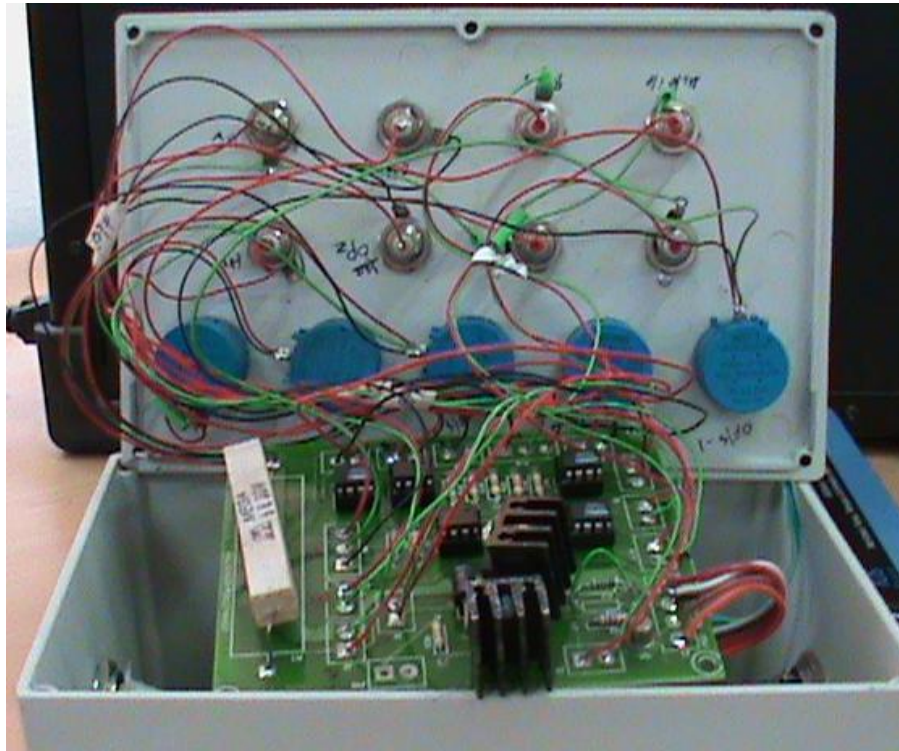


Figure 2.11. Internal circuit diagram of the excitation and receiver unit.

### 2.2.3 Signal processing unit

Detection of flaws located at deeper location is challenging in pulsed eddy current technique. This is due to the signal amplitude fluctuations in the order of  $100^s$  of  $\mu\text{V}$  due to noise and lift-off variations. Higher background noise can mask the feeble signals from deep subsurface flaws. Noise is caused by various factors and fall into different categories. Noise that spreads across the spectrum is detected in the acquired signals. Therefore, noise reduction is an important for improving the flaw detection sensitivity of the PEC system. Some of the commonly used techniques for noise reduction include: signal averaging, wavelet filtering and Gaussian filtering. Apart from signal averaging, all the techniques will change both the time and frequency characteristics of the PEC signals.

## 2.3 Performance evaluation of PEC instrument

Photograph of the developed PEC instrument is shown in Figure 2.12. Systematic studies have been carried out to assess the performance of the instrument by varying the pulse characteristics viz. pulse current, pulse width and pulse repetition frequency (PRF). The instrument is tested for detection of surface as well as subsurface flaws due to localised corrosion.

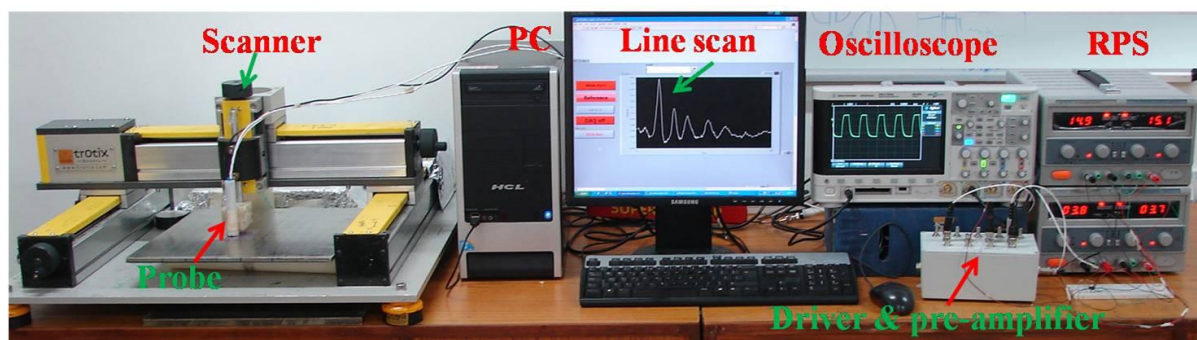


Figure 2.12. Photograph of the developed PEC instrument.

### 2.3.1 Test specimen

The performance of the PEC instrument is evaluated for detection of flaws in AISI type 304L stainless steel plate of size  $360.0 \times 100.0 \times 8.0 \text{ mm}^3$ . EDM notches shown in Figure 2.13 are introduced in the test plate to simulate localised corrosion. Six notches of length 25.0 mm and a width of 2.0 mm are machined at different depths in the range of 1.0 mm to 6.0 mm. For detection of subsurface flaws, the probe is moved from left to right on the top surface. Similarly, for surface flaws the probe is moved on the bottom surface from left to right. An air core send-receive type probe consisting of an excitation coil and a pickup coil is used and the dimensional details are given in Table 2.1.

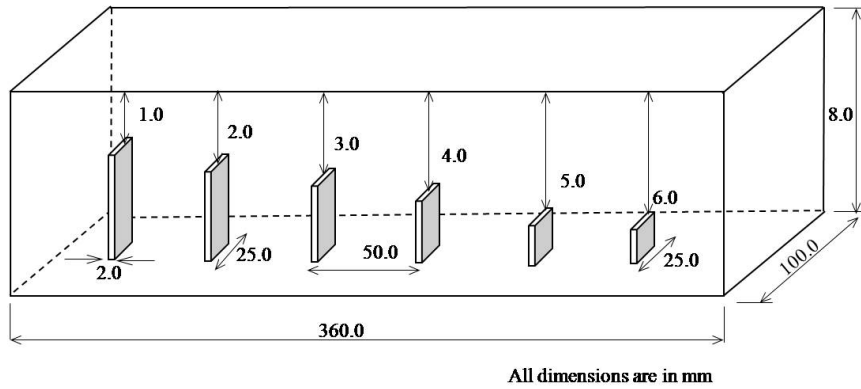


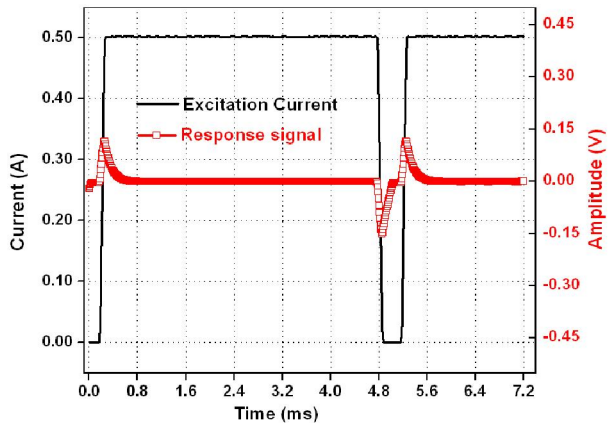
Figure 2.13. Details of stainless steel plate with subsurface EDM notches.

Table 2.1. Details of the air core PEC send-receive type probe used for performance evaluation of the PEC instrument

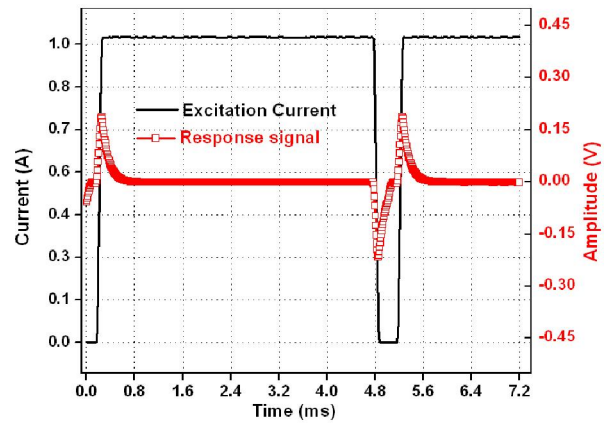
S. No.	Dimensions	Excitation coil	Receiving coil
1.	Inner Diameter (ID)	13.0 mm	2.0 mm
2.	Outer Diameter (OD)	22.0 mm	4.0 mm
3.	Height	26.0 mm	6.0 mm
4.	No. of turns	300	150

### 2.3.2 Pulse characteristics

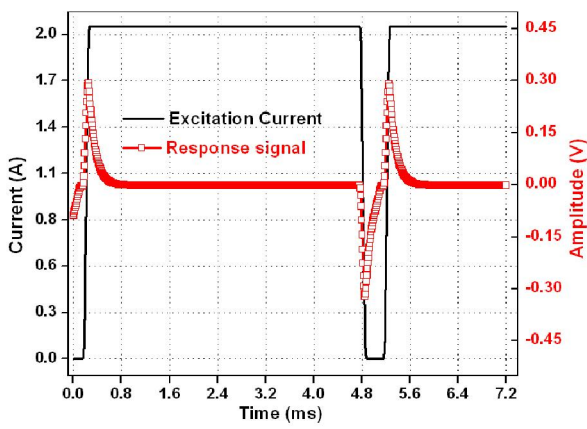
Firstly, the excitation current has been varied to check the current driving capability of the instrument. Typically four different excitation currents viz. 0.5, 1.0, 2.0 and 3.0 A are selected and the response signals obtained from a flaw-free region for these excitation currents are shown in Figure 2.14 (a), (b), (c) and (d) respectively. Peak amplitude ( $V_p$ ) is plotted as shown in Figure 2.14 (e) with respect to current. It is observed that the peak amplitude increases with an increase in excitation current from 0.5 to 3.0 A.



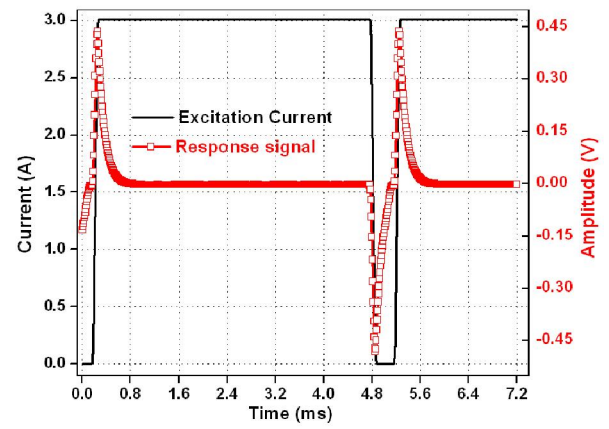
(a)



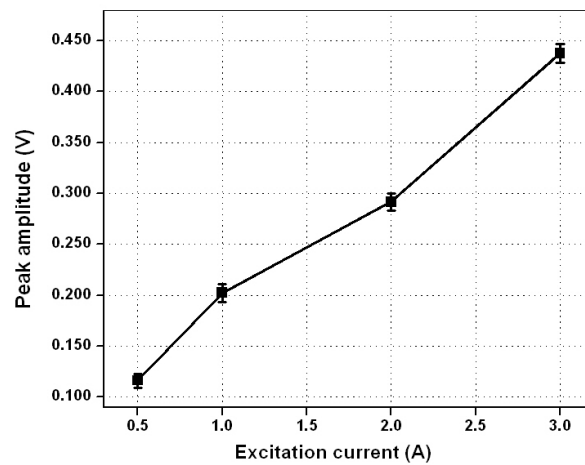
(b)



(c)



(d)



(e)

Figure 2.14. PEC signals for different excitation currents of (a) 0.5 A (b) 1.0 A (c) 2.0 A (d) 3.0 A and (e) peak amplitude with respect to current.

This is due to fact that higher excitation current increases the primary magnetic field strength. Repeated  $V_p$  measurements at different excitation current reveal that the variation in  $V_p$  at a constant current in the range of 0.5 to 3.0 A is  $< 5.0\%$ . Even though the excitation unit can deliver a peak current of 7.0 A, the experiments are carried out up to 3.0 A only to reduce heating losses ( $I^2R$ ) in the excitation coil. Further, to increase current, it may be necessary to use a coil with a lower standard wire gauge to avoid over heating of coil.

The PEC signals obtained from a flaw-free region at different pulse widths viz. 1.0, 2.0 and 4.0 ms while keeping current and pulse repetition frequency constant and the resulting PEC signals are shown in Figure 2.15.

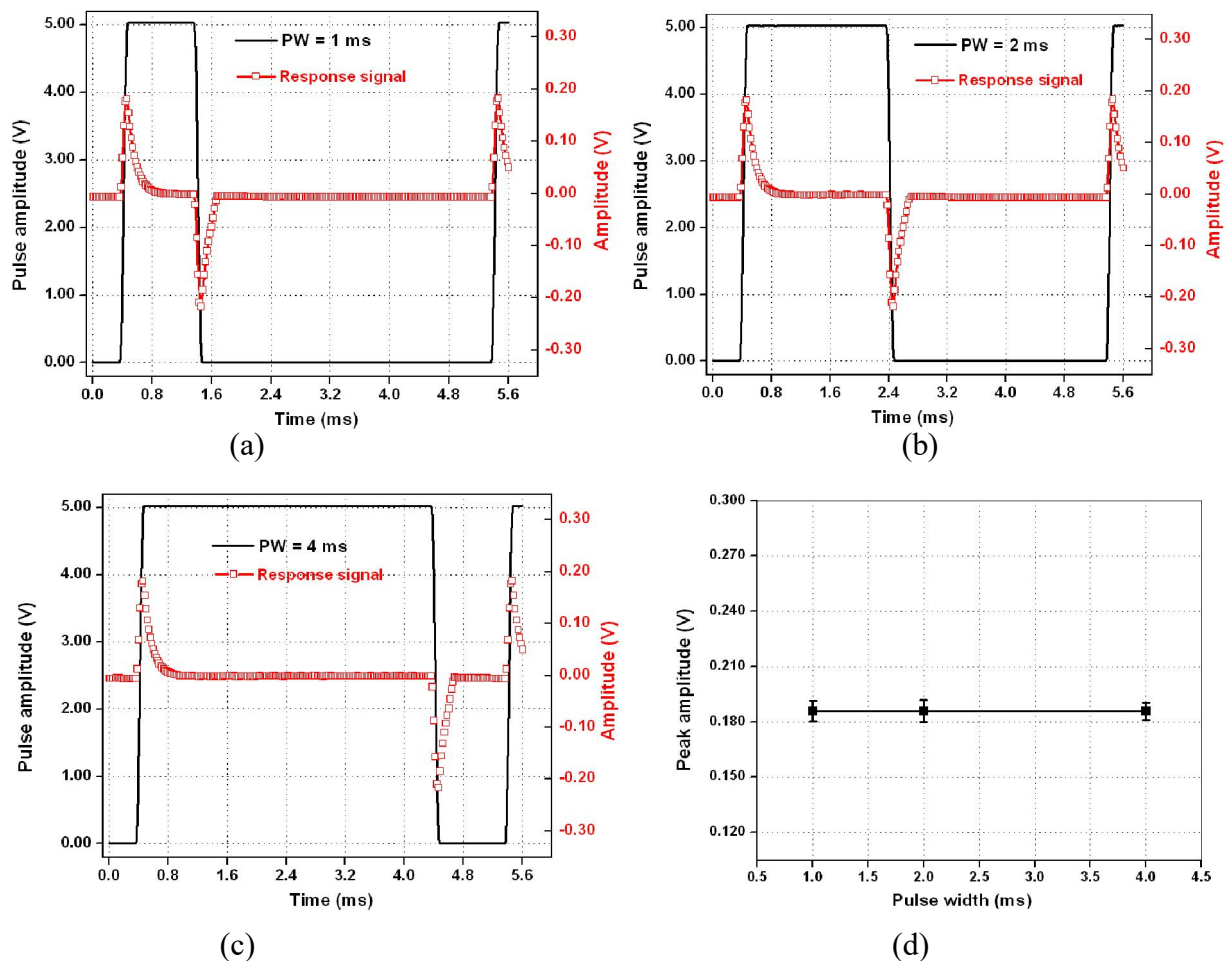


Figure 2.15. PEC signals for different pulse width of (a) 1.0 ms, (b) 2.0 ms, (c) 4.0 ms and (d) peak amplitude for different pulse widths.

As can be seen there is no change in the peak amplitude of the PEC signals with increasing pulse width. This is due to the fact that eddy currents perturb only during the rising and falling time of the pulse. Therefore, the effect of the pulse width is negligible on the peak amplitude of PEC signals.

Further, the pulse repetition frequency of the excitation source is varied as 200, 300 and 400 Hz and the response signals are shown in the Figure 2.16 (a), (b) and (c) respectively. Figure 2.16 (d) shows the variation of  $V_p$  with respect to PRF.

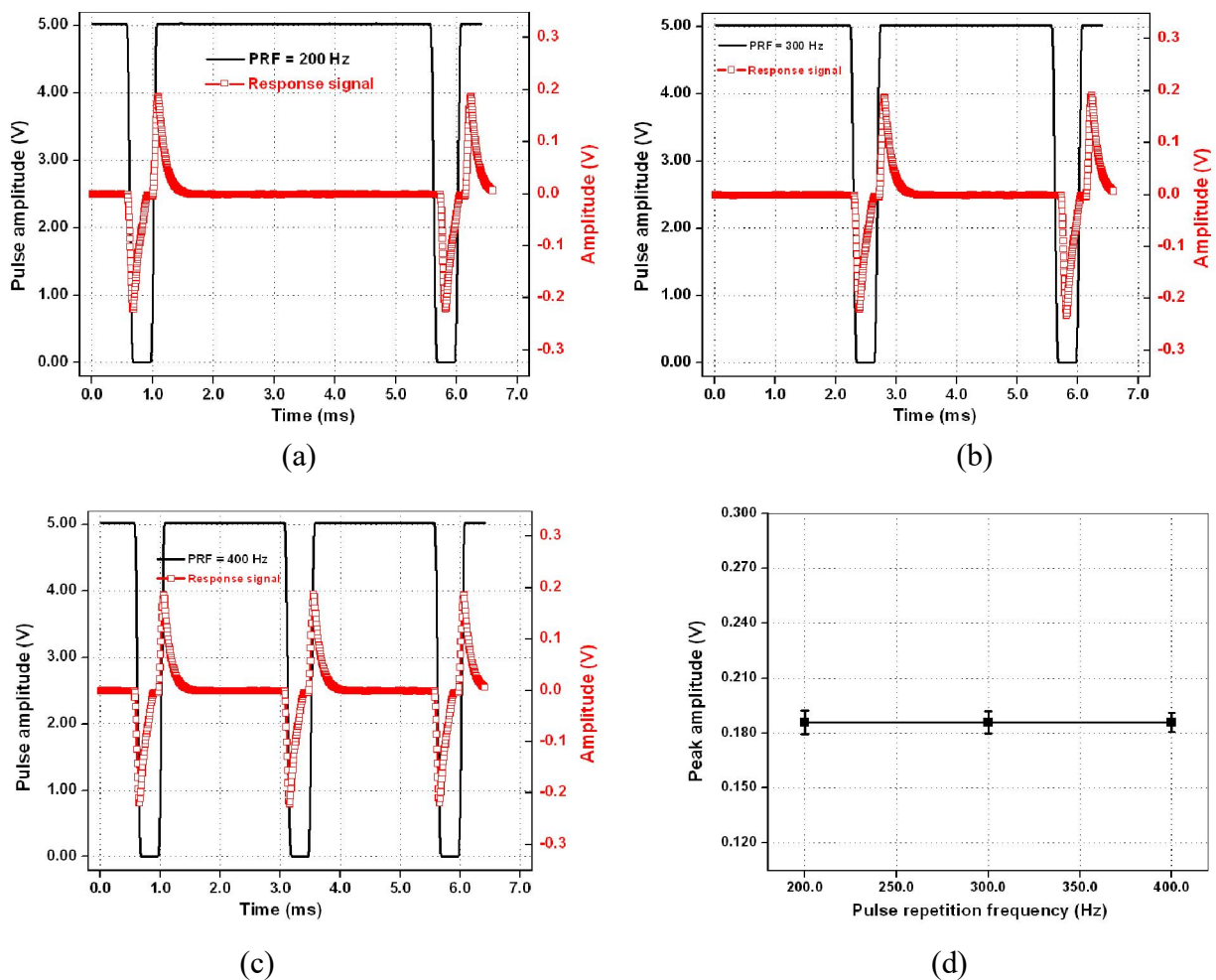


Figure 2.16. PEC signals for different pulse repetition frequencies of (a) 200 Hz (b) 300 Hz (c) 400 Hz and (d) peak amplitude variation with PRF.

From Figure 2.16 (d), it is evident that the peak amplitude doesn't change with PRF. Hence, the effect of PRF on the PEC signals is negligible similar to the pulse width (refer Figure 2.15 (d)).

The amplification capability of the receiver unit has been studied. The PEC response signal obtained from a flaw-free region which is having peak amplitude in the order of 0.177V is shown in Figure 2.17 (a) and that of a flaw at 1.0 mm below the surface is 0.182 V as shown in Figure 2.17 (b). For optimal utilization of the ADC card, typically, the signal has been amplified with a gain value of 10 and 31. As can be seen in Figure 2.17, it has improved the signal strength by 20dB and 30 dB. Moreover, the receiver unit can amplify the PEC signals up to 60 dB. It shows the potential capability of the receiver unit to amplify weak signals.

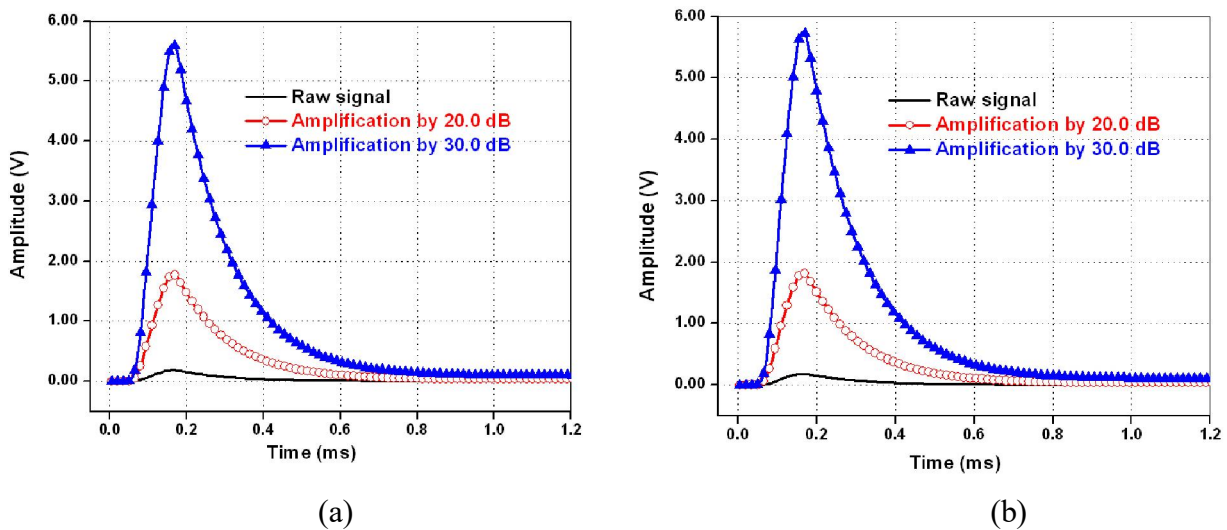


Figure 2.17. PEC signals amplified by 20 dB and 30 dB for (a) flaw-free signal and (b) flaw signal.

### 2.3.3 Detection of flaws due to localised corrosion

For detection of subsurface flaws due to localised corrosion, measurements have been carried out by placing the PEC probe centrally over the flaws. Figure 2.18 (a) shows the measured PEC signals from the subsurface flaws. Figure 2.18(b) shows the variation of peak amplitude with flaw location below the surface. From the results, it is observed that the peak amplitude decreases up to 3.0 mm below the surface, beyond which it saturates. This is essentially due to the exponential decay of the eddy currents and their reduced interaction with flaws located far below the surface. This saturation behavior is due to the fact that air core excitation coil has more magnetic flux leakage that weakens the electromagnetic coupling between the primary magnetic field and the test plate. And also the pickup coils are less sensitive to the slowly varying magnetic fields that come from flaws located beyond 3.0 mm below the surface.

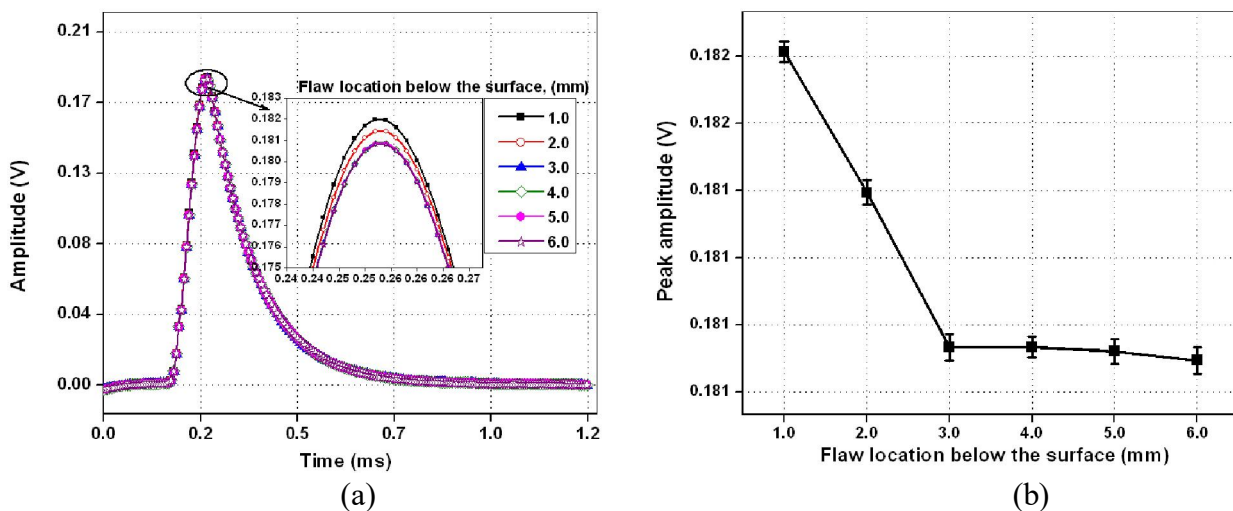


Figure 2.18. PEC response for (a) subsurface flaws and (b) Peak amplitude vs. flaw location below the surface.

Hence, to improve the flaw detection capability of the PEC instrument, one needs to optimise the excitation coil configuration. Next chapter discusses the work carried out to design and develop

an optimal PEC probe configuration for detection of flaws located beyond 3.0 mm below the surface. The studies reported in Section 2.3 clearly demonstrate the capability of the developed PEC instrument for detection of subsurface flaws in metallic materials.

## 2.4 Summary

A pulsed eddy current instrument has been designed and developed for detection of subsurface flaws thick stainless steel components. Systematic studies have been carried out for testing the performance of the instrument and the following are the main observations:

- ✓ The developed PEC instrument, designed based on MOSFET switching logic, has delivered a variable current in the range from 0.2 A to 7.0 A. It has shown the capability to vary the pulse width (50  $\mu$ s to 50.0 ms) and pulse repetitive frequencies (20 to 1000 Hz). The receiver unit has shown capability to amplify the PEC signals which is necessary to detect weak signals from deep subsurface flaws.
- ✓ Studies using the developed PEC instrument revealed that pulse width and PRF do not change the peak amplitude of the PEC signals.
- ✓ The performance of the PEC instrument has been demonstrated by detecting subsurface flaws located from in an 8.0 mm thick SS component with an un-optimal air core send-receive type coil probe.

## Development of PEC probe

---

### 3.1 Preamble

This chapter presents details of the design and development an optimal pulsed eddy current probe for detection of deep subsurface flaws due to localised corrosion using finite element modeling (FEM). It also discusses the optimisation of probe configuration among air core, ferrite core and ferrite core with outer shielding probes and the dimensions of the chosen probe configuration. It explains how the performance of these three probe configurations are compared using the two model predicted parameters viz. induced eddy current density ( $J_{\phi}$ ) and peak amplitude ( $V_p$ ). It discusses fabrication of the optimal probe and its capability to detect localised flaws.

### 3.2 Finite element (FE) modeling

For optimisation eddy current probes, model based studies are always preferred to practical trial and error approach which is expensive and time consuming. Traditionally, for modelling, analytical and numerical based approaches are used. Analytical modelling is ideal for solving the theoretical problems related to simple geometries. On the contrary, numerical modelling is more flexible and has the capability to model realistic problems in complex geometries and material nonlinearities [78]. Among various numerical modelling methods, FEM is widely used for electromagnetic NDE applications. FEM was first proposed in the 1940[79] and its use began in the 1960 for structural and continuum mechanics and later found a wide variety of applications in electromagnetic field problems[80].

FE modelling has been exploited well by the NDE research community [26]. It provides fast solution to specific electromagnetic problems and is capable of dealing with problems concerning multiphysics requirements e.g. electromagnetic issues coupling with heat diffusion [81]. Today, the FE modelling has become a powerful tool for designing eddy current probes for a variety of test situations [40,82].

In a FE model, the governing partial differential equation (refer, Section 1.31) is solved in the problem domain which is discretised into a number of sub-domains, called mesh elements. There are no restrictions (apart from computing power) on the size and number of the finite elements. The interconnecting points of elements are called nodes. The exact variation of the unknown function e.g. magnetic vector potential ( $A$ ) in electromagnetic problems is approximated by interpolation functions with unknown coefficients at each nodes associated with the elements. In other words, the original boundary value problem with infinite degrees of freedom is transformed into a problem with finite degrees of freedom. Then, a system of algebraic equations is obtained by applying the Ritz variational or Galerkin procedure and the magnetic vector potential is calculated by solving the system of equations. Finally, the desired parameters such as induced eddy current density, magnetic flux density, induced voltage and impedance change are computed from the vector potential at the nodes situated within the region of interest.

### **3.3 FE model for PEC testing**

The PEC problem can be solved by two methods. The first method is the Fourier transform (FT) method, in which time harmonic responses of significant harmonic components are computed using FEM steady state analysis. The contributions of the individual harmonic components are summed up to get the final response. But FT method suffers from the difficulty in the proper discretisation of the problem domain at various frequencies, as the *skin-depth* varies with

frequency. The second method is transient time stepping (TTS) method. In this method, transient pulse is divided into number of time steps and the response is calculated for each time step. This method is reported as the better approach for modelling of the PEC problems [26]. For FE model based optimisation PEC probe configuration, COMSOL multi-physics version 4.3 software is used. This is validated model for eddy current test applications. As the considered PEC probes are with cylindrical symmetry and 2D axisymmetry model is sufficient to give accurate solution quickly, studies are carried out in 2 dimensions.

### 3.3.1 Construction of model geometry

The modelled geometry consists of an excitation coil, a pickup sensor, a stainless steel plate with flaw in an air box shown in Figure 3.1. Table 3.1 gives the details of sub-domain parameters values i.e.  $\mu$  and  $\sigma$  used in the model. The conductivity of air sub-domain is set to a small non-zero value (10) to avoid computational errors that may be encountered during problem solving. The model is truncated into a finite region by defining an external air boundary which limits the solutions to be calculated inside the assigned region. Dirichlet boundary condition is applied at the line of symmetry and at the outer boundary.

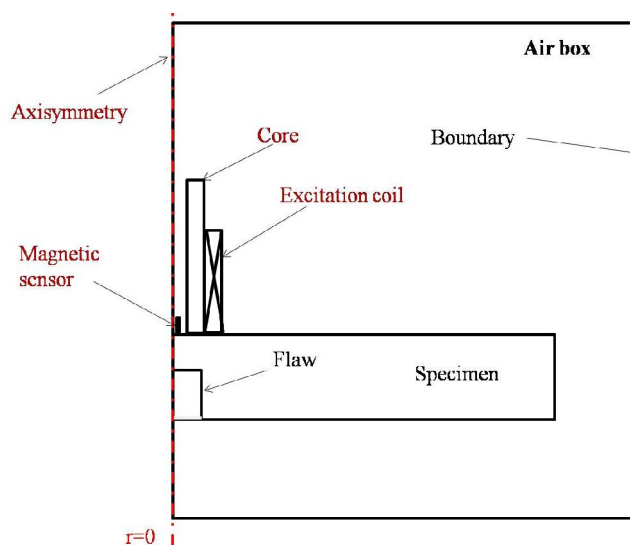


Figure 3.1: PEC model geometry in 2D.

Table 3.1.Details of the sub-domain parameters used in the FE modelling

S. No.	Material	Conductivity ( $\sigma$ ), S/m	Relative magnetic permeability ( $\mu_r$ )
1.	Air	10	1
2.	Copper	$5.88 \times 10^7$	1
3.	Ferrite	100	1500
4.	Stainless steel	$1.38 \times 10^6$	1

### 3.3.2 Meshing

In the model geometry, the region of interest is divided into a mesh of triangular-shaped elements. Higher accuracy is obtained by resorting to a fine mesh in the coil and flaw regions as they are the important regions to visualise the distribution of fields. In the modelled geometry, 41,676 number of mesh elements are generated. More than 50 mesh layers are chosen in the thickness region. This enhances the mesh quality around the flaw and the surrounding region where the direction and the magnitude of the magnetic field change rapidly. Figure 3.2 shows typical meshing employed. Mesh sensitivity analysis has been carried out.

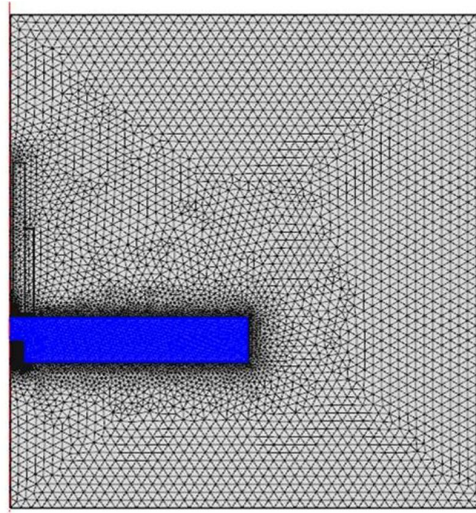


Figure 3.2: PEC geometry with mesh.

### 3.3.3 Solving the model

The problem is solved using the time stepping method. The frequency components in the pulse and accuracy of the solution depend on the step size. The time dependent solver is assigned with direct (UMFPACK) linear solver in the transient analysis mode. The solution is calculated for every time step. The time taken by the solver in order to solve the modelled geometry having mesh elements of 41, 679 and 83,696 degrees of freedom is 458 s in a PC with i5 processor and 8 GB RAM. Further, post processing is performed to calculate the magnetic flux density and induced eddy current density from the model predicted nodal vector potential data. Contour plots are generated for a few selected cases to visualize the EM fields and eddy currents and the interaction with flaws. The response signals are predicted by computing the induced voltage in the pickup coil. In the case of GMR sensor, the magnetic field value at the sensor location is computed and integrated to predict the PEC signals.

### 3.4 Optimisation PEC probe

The detection sensitivity of subsurface flaws due to localised corrosion depends mainly on

- i. The position of the pickup sensor in the probe to measure the resultant normal component of the magnetic field,
- ii. Type of excitation probe configuration and
- iii. Coil and sensor dimensions.

This section explains the optimum location of the pickup sensor and PEC probe configuration for detection of subsurface flaws in an 8.0 mm thick SS plate.

### 3.4.1 Position selection of pickup sensor in the probe

Typically, an air core probe is selected for excitation and a GMR sensor is used as pickup. The dimensional details of the probe are given in Table 3.2. There are two different kinds of magnetic fields are possible i.e. radial ( $B_r$ ) and normal component ( $B_z$ ). These fields are measured either at the center or adjacent to the excitation coil.

Based on the position of the pickup sensor and magnetic field measurement around the probe, the four different kinds of field measurements possible are:

- i. Normal component at the center of the probe ( $B_{zc}$ ),
- ii. Radial component at the center of the probe ( $B_{rc}$ ),
- iii. Normal component adjacent to the probe ( $B_{za}$ ) and
- iv. Radial component adjacent to the probe ( $B_{ra}$ ).

Table 3.2. Dimensional details of the air core probe

S. No.	Name of the parameter	Value
1.	Excitation coil inner diameter (ID)	6.0 mm
2.	Coil width (w)	1.0 mm
3.	Excitation coil outer diameter (OD)	8.0 mm
4.	No. of turns	250
5.	Excitation coil height ( $h_1$ )	16.0 mm
6.	Probe height ( $h_2$ )	28.0 mm

The cross-sectional view of the PEC probes and position of the pickup sensor are shown in Figure 3.3. Here the location of the pickup sensor is varied around the excitation coil to measure different field components. For optimisation of the sensor location, the outer diameter of the probe is selected as 8.0 mm which is the smallest practically feasible probe and also sensitive to subsurface flaws. An excitation current of 0.8 A with a rise time of 0.7 ms is considered. The PEC response signals obtained from a flaw-free region at different locations of the pickup sensor in and around the excitation coil are shown in Figure 3.4 (a). Figure 3.4 (b) shows the differential PEC signals, after subtraction of flaw-free signals.

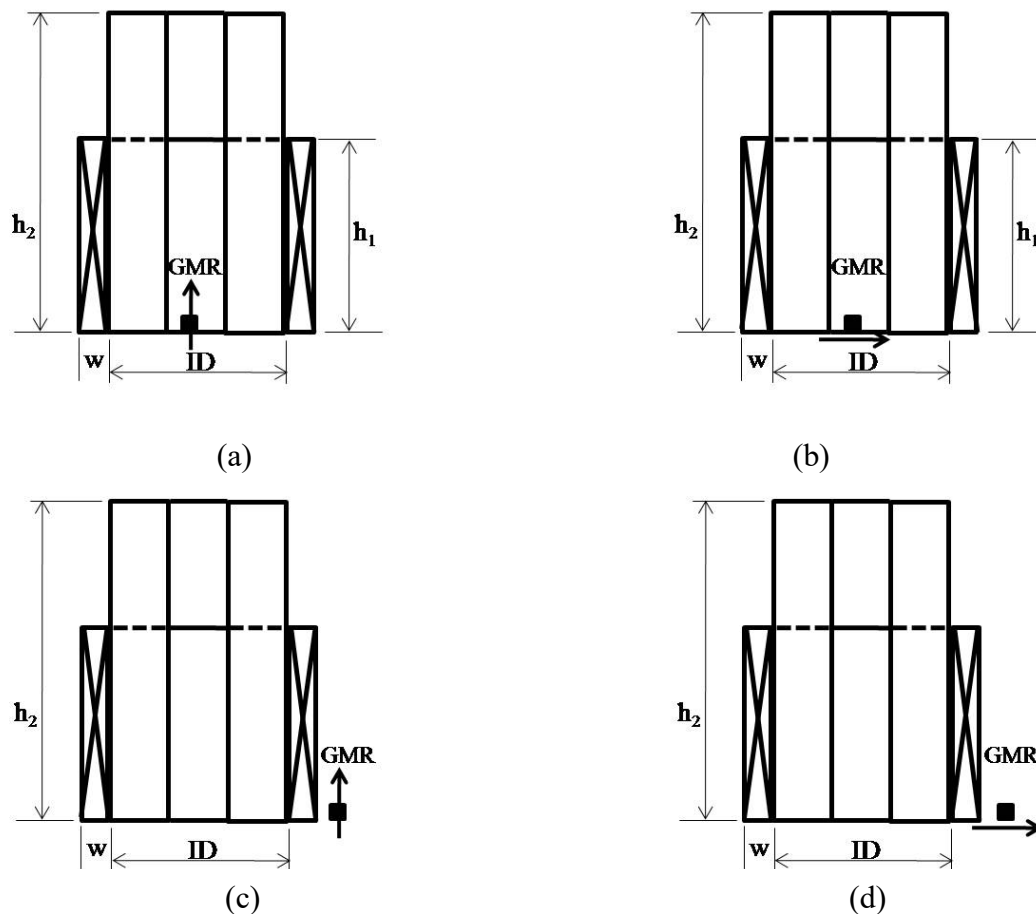


Figure 3.3. Four different field components analyzed (a)  $B_{zc}$  (b)  $B_{rc}$  (c)  $B_{za}$  and (d)  $B_{ra}$  around the excitation coil.

It is observed from Figure 3.4 (a) & (b) that  $B_{zc}$  shows the highest sensitivity among 4 studied magnetic field components. This is due to the fact that, the magnetic flux density at the center of the probe having maximum z-component as compared to other locations. Hence, keeping pickup sensor at the center of the probe and measuring  $B_z$  component is beneficial for detection of flaws located at deeper locations. Therefore, for the rest of the studies, the pickup sensor is kept at the center of the PEC probe to measure the  $B_{zc}$  component.

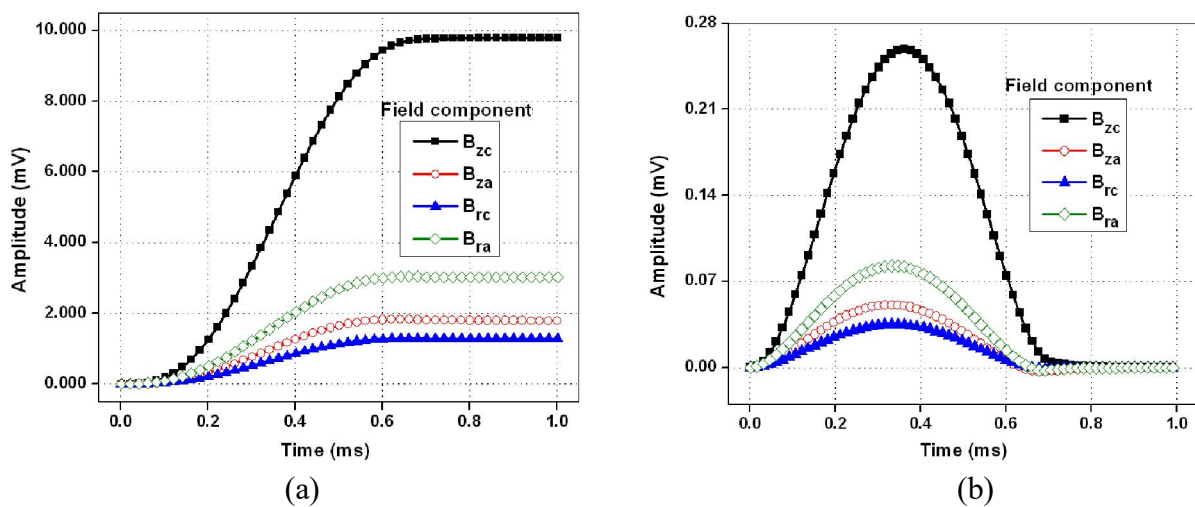


Figure 3.4. (a) Different field components around the PEC probe and (b) differential PEC signals for an excitation coil placed over a SS plate.

### 3.4.2 Selection of excitation coil configuration

Probe configurations like absolute, differential send-receive, and cup-core etc. are commonly used in pulsed eddy current testing. The depth of penetration of eddy currents is not same for all types of probe configurations. Hence, selection of a suitable probe configuration that ensures higher depth of penetration is important for detection of subsurface flaws. Even though the individual response of different probes towards transient magnetic fields had been reported for different NDE applications, their performances are not compared for detection of flaws in an 8.0 mm thick SS plate. Literature survey brought out the fact that send-receive probe is well suited

for PEC testing. GMR sensor is more sensitive to measure the  $B_z$  component at the centre of the probe. Thus, three most suitable send-receive probe configurations in pulsed eddy current NDE are:

- i. Air core probe (Probe-A),
- ii. Ferrite core probe (Probe-B) and
- iii. Ferrite core probe with ferrite outer shielding (Probe-C).

The cross-sectional view of the above probe configurations are shown in Figure 3.5. The dimensional parameters for Figure 3.5 (a) (b) and (c) are same as given in Table 3.2 except the outer diameter of Probe-C is fixed as 12.0 mm, in order to accommodate the outer ferrite shield.

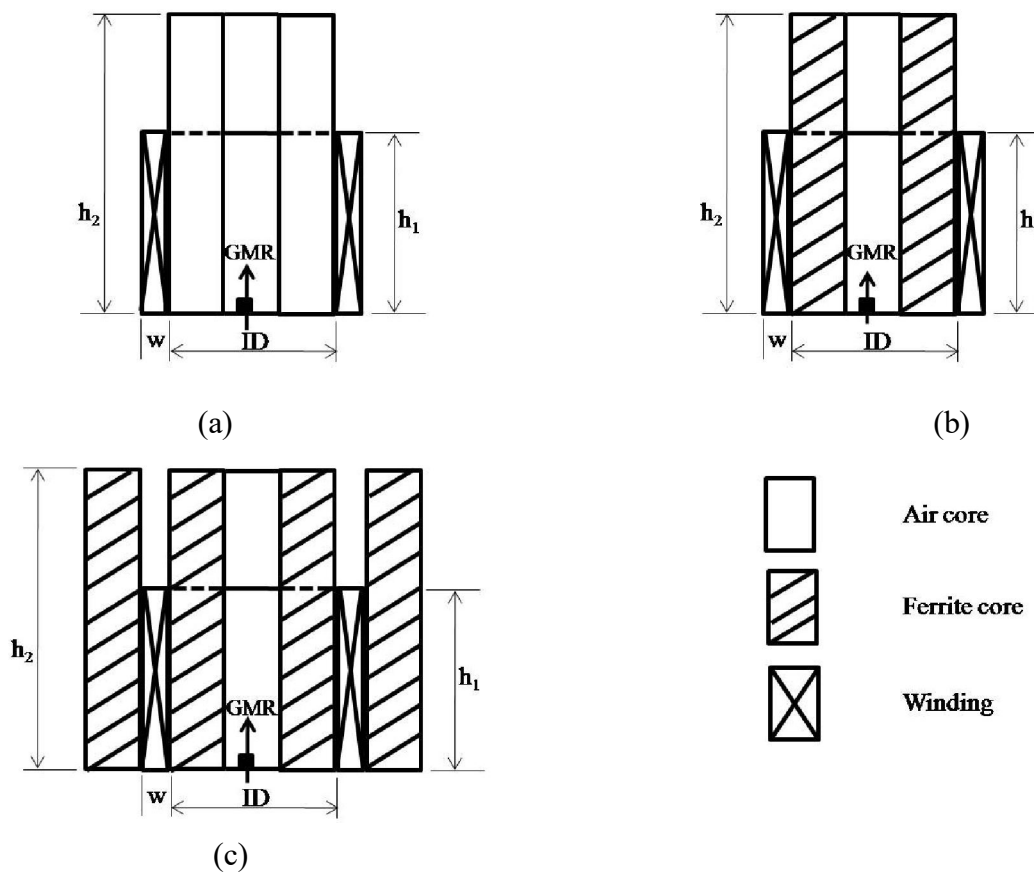


Figure 3.5. Three PEC probe configurations considered (a) Probe-A (b) Probe-B and (c) Probe-C

The test specimen selected for selection of optimal probe configuration is AISI type 304 stainless steel (SS) plate of 8.0 mm thickness having flat bottom holes (FBH) type of flaws (diameter, 5.0 mm) with subsurface depth varied from 1.0 mm to 7.0 mm. Model predictions for the three probe configurations with respect to flaw location below the surface are made and the results are shown in Figure 3.6. It is observed from the model predictions, that the peak amplitude and time-to-peak values saturate for Probe-A and Probe-C for the flaws located at 4.0 mm below the surface on the other hand Probe-B is able to detect flaws up to 5.0 mm below the surface as shown Figure 3.6(d) and (e).

In order to understand the reasons for this behavior, contours are drawn to the induced eddy current density ( $J_{\phi}$ ) for the three coil configurations and shown in Figure 3.7. From model predicted contours of the induced current density for Probe-A (b) Probe-B and (c) Probe-C are placed over a SS plate of 8.0 mm thickness and having a flat bottom hole (5.0 mm diameter) 5.0 mm below the plate surface. The contour intensity values for the contours are kept constant for all three probe configurations for ease of comparison. From Figure 3.7, it can be observed that more number of contours are intercepted for Probe-B as compared with other coil configurations for the flaw located at 5.0 mm below the surface.

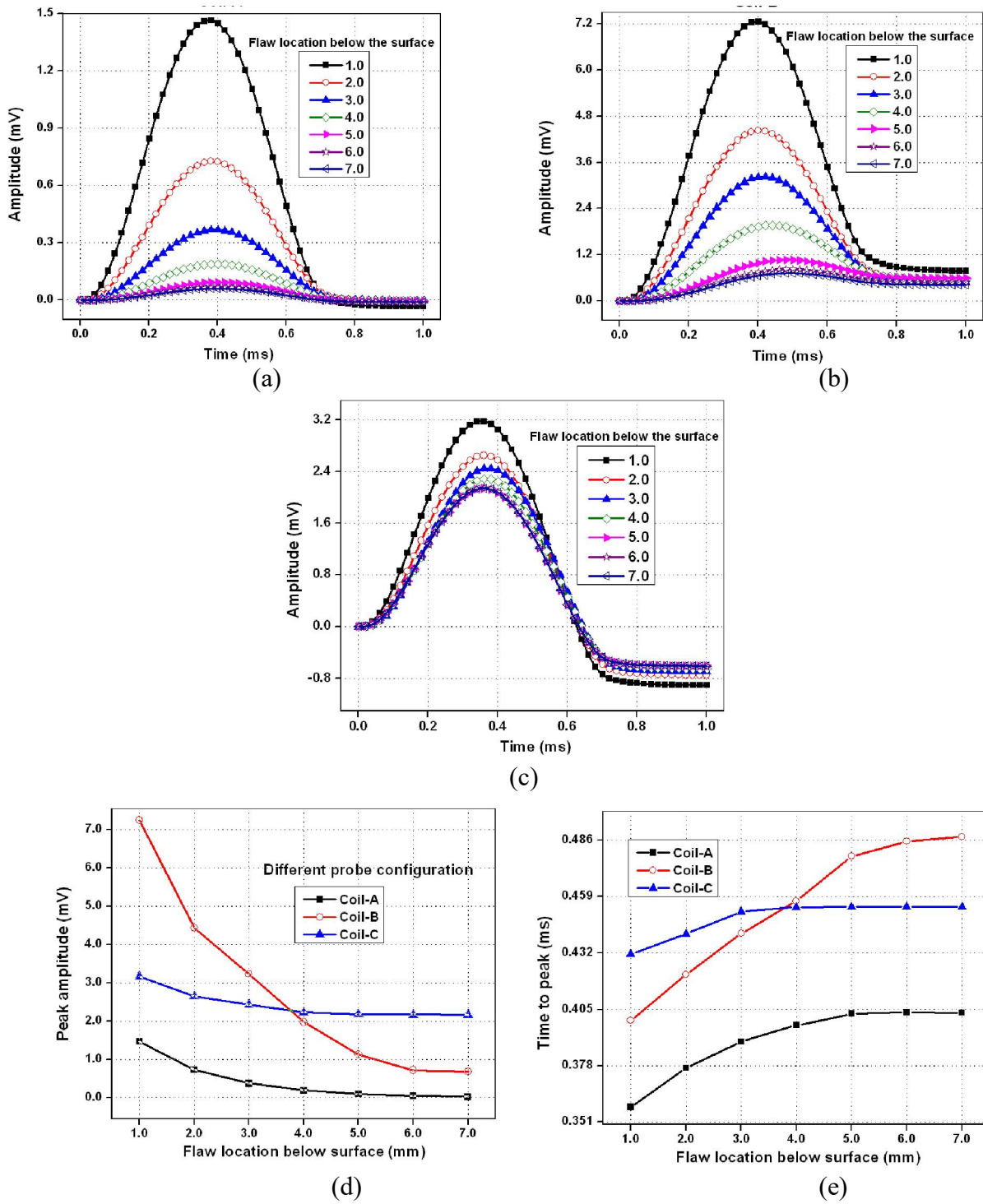


Figure 3.6. Model predicted PEC signals for (a) Probe-A (b) Probe-B (c) Probe-C. The predicted (d) peak amplitude and (e) time-to peak as a function of flaw location below the surface.

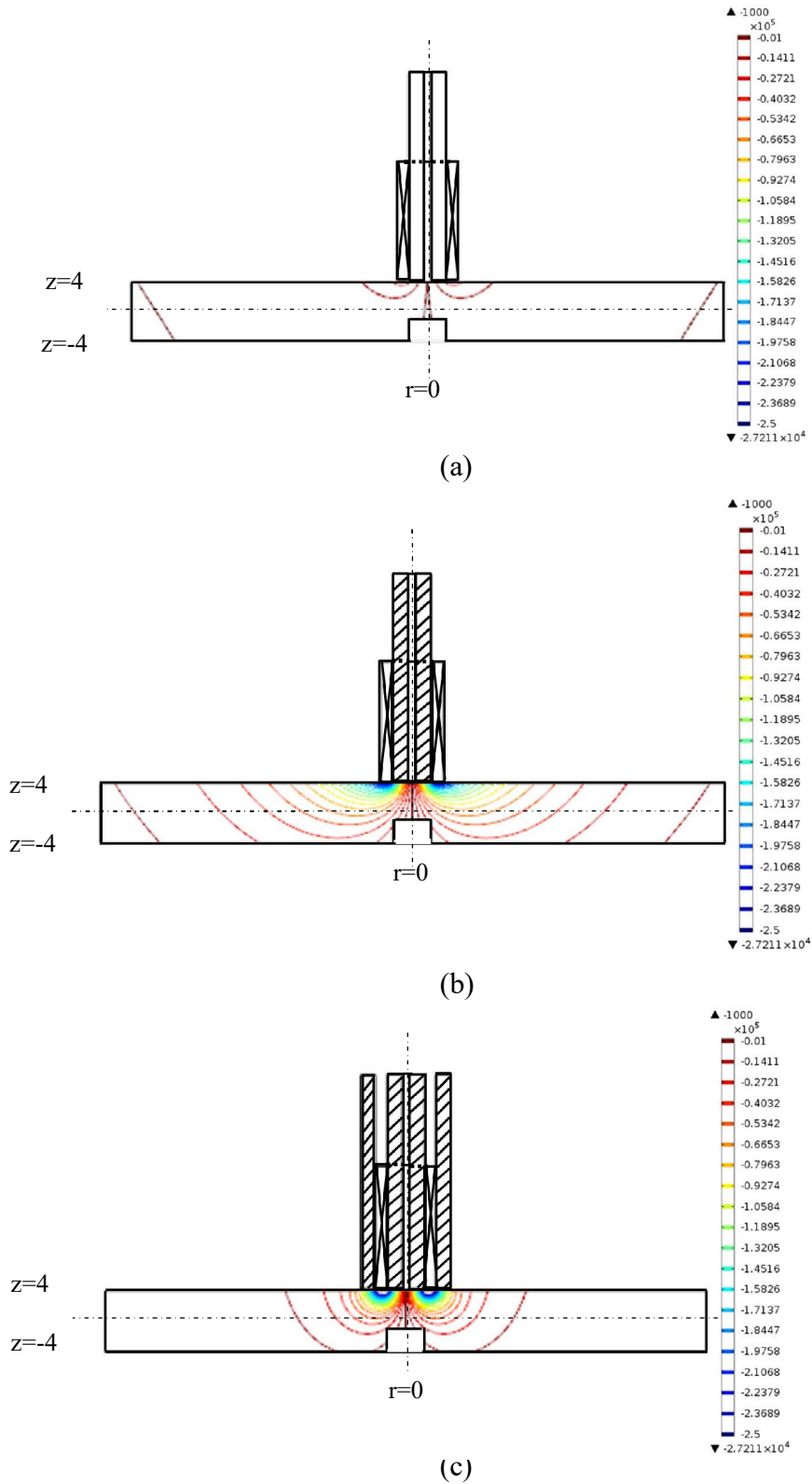


Figure 3.7. Model predicted contours of the induced current density for (a) Probe-A (b) Probe-B and (c) Probe-C placed over a SS plate of 8.0 mm thickness and having a flat bottom hole (5.0 mm diameter) 5.0 mm below the plate surface.

For further analysis, 2D cut-lines are drawn (cut line-1 at  $z = -1.0$ ,  $r = 0.0$  to  $6.0$  mm and cut line-2 at  $z = -5.0$ ,  $r = 0.0$  to  $6.0$  mm) inside the test plate in a flaw-free region to observe the distribution of induced eddy current density ( $J_\phi$ ) for the three configurations. The results are shown in the Figure 3.8.

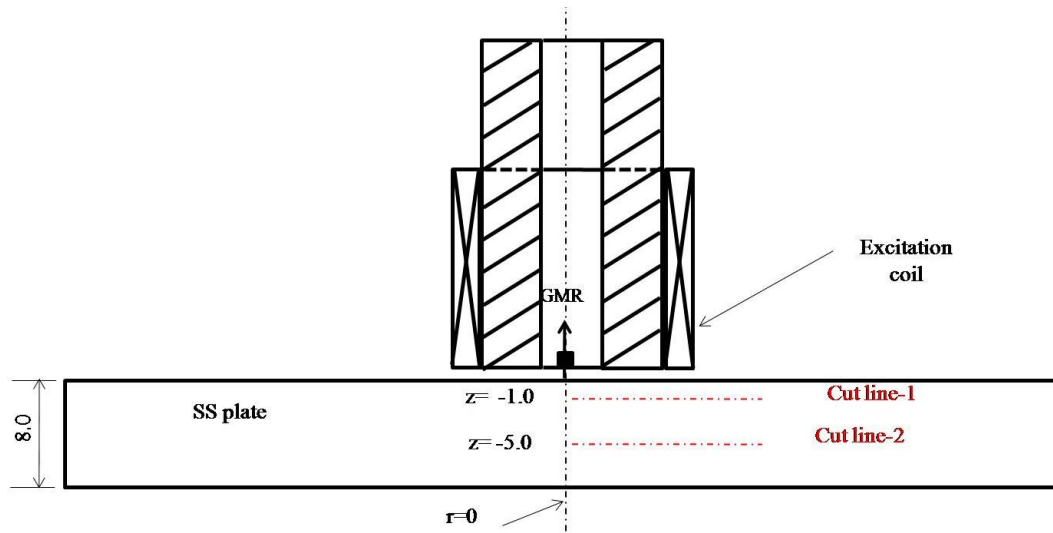


Figure 3.8. 2D cut lines inside the SS plate at  $z = -1.0$  (cut line-1) and  $-5.0$  mm (cut line-2) for different  $r=0.0$  to  $6.0$  mm.

The distributions of  $J_\phi$  inside the plate for two different cut lines are shown in Figure 3.9. The  $J_\phi$  value decreases with increase in thickness of the test plate. From Figure 3.9 (a) and (b) it is observed that the  $J_\phi$  value is lowest for Probe-A as compared to other configurations. This is essentially, due to the fact that with the air core more number of flux lines are leak from the excitation coil and also due to less EM coupling between the coil and plate. As can be seen in Figure 3.9 (a) and (b) for cutline-1 the  $J_\phi$  value is highest for Probe-C whereas for cutline-2 the  $J_\phi$  value is highest for Probe-B. This is due to the fact that the presence outer shielding (Probe-C) decreases flux lines leakage and focuses more fields near to the surface and decreases with

increase in the thickness of the test plate. The variation of  $J_\phi$  value towards flaw location below the surface is calculated by:

$$J_\phi = \frac{J_x}{J_0} \quad 3.1$$

where

$J_\phi$  is current density at any location, A/m<sup>2</sup>

$J_x$  current density at x mm location below the surface of the plate, A/m<sup>2</sup>

$J_0$  current density at the surface of the plate, A/m<sup>2</sup>

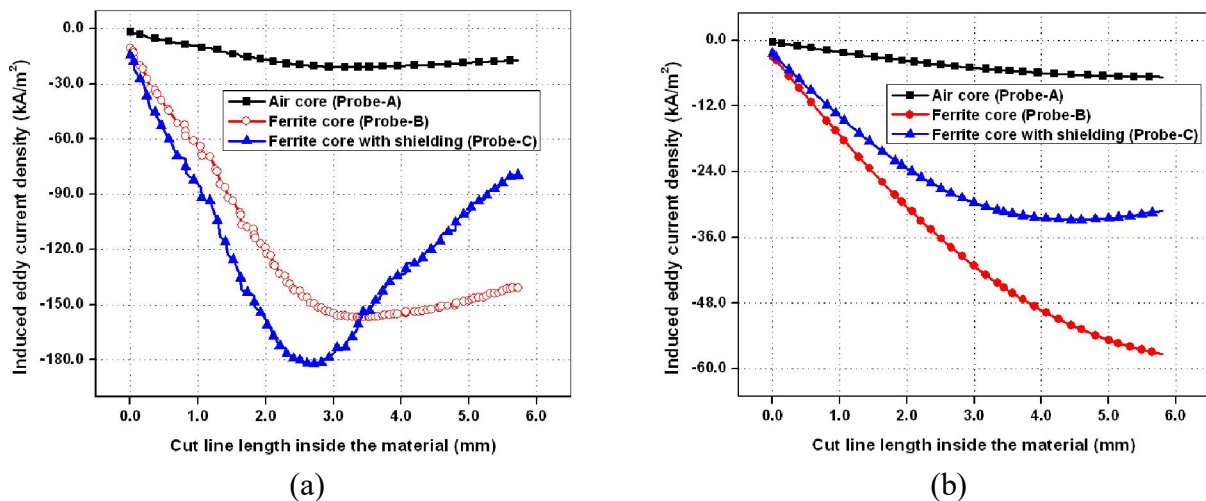


Figure 3.9. Radial distribution of induced eddy current at (a)  $z = -1.0$  mm (cut line-1) and (b)  $z = -5.0$  mm (cut line-2) inside the plate without flaw.

The percentage variation of  $J_\phi$  towards flaw location below the surface of the test plate is given in the Table 3.3. As can be noted the  $J_\phi$  value up to 4.0 mm is greater than  $1/e$  times of the surface  $J_\phi$  value for all the coil configurations. However, for the flaw located at 5.0 mm below the surface, the  $J_\phi$  value is less than the  $1/e$  times of the surface  $J_\phi$  value for Probe-A and Probe-C whereas, for Probe-B, it is greater. As a result, Probe-A and Probe-C are detected flaws located up to 4.0 mm below the surface, whereas Probe-B is detected up to 5.0 mm below the surface.

Hence, Probe-B is chosen as the optimal excitation coil configuration for detection of flaws located at deeper depth in thick SS plate.

Table 3.3. Variation of  $J_{\Phi}$  value with respect to subsurface flaw depth

Subsurface flaw depth, (mm)	Variation of $J_{\Phi}$ value, %		
	Probe-A	Probe-B	Probe-C
1.0	99.10	90.60	90.65
2.0	74.86	99.40	96.57
3.0	55.62	82.70	76.32
4.0	41.17	63.76	54.94
<b>5.0</b>	<b>29.78</b>	<b>46.92</b>	<b>35.06</b>
6.0	22.49	35.71	25.97
7.0	18.70	29.81	20.48

The increased sensitivity of Probe-B is due to:

- i. Presence of ferrite core between the excitation coil and the pickup sensor which reduces the primary magnetic field coupling with the pickup sensor and
- ii. Absence of outer shielding allows deeper penetration of the primary field and higher induced eddy currents as shown in Figure 3.9.

In order to enhance the flaw detection sensitivity of Probe-B up to 7.0 mm below surface in an 8.0 mm thick SS plate, the dimensions viz. outer diameter and height of Probe-B are to be optimal and details of these studies are discussed in the next Section.

### 3.4.3 Optimisation of outer diameter of the probe

After selection of the ferrite cored probe configuration, the next step is to optimize the outer diameter (OD) of the probe for detection of flaws at deeper locations. The outer diameter of Probe-B is varied as: (i) 12.0 mm, (ii) 16.0 mm, (iii) 20.0 mm, (iv) 25.0 mm and (v) 28.0 mm, keeping other dimensions as constant, as given in Table 3.2. A coil height of 16.0 mm is considered for this study. For each case, the PEC probe is positioned centrally over the flaws of varying location below the surface ( $d$ ) and  $B_{zc}$  in the pickup sensor is monitored as shown in Figure 3.10.

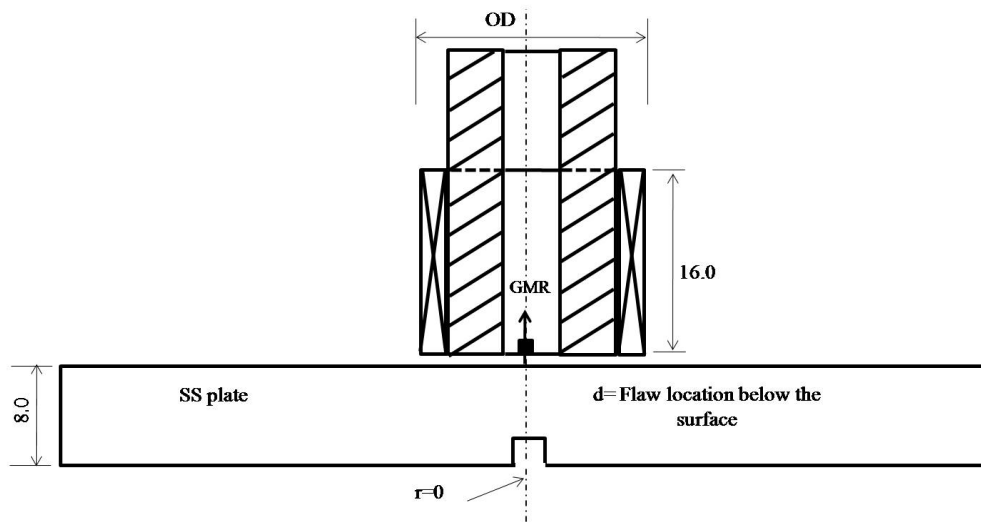


Figure 3.10. Cross-sectional view of the Probe-B for OD optimisation.

Figure 3.11 (a) shows the PEC signals predicted from a flaw-free region for different diameters of the probe. The flaw location below the surface,  $d$  is varied from 1.0 to 7.0 mm. Peak amplitude of PEC signal is obtained from the difference PEC signal. From the results it is observed that the peak amplitude increases from 12.0 to 20.0 mm and then decreases further up to 28.0 mm.

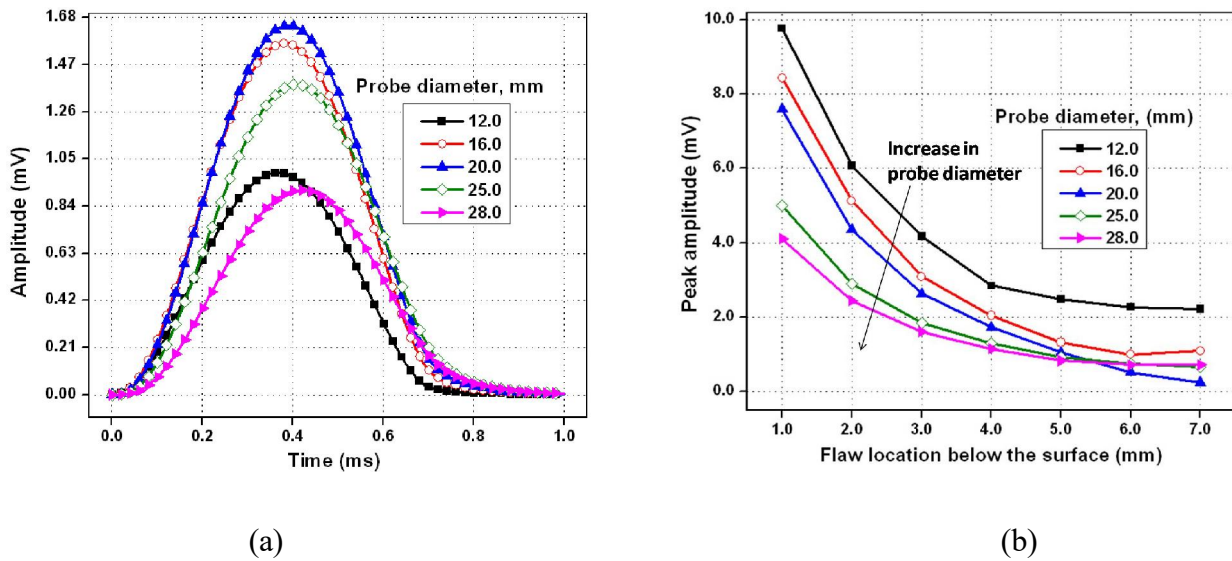


Figure 3.11. (a) PEC signals from a flaw-free region for different diameter of the probes and (b) the peak amplitude as function of flaw location below the surface.

Figure 3.11 (b) shows the variation of peak amplitude with respect to flaw location below the surface for different diameter probes. From the results, it is observed that the 20.0 mm OD probe has showed flaw good detection sensitivity up to 7.0 mm below the surface. A further increase in diameter of the probe has been found to result in lower  $V_p$ . This is attributed to be due to reduction in the interaction of induced eddy currents with flaws. Therefore, from the model predictions it is found that for enhanced detection of flaws in a 8.0 mm thick SS components, the optimal outer diameter of the send-receive type ferrite core probe (Probe-B) is 20.0 mm.

#### 3.4.4 Optimisation of height of the probe

To explore any further improvement in the flaw detection sensitivity, the height of Probe-B has been varied from 8.0 to 28.0 mm for 20.0 mm the OD of the probe. Here, also  $d$  is varied from 1.0 to 7.0 mm in steps (refer Figure 3.10) and  $V_p$  parameter is used to study the changes. Results are shown in Figure 3.12. Probe with 8.0, 12.0 and 16.0 mm height are able to detect flaws located up to 7.0 mm below the surface while probe with 25.0 and 28.0 mm height are able to detect

flaws located up to 5.0 mm only. This is due to fact that increase in height of the coil causes more primary magnetic field leakage and hence, reduced coupling of fields with flaws located at deeper depths.

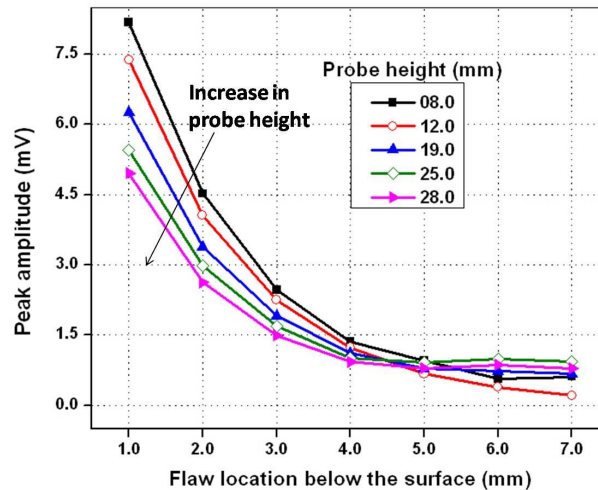


Figure 3.12. Optimisation of height of the Probe-B.

Detection of sensitivity of probes with different probe heights is determined. Clearly, the probe with 12.0 mm height is able to detect flaws located up to 7.0 mm below the surface with higher sensitivity of 1.167 mV/mm. Hence, 12.0 mm height is selected as the optimal height of Probe-B. Model predicted contours of the induced eddy current density for an optimal probe dimensions (outer diameter = 20.0 mm and height = 12.0 mm) for the flaw located at 7.0 mm below the surface as shown in Figure 3.13. From model predictions, the results reveal that the interaction of eddy currents is higher even though the flaw located at 7.0 mm below the surface. Therefore, Probe-B having an outer diameter of 20.0 mm and a height of 12.0 mm is optimal for detection of subsurface flaws located up to 7.0 mm below the surface in 8.0 mm thick SS components.

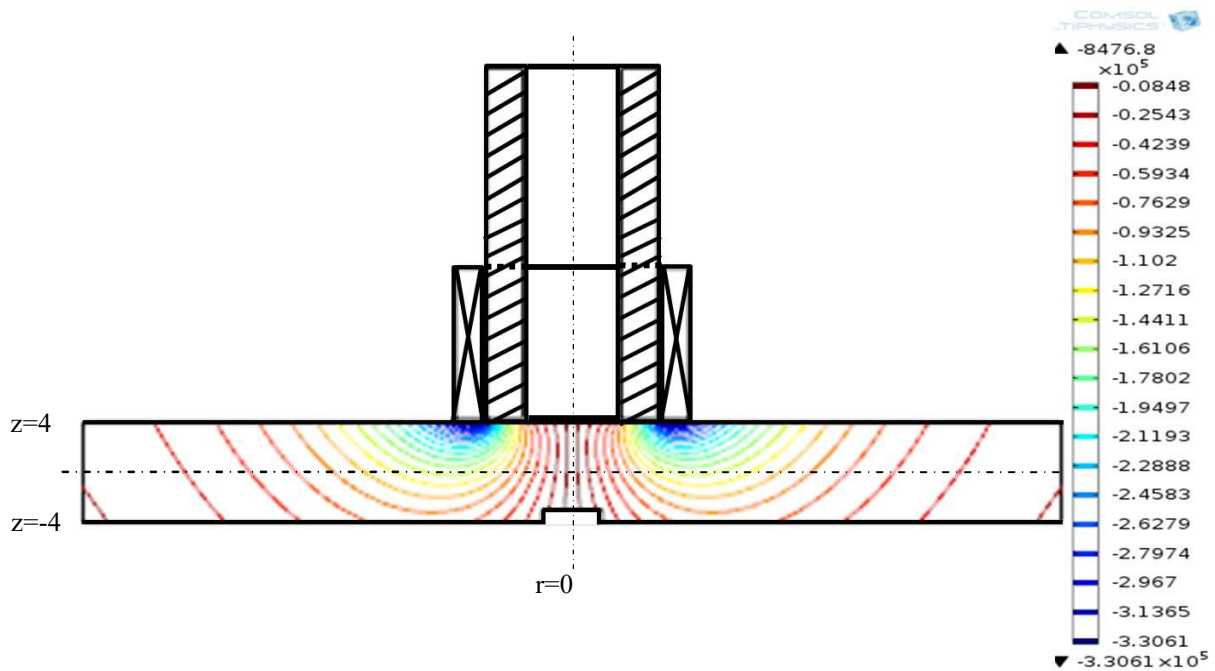


Figure 3.13. Model predicted contours of the induced eddy current density for an optimal probe dimensions (outer diameter = 20.0 mm and height = 12.0 mm) for the flaw located at 7.0 mm below the surface.

The optimal PEC probe configuration has also been used for detection of surface flaws whose depth ( $D$ ) varied from 1.0 to 7.0 mm as shown in Figure 3.14. Here the PEC probe is moved over the surface flaws and the corresponding PEC differential signals are obtained by subtracting the flaw-free signal from the PEC signals from flaw. Model predicted contours of the induced eddy current density for an optimal probe dimensions (outer diameter = 20.0 mm and height = 12.0 mm) for surface flaw depth of 1.0 mm, as shown in Figure 3.15. Model predictions reveal that the interaction of eddy currents is higher for the surface flaw depth of 1.0 mm.

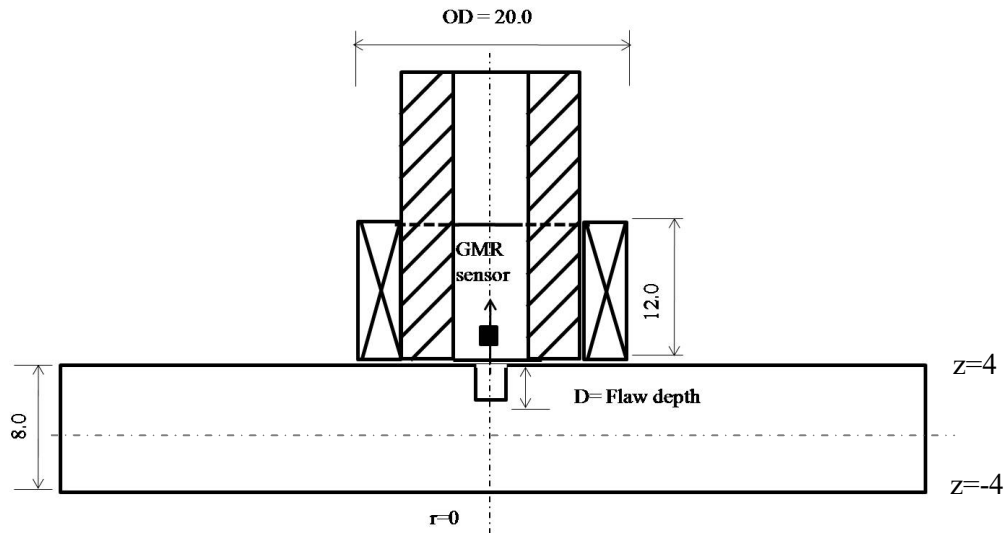


Figure 3.14. PEC probe for detection of surface flaws.

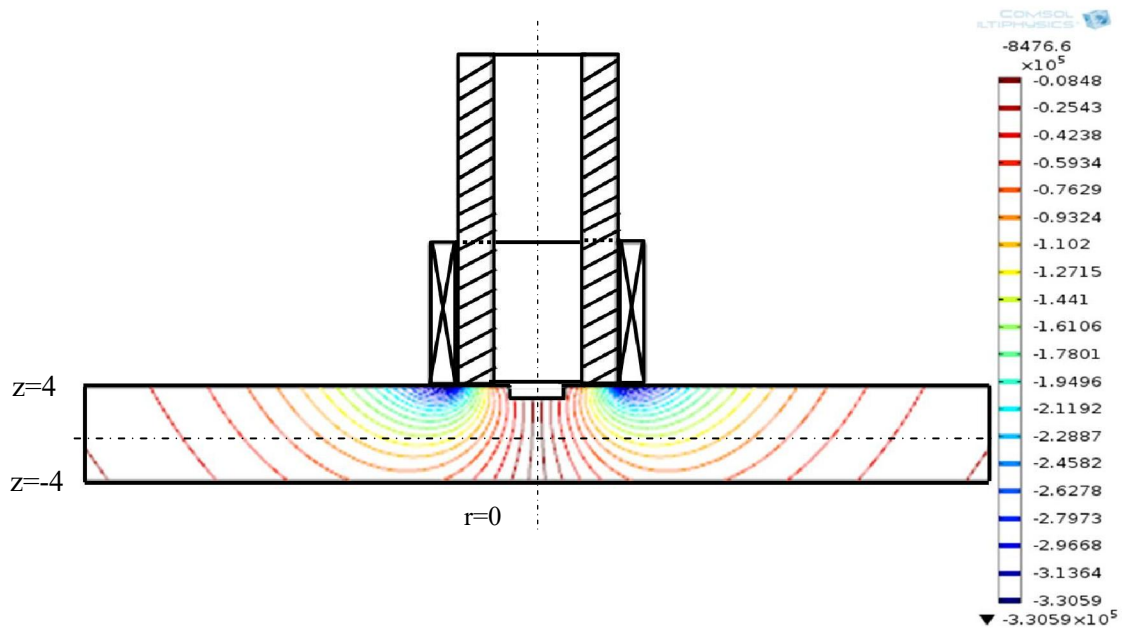


Figure 3.15. Model predicted contours of the induced eddy current density for an optimal probe dimensions (outer diameter = 20.0 mm and height = 12.0 mm) for surface flaw depth of 1.0 mm.

Figure 3.16(a) shows the PEC differential signals obtained from the surface flaws. Figure 3.16 (b) shows the variation of  $V_p$  and  $T_p$  with surface flaw depth. The value of  $V_p$  is found to

increase with increase in flaw depth. This is essentially; due to increased opposition to the flow of induced eddy currents which causes decrease in secondary magnetic field. The value of  $T_p$  is also found to increase with increase in surface flaw depth. This is essentially; due to increase in phase lag of the induced eddy currents with increase in surface flaw depth. Therefore, Probe-B having an outer diameter of 20.0 mm and a height of 12.0 mm can also be used for detection of surface flaws of depth 1.0 to 7.0 mm in 8.0 mm thick SS components.

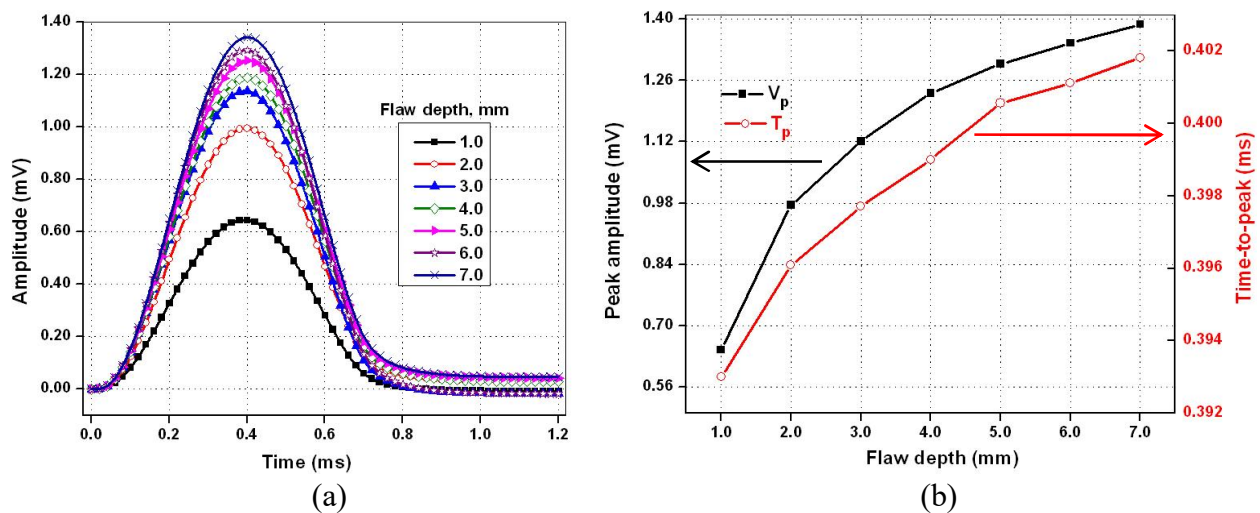


Figure 3.16. (a) PEC signals of surface flaws of different depths and (b) variation of peak amplitude and time-to-peak with surface flaw depth.

The PEC signals of subsurface flaws are shown in Figure 3.17(a). Figure 3.17(b) shows the variation of  $V_p$  and  $T_p$  with flaw location below the surface. The  $V_p$  is found to decrease with an increase in subsurface flaw depth. This is essentially due to reduced opposition to the flow of eddy currents which causes increase in secondary magnetic field. On the other hand,  $T_p$  is found to increase with increase in subsurface flaw depth. This is due to increase in phase lag of the eddy currents with increase in flaw location below the surface. Thus, the above model predictions confirm that the ferrite core send-receive probe can detect both surface flaws and subsurface flaws up to a depth of 7.0 mm below the surface.

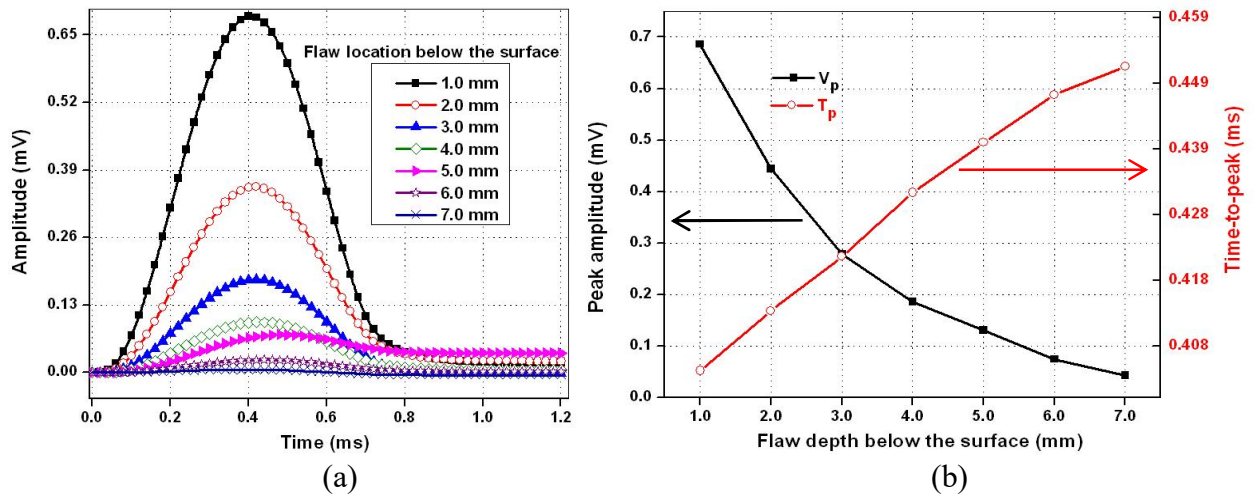


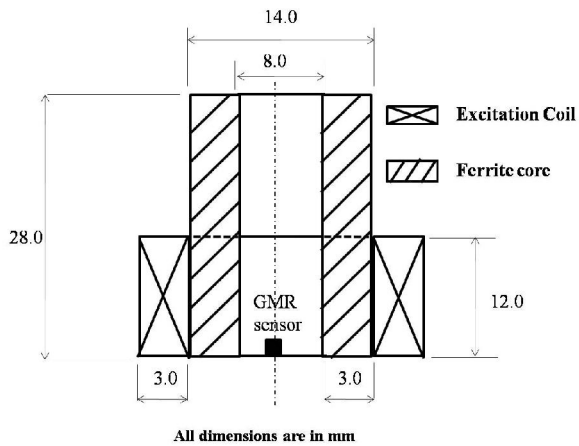
Figure 3.17. (a) PEC signals of subsurface flaws and (b) variation of  $V_p$  and  $T_p$  with flaw location below the surface.

### 3.5 Fabrication of the PEC probe and testing

Following the model predictions, a ferrite core send-receive type PEC probe with optimal dimensions given in Table 3.4 have been fabricated. The probe uses a GMR sensor to measure the  $B_{zc}$  component. Figure 3.18(a) shows the cross-sectional view and Figure 3.18(b), (c) the photograph and zoomed portion of the fabricated PEC probe.

Table 3.4. Dimensions of the fabricated PEC probe

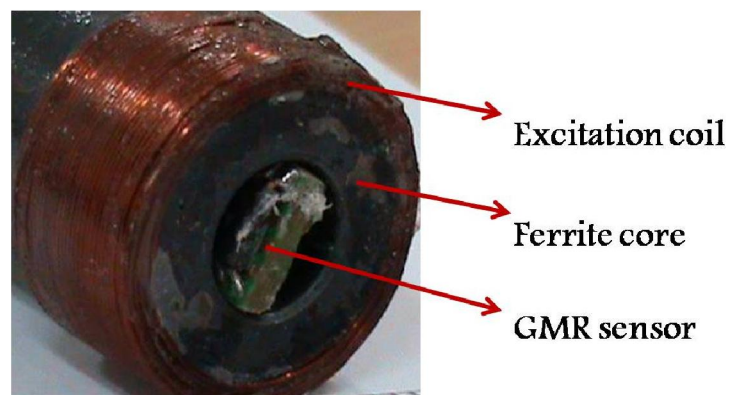
S. No.	Exciter coil	Dimensions
1.	Inner Diameter (ID)	8.0 mm
2.	Outer Diameter (OD)	20.0 mm
3.	Height of the coil	12.0 mm
4.	No. of turns	250
5.	Coil gauge (SWG)	32



(a)



(b)

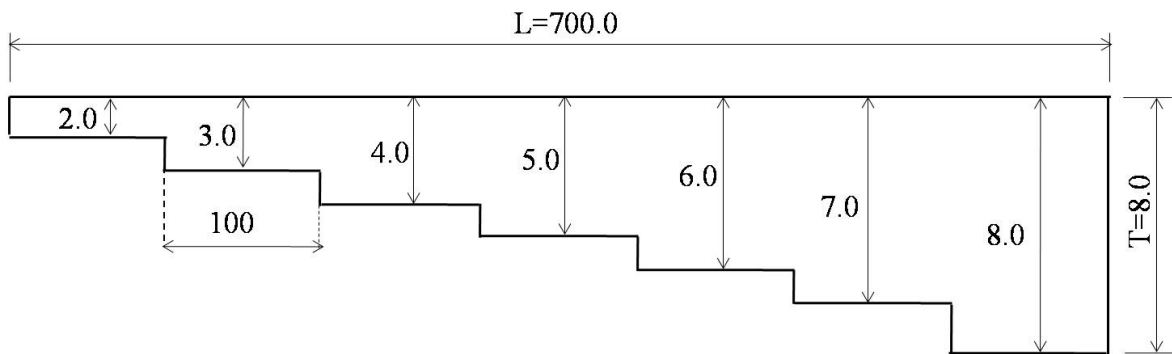


(c)

Figure 3.18. Design of the optimal PEC probe, (b) photograph of the fabricated probe and (c) close up view of the probe.

### 3.6 Testing of the PEC probe

The performance of the fabricated PEC probe has been tested by detecting surface and subsurface flaws due to localised corrosion shown in Figure 2.13 and reduction in thickness of SS plate due to uniform corrosion shown in Figure 3.19. PEC signals have been recorded by placing probe on a flaw-free region and then centrally over the flaws. Differential PEC signals have been obtained by subtracting the flaw-free signal from that of the flaw signals. From the differential PEC signal,  $V_p$  has been determined.



All dimensions are in mm

Figure 3.19. Schematic of the thickness reduction of SS plate to simulate uniform corrosion.

Figure 3.20 (a) shows the differential PEC signals obtained for the surface flaws with varying flaw depth. It is observed from Figure 3.20 (a) that, PEC signals are noisy due to electromagnetic interference from the adjacent instrument or within the electronic circuit (internal noise). Irrespective of presence of noise in the measurements, the instrument and probe are able to detect all the flaws effectively. Figure 3.20 (b) shows the variation of peak amplitude with flaw depth from 5 PEC measurements. It is observed that the peak amplitude increases with surface flaw depth from 1.0 to 6.0 mm. The results are in line with the model predictions as shown in Figure 3.16.

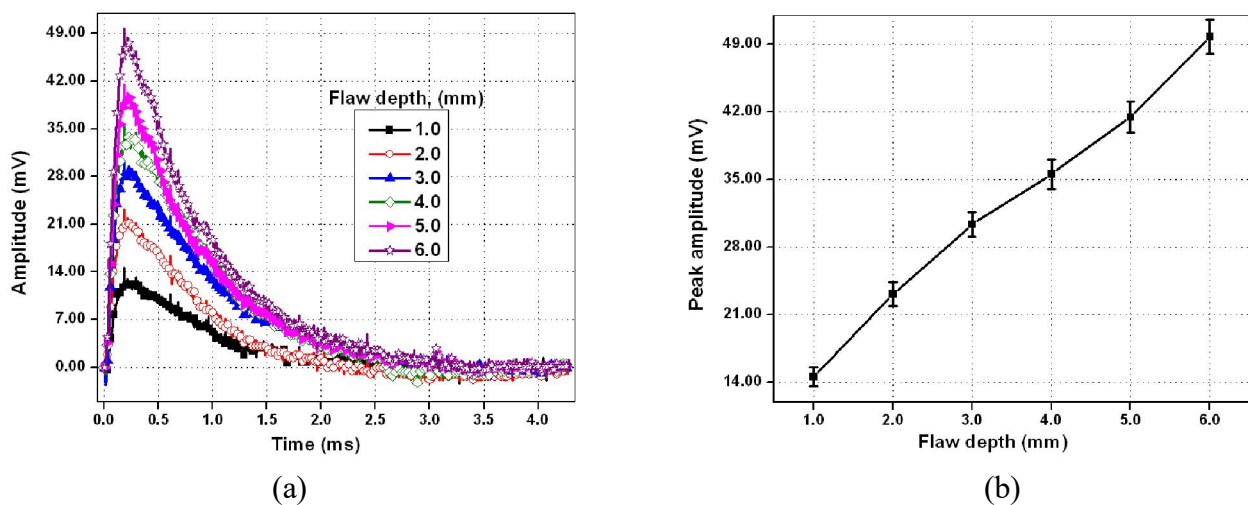


Figure 3.20. PEC signals for (a) surface flaws and (b) peak amplitude vs. flaw depth.

The sensitivity (S) of the PEC technique i.e. instrument and optimal probe for detection of surface flaws is defined as the ratio of change in  $V_p$  and the change in flaw depth (from 1.0 to 6.0 mm).

$$S = \frac{\text{change in peak amplitude}}{\text{change in depth}} \quad 3.2$$

The sensitivity is found to be 7.034 mV/mm. This sensitivity can overcome the noise and can detect surface flaws.

Figure 3.21 (a) shows the differential PEC signals obtained for thickness reduction of the plate. Figure 3.21(b) shows the variation of peak amplitude of the PEC signal with respect to thickness reduction for 5 PEC measurements. From the results, it is observed that the peak amplitude value increases with increase in thickness reduction of the plate from 2.0 to 7.0 mm. This is essentially due to induction of lesser eddy currents at higher thickness reduction region and associated to increase in  $B_{zc}$ . The sensitivity of PEC technique for thickness reduction is 7.644 mV/mm.

In addition to sensitivity there is another parameter called limit of detection (LOD) [83] which is an important figure of merit estimated in validation studies or when reporting the performance of a particular system. LOD is defined as

$$LOD = \frac{3 \sigma}{S} \quad 3.3$$

where,

$\sigma$  is standard deviation and S is slope. Here S is sensitivity.

The standard deviation ( $\sigma$ ) is calculated for a PEC signal by point by variation from the mean of a signal. It is found that the standard deviation of the PEC signal is 1.4 mV. The LOD for surface

flaws found to be 0.59 mm and for thickness reduction is 0.54 mm. This parameter is comparatively smaller than the variation of flaw depth and thickness variation i.e. in step of 1.0 mm and hence, the experimental measurements are more reliable. However, it would be advantageous to use processing techniques to reduce the noise for much higher sensitive detection and classification of flaws.

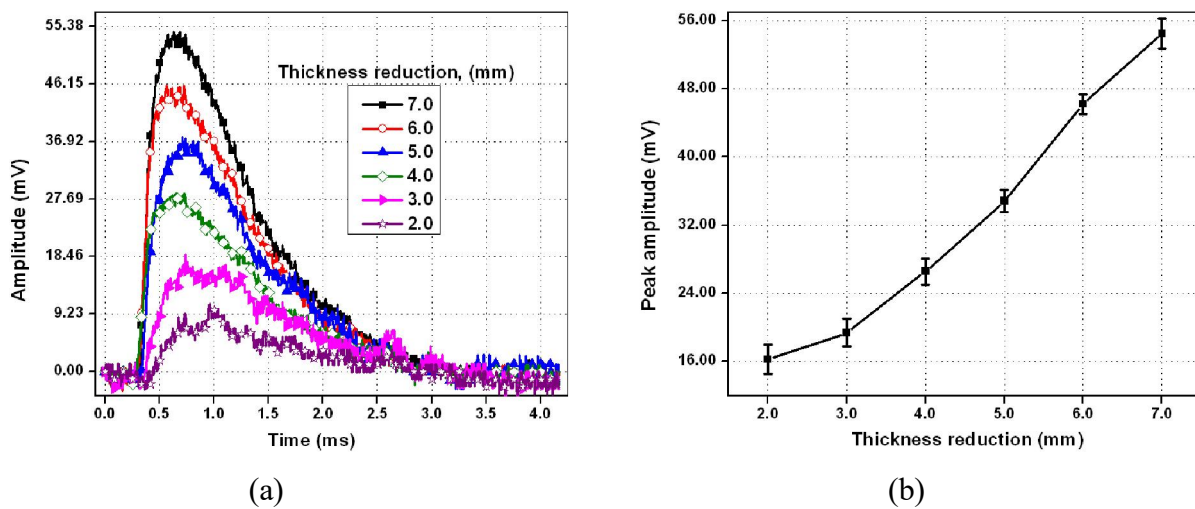


Figure 3.21. (a) PEC signals for thickness reduction and (b) variation of peak amplitude with thickness reduction.

The PEC technique has been used for detection of deep subsurface flaws shown in Figure 2.13. The probe is scanned over the flaws located at 3.0 mm and 6.0 mm below the surface and the differential PEC signals are shown in Figure 3.22. As can be seen the amplitude decreases with increase in flaw location below the surface similar to the model predicted results shown in Figure 3.17. The optimal probe has shown improved flaw detection (4.0 mm below the surface) as compared to the un-optimal air core type probe that could detect flaws located up to 3.0 mm only (refer Figure 2.18). Noise is observed in the PEC signals as a result flaw located at 6.0 mm below surface could not be detected. In this connection, for detection of flaws located at deeper

location (beyond 4.0 mm below the surface) in the presence of noise a new technique will be discussed in the next chapter.

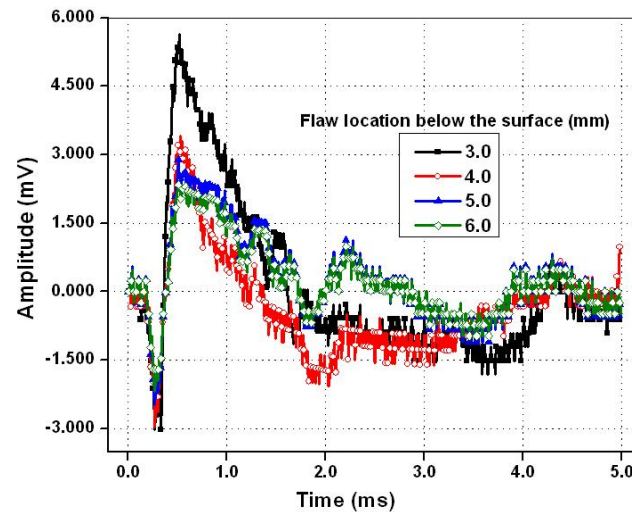


Figure 3.22. PEC signals for subsurface flaws located at 3.0 mm and 6.0 mm below surface in an 8.0 mm thick SS plate.

### 3.7 Summary

For detection of subsurface flaws in stainless steel components, FE model studies have been carried out for optimal location of the pickup sensor, probe configuration, and excitation coil dimensions. Three different types of coil configurations viz. air core (Probe-A), ferrite core (Probe-B) and ferrite core with outer shielding (Probe-C) have been studied by finite element modeling in order to design an optimal coil configuration for detection. The model predicted induced eddy current density ( $J_{\phi}$ ) has been calculated at 5.0 mm location inside the test component for three coil configurations with un-optimal coil dimensions. The following results are observed:

- ✓  $J_{\phi}$  for Probe-B is 47.0 % whereas for Probe-A and Probe-C are 30.0% and 35.0 % respectively. The higher induced current density for the Probe-B is essentially due to reduced direct field to the sensor and focused fields which lead to deeper penetration of eddy currents.
- ✓ From the model predictions it is observed that the Probe-B detected flaws located up to 6.0 mm below the surface whereas 5.0 mm for Probe-C and 3.0 mm for Probe-A. This shows Probe-B has the capability to penetrate magnetic field deeper into the test plate.
- ✓ Model studies have been extended further to enhance the flaw detection sensitivity of Probe-B up to 7.0 mm below surface in an 8.0 mm thick SS plate. Probe-B with 20.0 mm outer diameter and 12.0 mm height has been found to be optimal for detection of subsurface as well as surface flaws.
- ✓ A PEC probe with optimal dimensions has been fabricated. The developed PEC instrument and optimal probe have detected surface flaws with a sensitivity of 7.034 mV/mm and thickness reduction with a sensitivity of 7.644 mV/mm.
- ✓ The optimal probe also detected flaws located at 4.0 mm below the surface in an 8.0 mm thick SS component even in the presence of noise. For detection of flaws located beyond 4.0 mm there is a benefit if noise effects are handled properly.

# Development of technique for detection of flaws due to localised corrosion

---

# 4

## 4.1 Preamble

This chapter addresses ways to handle noise in PEC signals and presents a new technique for enhanced detection of deep subsurface flaws due to localised corrosion. This chapter also presents the effect of excitation rise time ( $E_r$ ) on detection of deep subsurface flaws and discusses the details of two new signal parameters proposed for detection and classification of flaws in stainless steel components.

## 4.2 Detection of subsurface flaws

The PEC instrument and optimal send-receive type PEC probe with GMR sensor have been used and the PEC difference signals obtained from six subsurface flaws (refer Figure 2.13) are shown in Figure 4.1(a). The traditional signal parameters viz.  $V_p$  and  $T_p$  are plotted in Figure 4.1 (b). The  $V_p$  decreases with an increase in flaw location below the surface while  $T_p$  increases. A close observation of Figure 4.1 (b) reveals that  $T_p$  does not increase beyond 3.0 mm below the surface and this is

- i. due to the presence of noise in the PEC signal during the initial part (0-10 %) and the settling part (98-100 %),
- ii. due to power supply fluctuations and
- iii. due to the MOSFET switching characteristics [84,85] that are shown in Figure 4.1 (c).

This noise influence on  $T_p$  is in agreement with that referred in [86]. To reduce the influence of noise on the measurement of  $V_p$  and  $T_p$ , a new technique is proposed for detection of deep subsurface flaws due to localised corrosion.

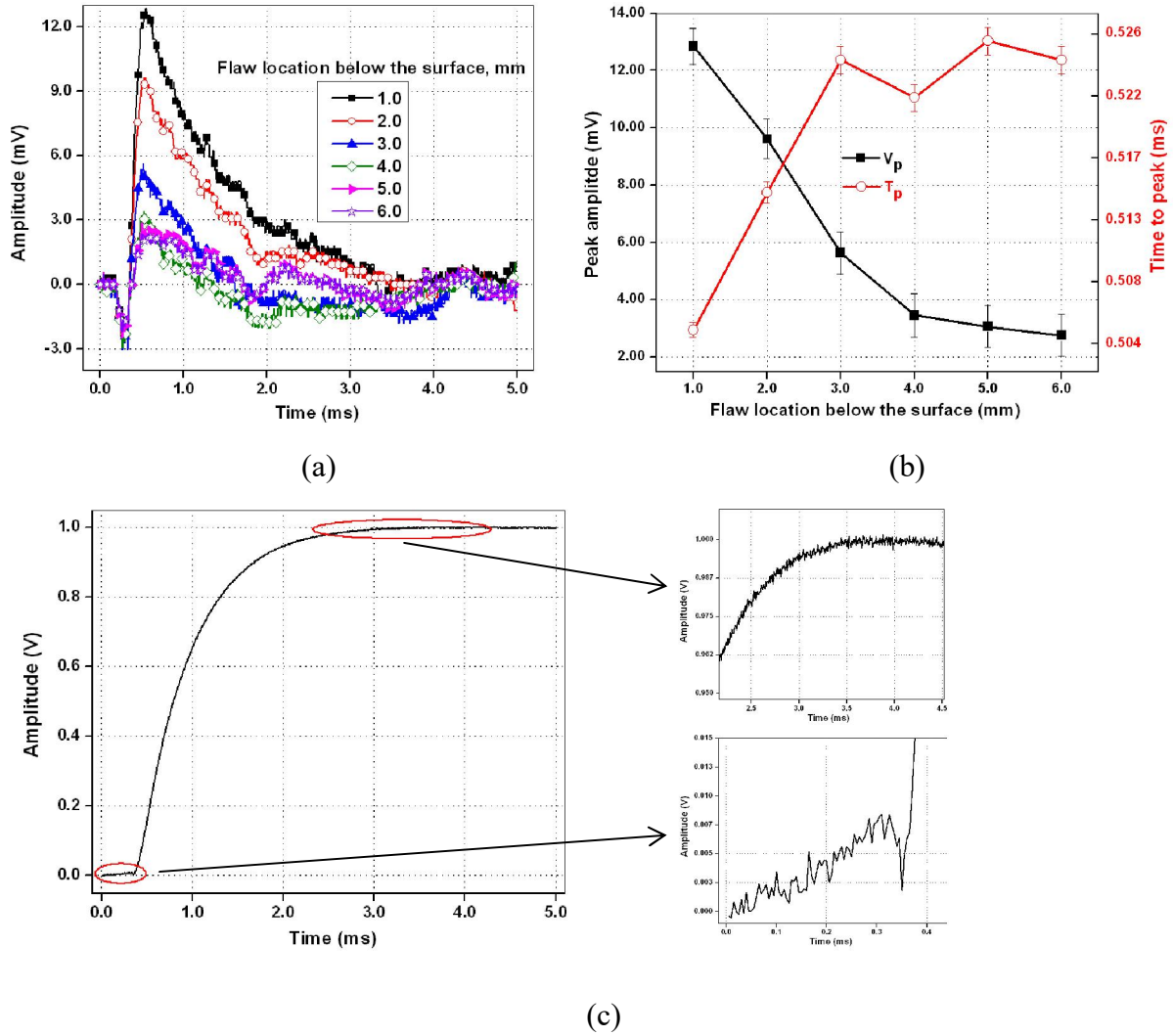


Figure 4.1. (a) PEC difference signals (b) peak amplitude and time-to-peak with flaw location below the surface and (c) a close look at the PEC signal from a flaw-free region.

### 4.3 Proposed technique

The equivalent circuit of an inductive coil has R in series with L and a capacitor in parallel to R and L. The value of C is negligible as compared with R and L in the frequency ranges of PEC technique. The current flowing through the PEC excitation coil is given by[87,88]:

$$I_L = I_0 \times (1 - e^{(-t/\tau)}) \quad 4.1$$

where

$I_L$  is the current flowing through the coil, Ampere

$I_0$  is the peak current, Ampere

R is the resistance of the coil, Ohms

t is the time, seconds

$\tau$  is the time constant of the coil, i.e. L/R in seconds

Since the GMR sensor measures the direct magnetic field which is proportional to the current flowing through the coil, the output voltage of the sensor (V) follows the equation (4.1). The sensor response is influenced by location of the flaw (signal) and variations in lift-off (due to material irregularities) and electromagnetic interference leading to noise in the signal. To detect flaws located beyond 4.0 mm below surface (as shown in Figure 4.1) in the noisy environment, a new technique is proposed. The flow chart of the proposed technique is shown in Figure 4.2. In the proposed technique, GMR response from flaws are normalized with respect to the maximum value of the flaw-free signal and these signals are iteratively fitted to a modified equation that closely describes the underlying physical process:

$$V = V_0 - V_1 \times e^{(-t/\tau)} \quad 4.2$$

where

V is the GMR sensor output, volts

$V_0$  and  $V_1$  are the voltage parameters, volts

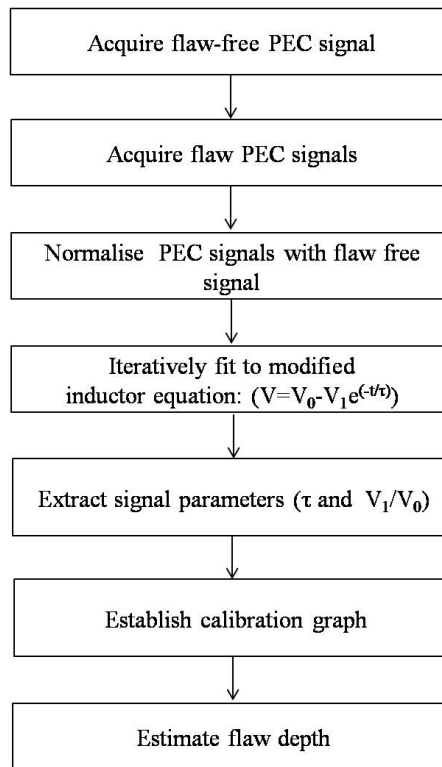


Figure 4.2. Flow chart of the proposed technique.

During the fit process, the parameters  $V_0$ ,  $V_1$  and  $\tau$  are extracted for detection of flaws. The statistical correlation parameter,  $R_c$  is maximised to a value close to 1.0 for ensuring the best fit. The parameters,  $V_0$  and  $V_1$  vary due to the changes in excitation currents and location of the flaw, whereas  $\tau$  measures the delay in the response pulses and is sensitive to location of the flaw.

For a constant excitation current and lift-off,  $V_0$  value changes marginally due to noise and it is independent of flaw location whereas  $V_1$  varies with flaw location. Therefore, the voltage ratio,  $V_r$  i.e.  $V_1/V_0$  a new parameter proposed for the first time, increases with an increase in flaw location below the surface. The time constant,  $\tau$  measures the delay in the response pulses and is sensitive to location of the flaw.

As discussed earlier in Section 1.3, a pulse consists of a spectrum of frequencies, it is broadened and delayed as it travels deeper into a highly dispersive material [89]. Therefore, with an increase in flaw location below the surface, the response pulse will be delayed more. The depth of penetration,  $z$  of the pulsed electromagnetic field at a given time,  $t$  in a conducting test plate is governed by [90]:

$$z = \sqrt{\frac{t}{\pi\sigma\mu}} \quad 4.3$$

From Equation 4.3 it can be inferred that the response pulse occur earlier in time for the flaws closer to the surface than that of the flaws that are at the deeper location. The new parameters  $V_r$  and  $\tau$  are used for estimation of the subsurface flaw depth for various excitation rise times ( $E_r$ ). The following analysis is presented for a typical  $E_r$  of 0.7 ms.

The GMR signal when the probe is in air is shown in Figure 4.3 (a) (with open circles) along with the fitted signal (continuous line) as per equation 4.2 with a  $R_c$  value of 0.999. The PEC signal is obtained by substituting the  $t$  values in equation (4.2), knowing  $V_0$ ,  $V_1$  and  $\tau$  values. The parameters ( $V_0$ ,  $V_1$  and  $\tau$ ) obtained from signals at flaws located at different depth below the surfaces (from 1.0 to 6.0 mm) are given in Table 4.1. It can be observed from Table 4.1 that the  $V_0$  varies marginally whereas  $V_1$ ,  $V_r$  and  $\tau$  are found to increase in flaw location below the surface. Figure 4.3 (b) shows how the fit equation handles the noise in the measured PEC signal. The corresponding signals obtained from the subsurface flaws are shown in Figure 4.3 (c). The inset to Figure 4.3 (c) shows the signals during the rising part. Herein, the signals are clearly distinguishable.

The variation of parameters viz. voltage ratio ( $V_r$ ) and time constant ( $\tau$ ) with flaw location below the surface (1.0 to 6.0 mm) are shown in Figure 4.3 (d) with a linear fit. The correlation

coefficient for linear fit of  $V_r$  and  $\tau$  is 0.985. The error in  $V_1/V_0$ , and  $\tau$  are 0.1 mV and 4  $\mu$ s respectively. From the results, it is observed that the parameters  $V_r$  and  $\tau$  increases with increase in flaw location below the surface. Therefore, from the results it can be observed that the proposed technique is able to detect flaws located at 1.0 to 6.0 mm below the surface in an 8.0 mm thick SS plate effectively irrespective of presence of noise in the measurements. The advantage of the proposed technique is that, it does not require either reference signal subtraction or signal processing methods for detection and classification of flaws in a noisy environment.

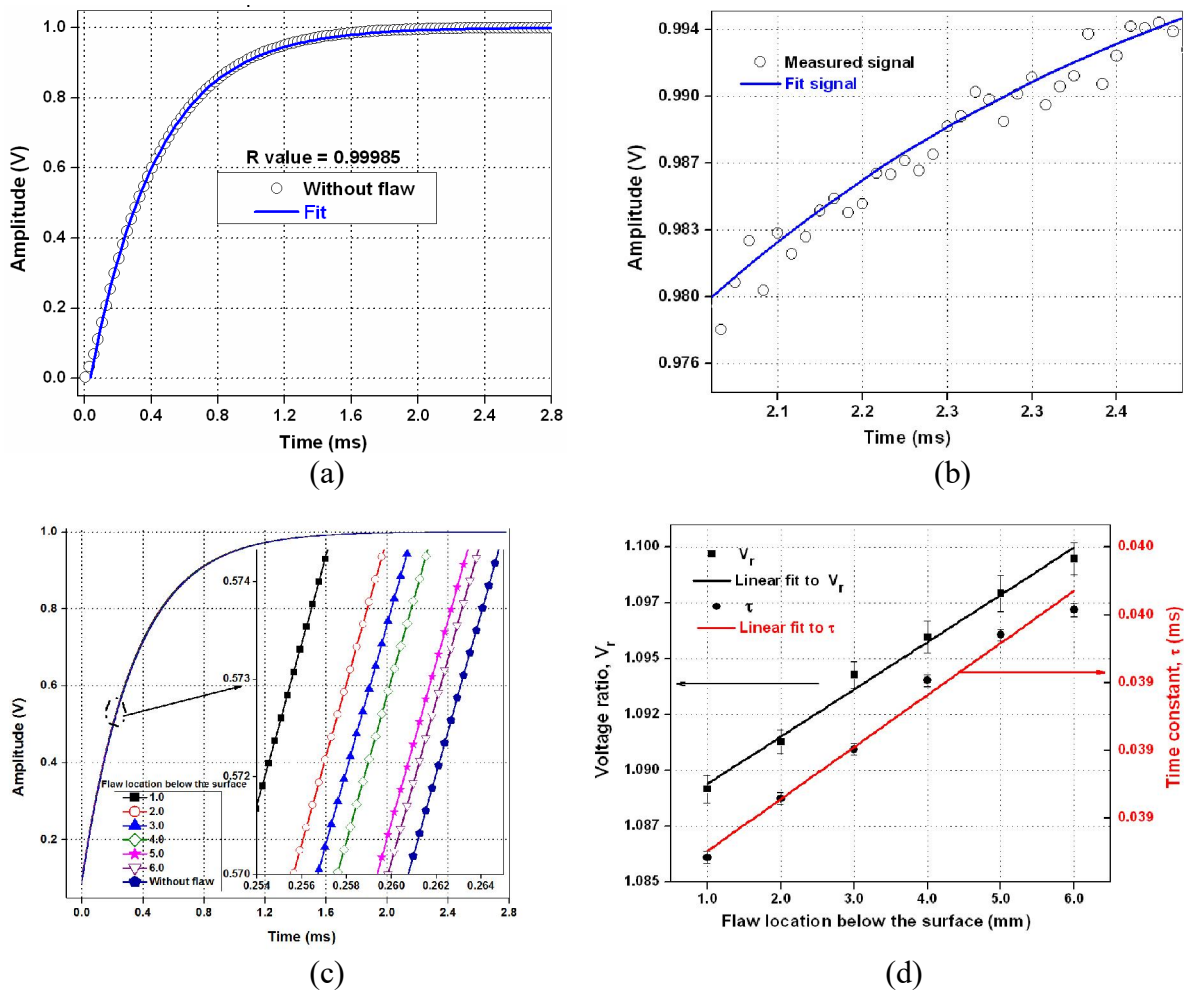


Figure 4.3. PEC response for probe in (a) air (b) noise signal with fit (c) for subsurface flaws and (d) the calibration graph in SS plate.

Table 4.1. PEC signal parameters for subsurface flaws

Subsurface flaw depth (mm)	$V_0$ (V)	$V_1$ (V)	$V_r$	$\tau$ (ms)
1.0	1.0043	0.9991	0.9947	0.3906
2.0	1.0050	1.0026	0.9975	0.3919
3.0	1.0037	1.0053	1.0016	0.3930
4.0	1.0072	1.0109	1.0037	0.3945
5.0	1.0049	1.0098	1.0048	0.3955
6.0	1.0051	1.0119	1.0068	0.3961

#### 4.4 Effect of excitation rise time on detection of flaws

The time taken by the PEC signal to reach from 10 % to 90 % of its maximum value is taken as the rise time. The rise time of the exciter coil ( $E_r$ ) depends on the resistance and inductance values of the coil. Therefore, by connecting a variable resistor and an inductor in series with the excitation coil, the  $E_r$  value and the frequency range can be varied. For a fixed value of inductance, by increasing the resistance, the time constant of the coil decreases and hence,  $E_r$ . Thus, by proper selection of R and L, appropriate  $E_r$  can be chosen with suitable frequency components.

The frequency components present in an excitation pulse depends on the rise time [91]. Therefore, to study the influence of  $E_r$  on detection of subsurface flaws, the rise time of the coil is varied. For the present study five different  $E_r$  viz. 0.25 ms, 0.5 ms, 0.7 ms, 1.0 ms and 1.4 ms are

selected by connecting an external variable resistor and an inductor in series with the excitation coil. Figure 4.4 shows the normalised PEC signals for different  $E_r$  when the PEC probe is placed on air.

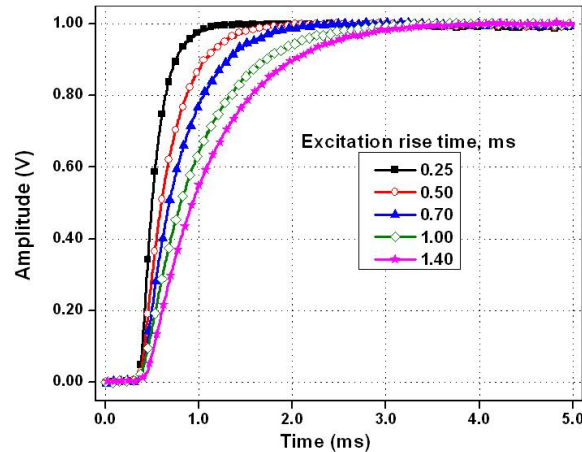
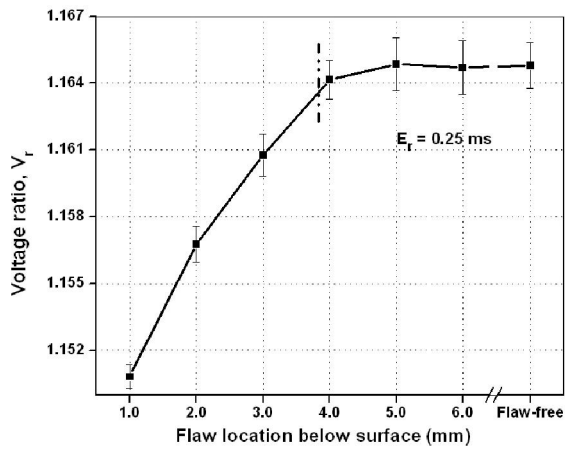


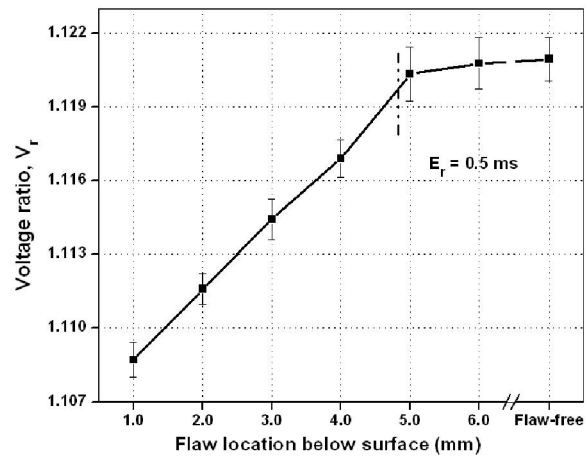
Figure 4.4. PEC signals from different excitation rise time.

With an increase in excitation rise time, the response pulses are delayed more. This delay in response is due to the presence of low-frequency components in the excitation pulse. For each  $E_r$ , the PEC probe is scanned over the flaws (as shown in Figure 2.13) and the response pulses are normalised with respect to the flaw-free region and fitted to the modified equation 4.2 and the results are shown in Figure 4.5. It can be observed that the  $V_r$  increases with an increase in flaw location below the surface (1.0 to 6.0 mm).

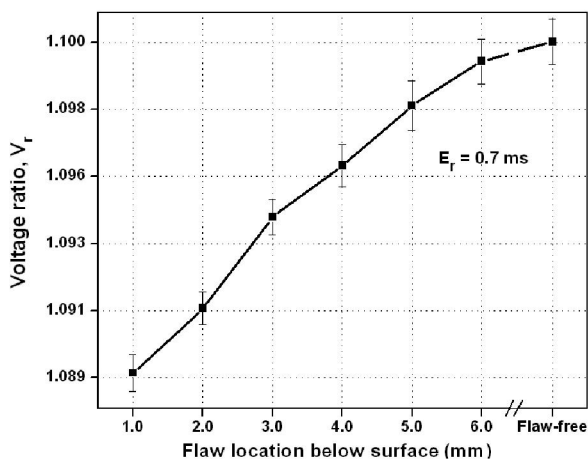
However, for excitation rise times of 0.25 ms and 0.5 ms,  $V_r$  is found to saturate for flaws located 4.0 and 5.0 mm below the surface. For other  $E_r$  of 0.7, 1.0 and 1.4 ms the  $V_r$  is found to be sensitive to flaws located 6.0 mm below the surface. The change in  $V_r$  value with flaw location for different excitation rise times is less and is found to vary between 0.01 and 0.014. This small change is not encouraging to detect and classify flaws.



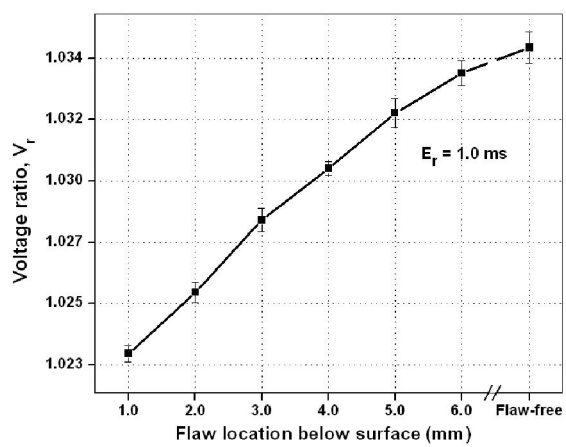
(a)



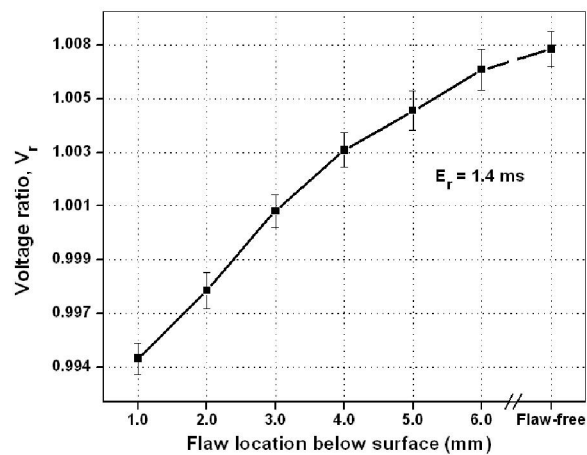
(b)



(c)



(d)



(e)

Figure 4.5.  $V_r$  for subsurface flaws  $E_r$  values of (a) 0.25 ms, (b) 0.5 ms, (c) 0.7 ms, (d) 1.0 ms, and (e) 1.4 ms.

Figure 4.6 shows the results for  $\tau$  for different  $E_r$ . As can be observed  $\tau$  values are saturated for flaws located beyond 4.0 mm below the surface for  $E_r$  of 0.25 and 0.5 ms. However, for  $E_r$  of 0.7, 1.0 and 1.4 ms,  $\tau$  is found to increase systematically with respect to flaw location below the surface as shown in Figure 4.6. Table 4.2 shows the variation of  $\tau$  with respect to flaw location for 5 different  $E_r$ .

Table 4.2. Measured  $\tau$  for different  $E_r$  and flaw depth below the surface

Subsurface Flaw depth (mm)	$\tau$ (ms)				
	$E_r = 0.25$ ms	$E_r = 0.5$ ms	$E_r = 0.7$ ms	$E_r = 1.0$ ms	$E_r = 1.4$ ms
1.0	0.1416	0.2721	0.3551	0.5582	0.6622
2.0	0.1434	0.2729	0.3563	0.5603	0.6635
3.0	0.1449	0.2740	0.3573	0.5623	0.6652
4.0	0.14530	0.275	0.3588	0.5638	0.6661
5.0	0.1454	0.2762	0.3596	0.5653	0.6671
6.0	0.1455	0.2763	0.3600	0.5666	0.6679

Table 4.3 shows the maximum change in  $\tau$  value ( $\Delta\tau$ ) i.e. the difference between  $\tau$  values at 1.0 mm below the surface from that of the flaw-free region. For the  $E_r$  of 0.25 and 0.5 ms the  $\tau$  value is saturated up to 5.0 mm below the surface whereas it changes up to 6.0 mm below the surface for other  $E_r$ . The change in  $\tau$  value is maximum observed for 1.0 ms excitation rise time pulse as shown in Table 4.3.

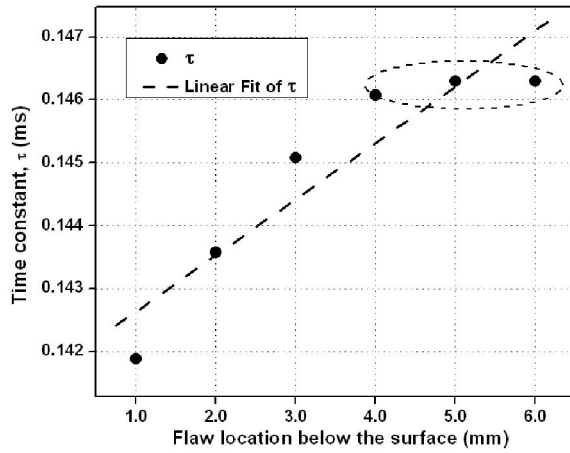
Table 4.3. Change in  $\tau$  for different  $E_r$ 

S. No	$E_r$ , ms	Change in $\tau$ value, $\mu\text{s}$
1.0	0.25	3.94
2.0	0.50	4.34
3.0	0.70	5.21
4.0	1.00	9.61
5.0	1.40	6.17

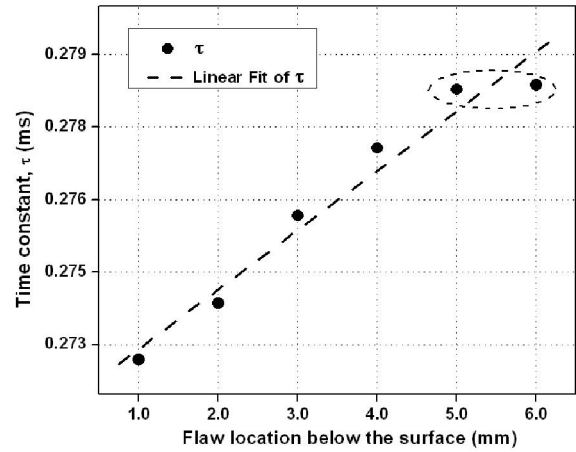
Figure 4.6 also shows the linear fit obtained for the  $\tau$  and the slope is evaluated. The correlation coefficient for the linear fit is above 0.945 for  $E_r$  of 0.7, 1.0 and 1.4 ms. This slope gives the sensitivity of  $\tau$  to detect flaws located at different locations. The flaw detection sensitivity is defined as the ratio of change in  $\tau$  to the change in subsurface flaw depth. The sensitivity for different  $E_r$  is shown in Figure 4.7. The sensitivity of  $\tau$  for rise time of 0.25 and 0.5 ms is less as compared with 0.7, 1.0 and 1.4 ms. However, it is found to be maximum for  $E_r$  at 1.0 ms.

For excitation rise times of 0.7, 1.0 and 1.4 ms, both  $V_r$  and  $\tau$  increase with increase in flaw location below the surface from 1.0 to 6.0 mm. This is attributed to the combined effect of

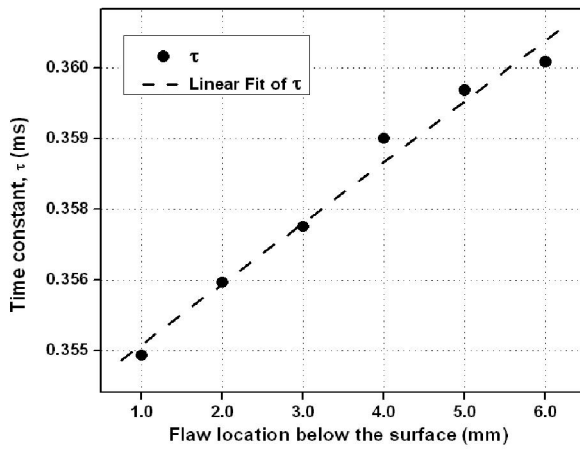
- i. multiple frequency components present in the input pulse, leading to different levels of attenuation of eddy currents in the plate and
- ii. variation of mutual inductance between the excitation coil and the plate with flaws present.



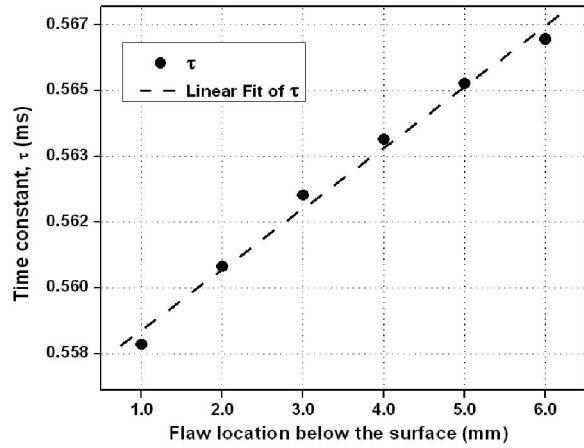
(a)



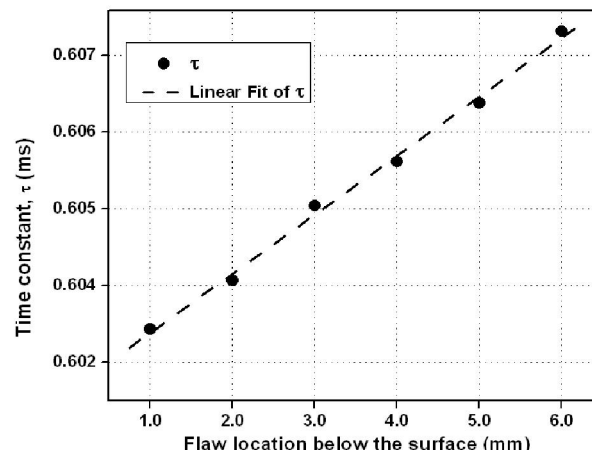
(b)



(c)



(d)



(e)

Figure 4.6. Linear fit for time constant with respect to flaw location below the surface for  $E_r$  of (a) 0.25 ms, (b) 0.5 ms, (c) 0.7 ms, (d) 1.0 ms and (e) 1.4 ms.

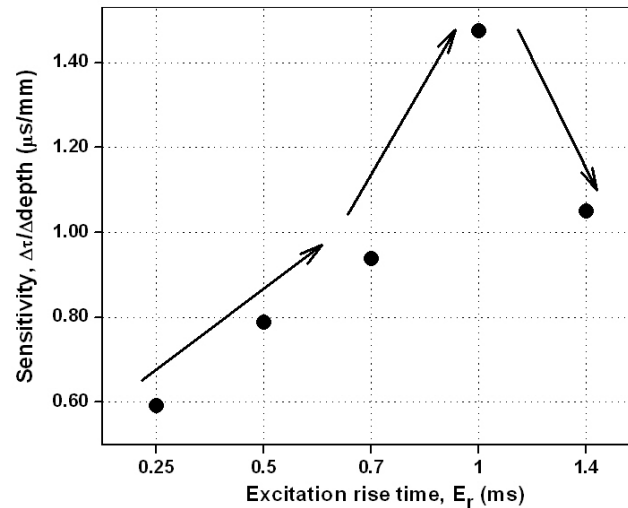


Figure 4.7. Variation of sensitivity of time constant with respect to  $E_r$ .

The increase in  $\tau$  with subsurface flaw depth is in-line with the TD (Time-to-descending point) parameter represented by Chen et al. [33]. Based on the estimated higher sensitivity (from Figure 4.7) to flaw detection by  $\tau$ , an excitation rise time of 1.0 ms can be used for detection of subsurface flaws in 8.0 mm thick SS plate.

In order to understand the change in sensitivity  $E_r$ , frequency analysis is carried out. Figure 4.8(a) shows the fast Fourier transform (FFT) of excitation pulses with 5 rise times. There exist crossovers in the frequency response plot. This is due to the fact that pulses with larger rise time have dominant amplitude components at low frequencies and vice versa [91].

The variation of FFT amplitude with respect to skin depth (corresponding to the frequency range of 3.0 – 3.5 kHz) for the different rise time pulses is shown in Figure 4.8 (b). Skin depth value is calculated based on the Equation (1.2) with a conductivity value of  $1.34 \times 10^6 \text{ S/m}$  and relative permeability value of 1 at different frequency components in the excitation pulse. It is observed that the FFT amplitude of 1.0 ms rise time pulse is highest among all the other rise times and this

frequency range corresponds to a skin depth of 7.5-8.0 mm for stainless steel. The observed higher sensitivity of  $\tau$  at 1.0 ms excitation rise time is consistent with this observation.

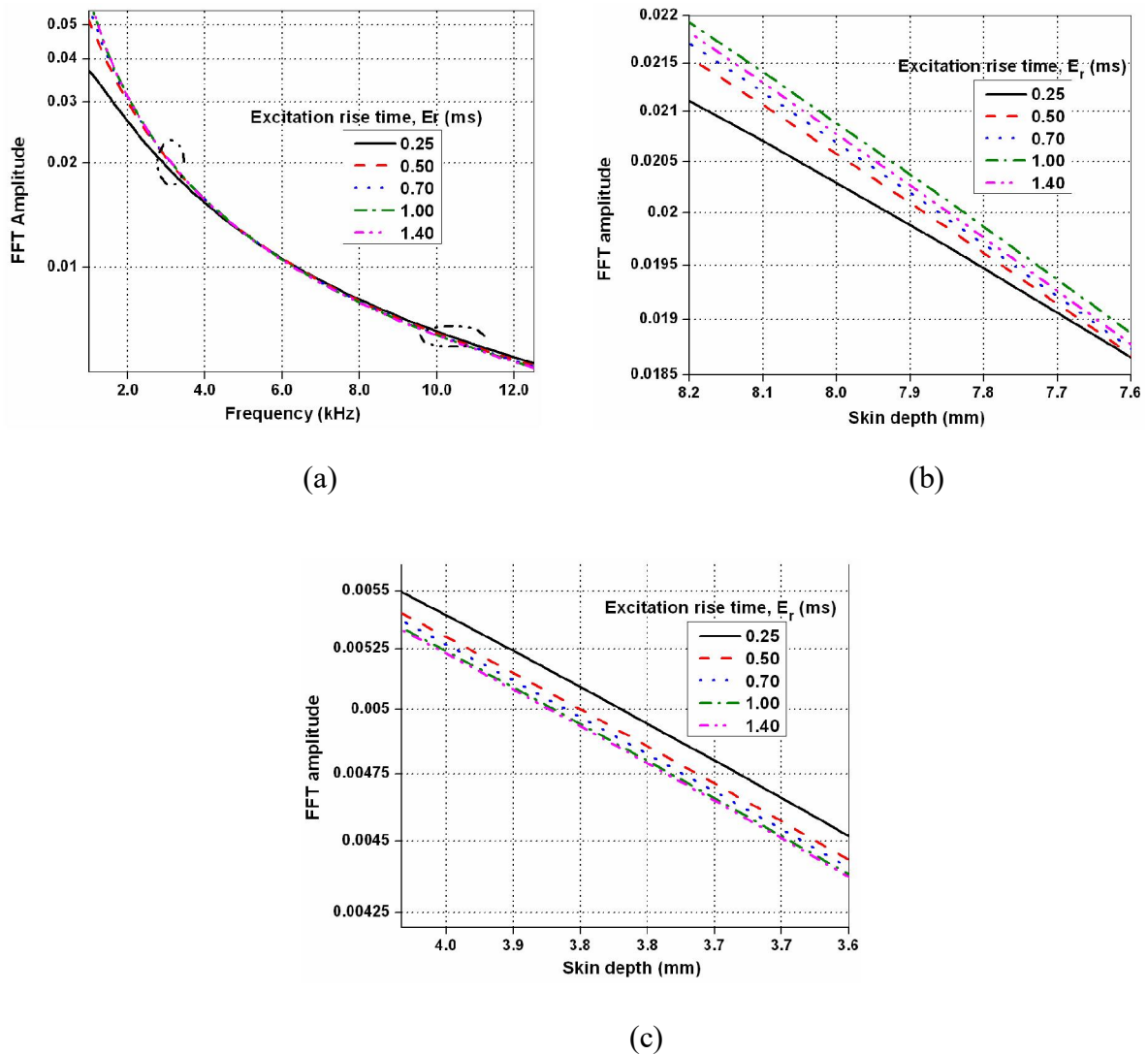


Figure 4.8. FFT amplitude for different excitation rise time pulses in the (a) 1 - 12 kHz range (b) 3 - 3.5 kHz in range (skin depth 7.6 to 8.2 mm) and (c) 10 -11 kHz in (skin depth 3.5 to 4.0 mm).

Similarly, the frequency range of 10.0 – 11.0 kHz corresponds to a skin depth range of 3.5-4.0 mm, and the variation of FFT amplitude with respect to skin depth is shown in Figure 4.8(c) for all the excitation rise time pulses. From Figure 4.8(c) it is observed that the FFT amplitude is highest in this skin depth range for the pulse with a rise time of 0.25 ms. The observed flaw depth detection using  $\tau$  (refer, Figure 4.5 (a)) is consistent with this finding.

From the results, it is clear that  $E_r$  of 1.0 ms has dominant low-frequency components which are useful to detect flaws in 8.0 mm thick SS components. This ensures improved sensitivity for  $\tau$  value and hence,  $E_r$  of 1.0 ms is found to be optimal for detection of flaws in 8.0 mm thick SS components. Studies also reveal that  $E_r$  of 0.25 and 0.5 ms are useful for detection of surface as well as near subsurface flaws up to a depth of 4.0 mm from the surface.

#### 4.5 Extraction of conventional PEC parameters

To compare the performance of the proposed technique, the traditional PEC time-domain signal parameters viz. peak amplitude ( $V_p$ ) and time-to-peak ( $T_p$ ) are extracted from difference PEC signals by subtracting fit reference signal from that of a fit flaw signals. The difference signals obtained for different excitation rise time pulses are shown in Figure 4.9. The maximum amplitude of the difference PEC signals is found to decrease with an increase in  $E_r$ . This is due to the decrease in the rate of change of current in the coil i.e. presence of low-frequency components in the pulse. From the difference PEC signals,  $V_p$  and  $T_p$  are determined. Variations of these parameters with flaw location below the surface are shown in Figure 4.10 for different  $E_r$  of the pulses. It is observed that for a given  $E_r$ ,  $V_p$  decreases with increase in flaw location below the surface (1.0 to 6.0 mm). On the contrary, the  $T_p$  is found to increase as expected. This is attributed to the contribution of the low-frequency components in the excitation pulse and phase lag of the eddy currents with an increase in flaw location below the surface.

It is observed from Figure 4.10 (a) and (b) that  $E_r$  of 0.25 ms and 0.5 ms,  $V_p$  and  $T_p$  values are seen saturated for the flaws located beyond 4.0 mm. However, for  $E_r$  of 0.7, 1.0, and 1.4 ms, these parameters are seen changing with respect to flaw location below the surface (up to 6.0 mm) which is in-line with proposed parameters behaviour as discussed in Figure 4.5 and Figure 4.6. Hence, for detection of flaws located beyond 4.0 mm below the surface, a minimum of 0.7 ms rise time pulse is required. Therefore, the proposed technique can be used effectively

for detection of flaws in electrically conductive materials by suitably tuning the excitation rise time.

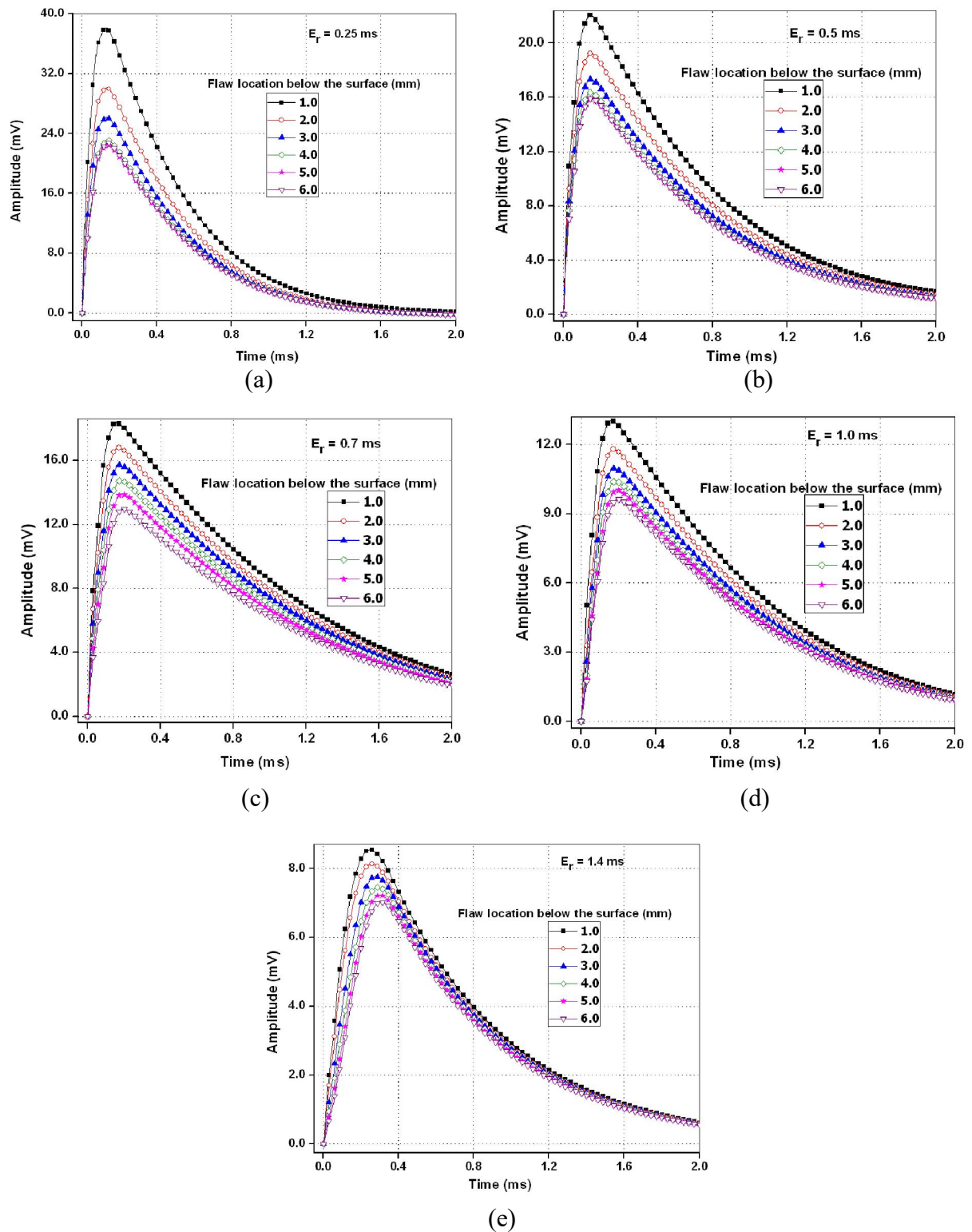


Figure 4.9. PEC differential signals for  $E_r$  of (a) 0.25 ms, (b) 0.5 ms, (c) 0.7 ms, (d) 1.0 ms and (e) 1.4 ms.

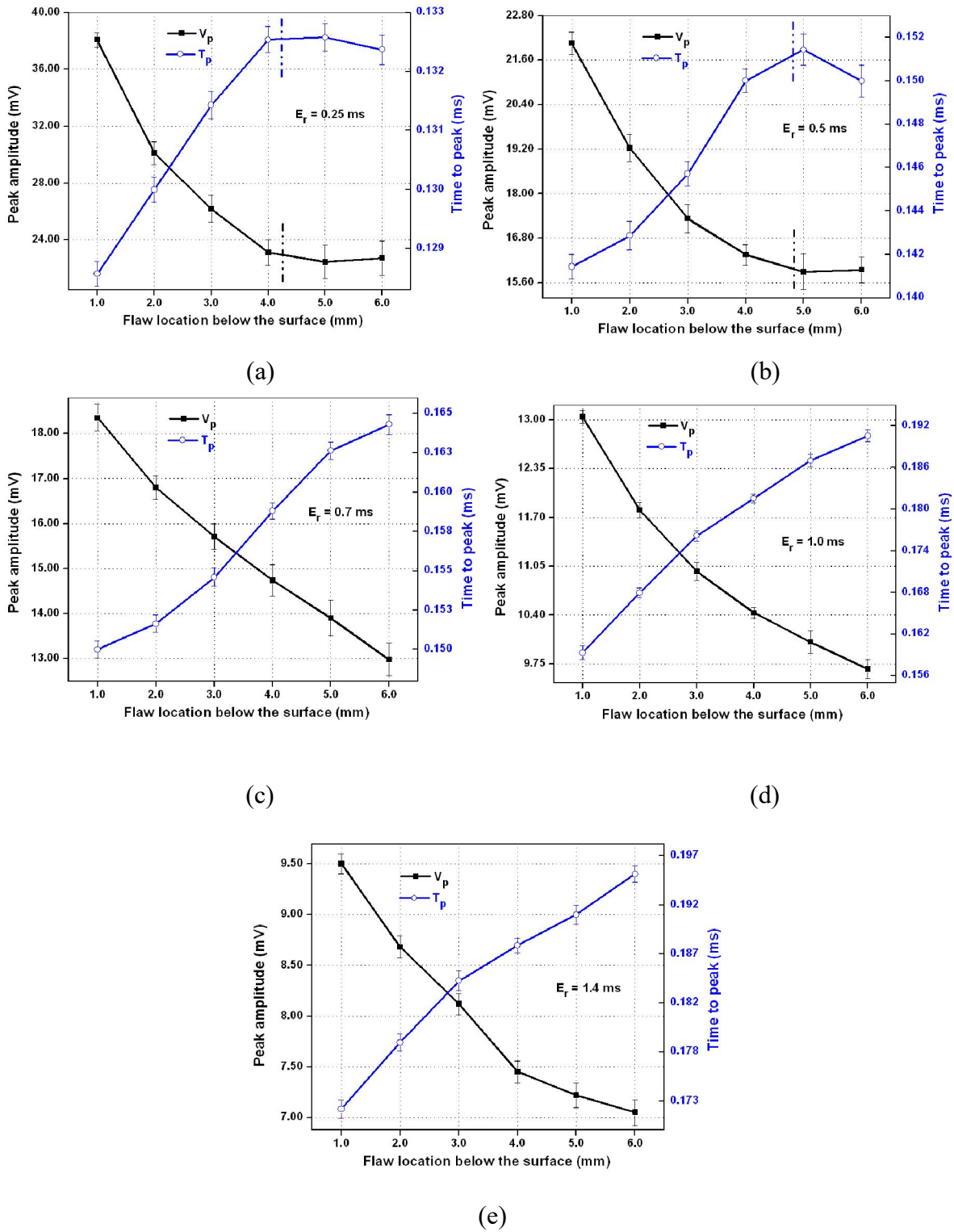
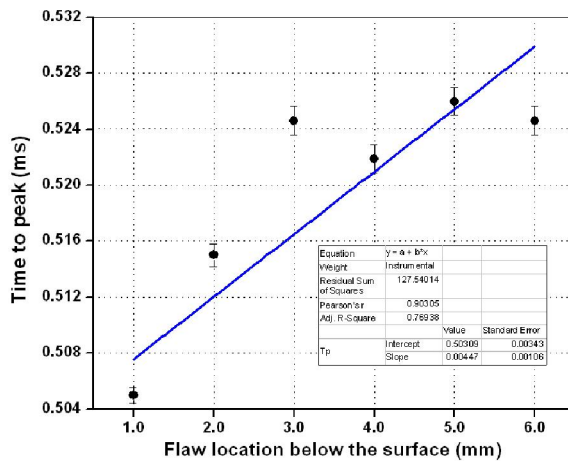


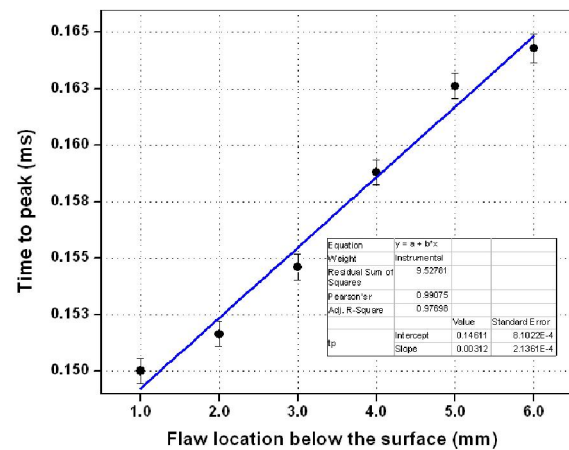
Figure 4.10. Peak amplitude and time-to-peak for  $E_r$  of (a) 0.25 ms, (b) 0.5 ms, (c) 0.7 ms, (d) 1.0 ms and (e) 1.4 ms as a function of location below the surface.

The variation of the flaw parameter  $T_p$  obtained from the conventional PEC technique (as discussed in Section 4.2) and the proposed technique (discussed in Section 4.5) with flaw location is shown in Figure 4.11 with a linear fit. From Figure 4.11 (a) it is observed that the  $T_p$  value obtained by the conventional technique is able to detect flaws located only up to 3.0 mm below the surface with a correlation coefficient value of 0.76938. However, from Figure 4.11 (b) the  $T_p$  values obtained from the proposed technique increases with respect to flaw location below the surface up to 6.0 mm with a correlation coefficient value of 0.97698 which is greater than the  $T_p$  value obtained by conventional method.

Therefore, the parameter  $T_p$  derived from the fit signals shows enhanced flaw detection sensitivity with higher correlation than that derived from direct subtraction (as received). Hence, with the proposed technique, even the conventional PEC signal parameters are also preserved irrespective of presence of noise in the measurements.



(a)



(b)

Figure 4.11. Comparison of time-to-peak parameter from (a) the conventional PEC technique and (b) the proposed technique.

## 4.6 Detection and classification of flaws

Previous sections focused only on detection of subsurface flaws. However in a component surface flaws also may be present. When a flaw is detected, it must be possible to classify whether the flaw is a surface or a subsurface, using certain signal parameters or processing techniques. The width of the flaws also affects the PEC signal parameters. Therefore, the following section describes the influence of width and location of the flaw on  $V_r$  and  $\tau$  for possible detection of surface flaws as well as classification of subsurface and surface flaws.

### 4.6.1 Dimensional details of flaws

Flaws with different widths viz.  $w = 1.0$  and  $3.0$  mm are selected in an  $8.0$  mm thick SS plate by keeping the other dimensions of the flaws similar to that mentioned in Section 4.2. Overall 24 different types of flaws are considered in this study. Out of them 12 are surface flaws, and the remaining 12 are subsurface flaws. The schematic of the test plate with EDM notches is shown in Figure 4.12. The PEC signals obtained for these flaws are analysed.

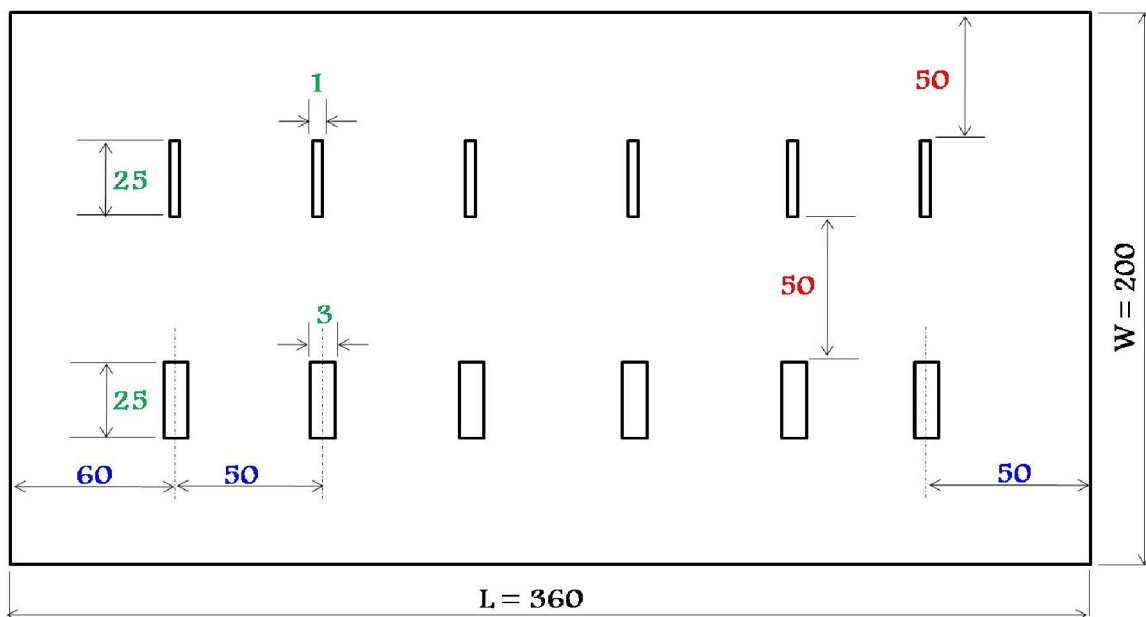


Figure 4.12. Schematic of a SS plate having surface flaws of two different widths.

#### 4.6.2 Detection of surface flaws

Figure 4.13(a) shows the variation of  $V_r$  with respect to the surface flaw depth (1.0 to 6.0 mm) for two different flaw widths (1.0 and 3.0 mm). The  $V_r$  is found to decrease with an increase in the flaw depth. As discussed in Section 4.3,  $V_1$  measures the resultant magnetic field due to induced eddy currents in the test plate. As a result, increase in surface flaw depth points to more volume loss and lesser induced eddy currents and hence, decrease in  $V_1$ . The  $V_r$  is found to be higher for 1.0 mm flaw width as compared to that of 3.0 mm. This is due to the fact that at a constant flaw dimensions, flaw width of 1.0 mm having less volume loss as compared to 3.0 mm flaw width.

Figure 4.13 (b) shows the variation of  $\tau$  for flaw depth. It can be observed that  $\tau$  value is found to decrease with an increase in flaw depth. This is essentially due to the attenuation of different frequency components for flaws located at different depths.

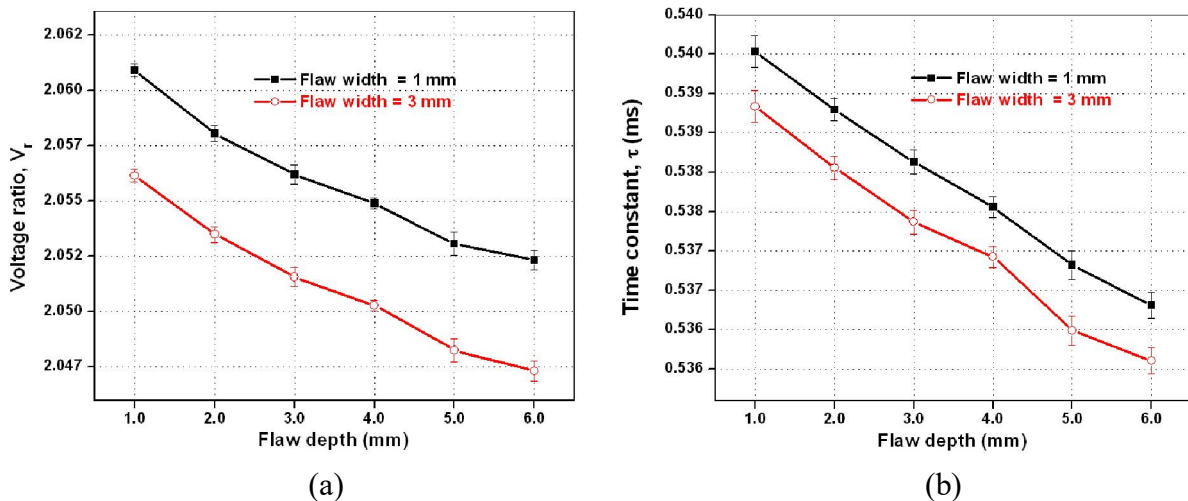


Figure 4.13. Variation of (a)  $V_r$  and (b)  $\tau$  with surface flaw depth (flaw width 1.0 and 3.0 mm).

### 4.6.3 Detection of subsurface flaws

PEC signals of subsurface flaws are detected by keeping the PEC probe over the inverted plate surface where the flaws opened to the opposite side. Figure 4.14 (a) shows the variation of  $V_r$  with flaw location below the surface (1.0 to 6.0 mm) for two different flaw widths (1.0 and 3.0 mm). As expected  $V_r$  is found to increase with increase in flaw location below the surface. Similarly, its value is higher for the flaw width of 1.0 mm than 3.0 mm as discussed in Section 4.6.2. Figure 4.14 (b) shows the variation of  $\tau$  with flaw location below the surface for two different flaw widths. As can be seen  $\tau$  increases with increase in flaw location below the surface and it is higher for 1.0 mm flaw width. Table 4.4 explains summarises parameters for surface and subsurface flaws.

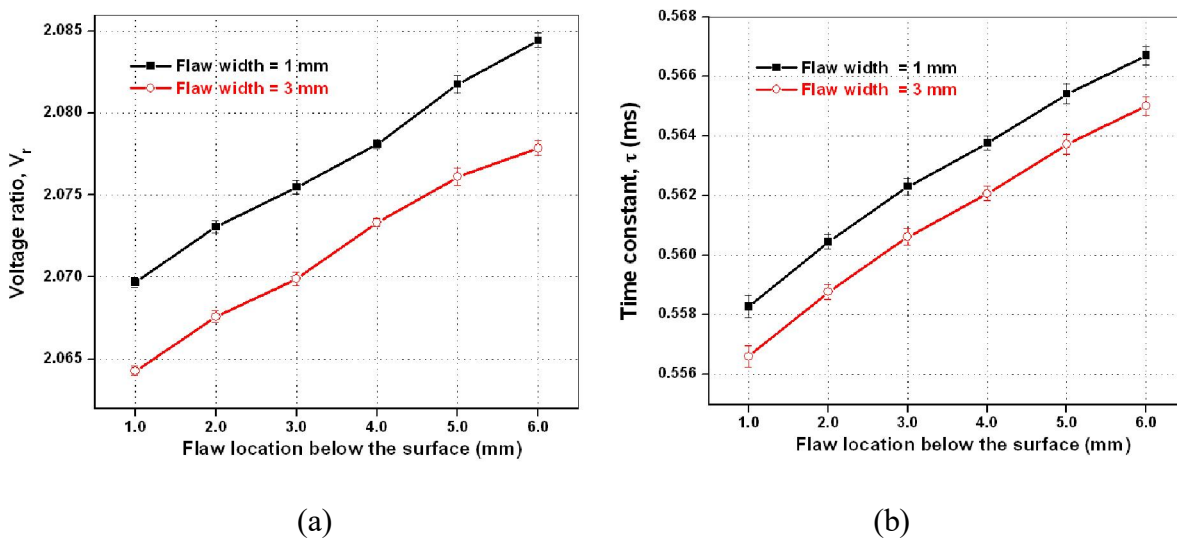


Figure 4.14. Variation of (a)  $V_r$  and (b)  $\tau$  with flaw location below the surface for two different flaw widths (1.0 and 3.0 mm).

Table 4.4. Variation of the fit parameters with flaws

Parameter	Surface flaws	Subsurface flaws	Description
$V_r$	Decreases with an increase in flaw depth	Increases with increase in flaw location below the surface	Depends on the amount of induced eddy currents in the plate
$\tau$	Decreases with an increase in flaw depth	Increases with increase in flaw location below the surface	Depends on the attenuation of frequency components and also variation mutual inductance between probe and flaws located in the plate

#### 4.6.4 Classification flaws

Based on the observed trends in  $V_r$  and  $\tau$ , possible classification of subsurface and surface flaw is studied. Figure 4.15 shows the plot between  $V_r$  and  $\tau$  for flaws with two different flaw widths. It can be seen from Figure 4.15 that the plot between  $V_r$  and  $\tau$  can be effectively used for classification of surface and subsurface flaws for both the widths (1.0 and 3.0 mm without any need for signal processing or statistical analysis.

The sensitivity of the voltage ratio and time constant are  $2.9 \text{ mm}^{-1}$  and  $1.43 \text{ } \mu\text{s}/\text{mm}$  respectively for subsurface flaws whereas it is  $1.6 \text{ mm}^{-1}$  and  $0.652 \text{ } \mu\text{s}/\text{mm}$  for surface flaws. The proposed technique is able to differentiate surface and subsurface flaws with a very good sensitivity for estimating the depth of the flaws. For quantitative NDE of flaws with different width, lengths and

the invariance of the derived parameters to variations in experimental conditions are to be addressed.

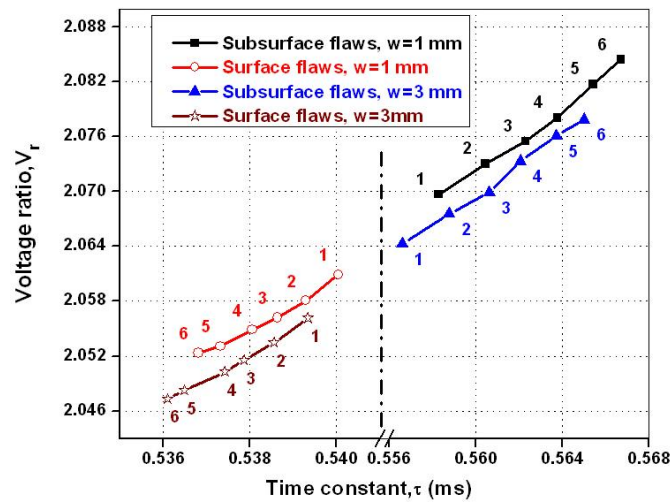


Figure 4.15. Classification of surface and subsurface flaws using a plot between  $V_r$  and  $\tau$ .

The studies carried out in this Chapter are the detection of flaws that occur due to localised corrosion in 8.0 mm SS plates only. Further, studies can be extended for detection and classification of flaws in higher thick plates ( $> 8.0$  mm) and other electrically conductive materials such as copper and aluminium.

## 4.7 Summary

To reduce influence of noise on PEC measurements to detect flaws located up to 6.0 mm below the surface, studies have been carried. The following observations have been drawn:

- ✓ A new technique has been proposed based on fitting the response pulse from a GMR sensor to a modified inductor current equation to extract two new PEC signal parameters viz. voltage ratio,  $V_r$  and time constant,  $\tau$ . Using these two parameters flaws located up to 6.0 mm below the surface has been detected.

- ✓ The two new parameters have been found to be superior to the traditional parameters namely,  $V_p$  and  $T_p$  which are able to detect flaws only up to 4.0 mm below the surface.
- ✓ A study has been carried out by varying the excitation rise time ( $E_r$ ) of the pulse in the range of 0.25, 0.50, 0.70, 1.00 and 1.40 ms for detection of flaws in 8.0 mm thick SS components.  $E_r$  of 1.0 ms has shown enhanced detection sensitivity for subsurface flaws while  $E_r$  of 0.25 and 0.5 ms appear good for detection of surface flaws.
- ✓ The proposed technique has been able to detect subsurface flaws as well as surface flaws.
- ✓ The experimental study clearly demonstrates that using a plot between  $V_r$  and  $\tau$  it is possible to classify subsurface flaws and surface flaws.
- ✓ The parameters  $V_r$  and  $\tau$  have shown a sensitivity of  $0.0029 \text{ mm}^{-1}$  and  $1.43 \text{ }\mu\text{s/mm}$  respectively for detection of subsurface flaws and a sensitivity of  $0.0016 \text{ mm}^{-1}$  and  $0.652 \text{ }\mu\text{s/mm}$  for surface flaws.

# **Development of technique for estimation of thickness reduction due to uniform corrosion**

---

# 5

## **5.1 Preamble**

PEC instrument and probe developed have been used for detection of uniform corrosion apart from detection of flaws due to localised corrosion. This chapter presents application of continuous wavelet transform (CWT) based technique to PEC signals for accurate estimation thickness reduction due to uniform corrosion in 8.0 mm thick stainless steel components.

## **5.2 Estimation of thickness reduction**

Previous chapter discussed the detection of flaws due to localised corrosion with the use of novel parameters  $V_r$  and  $\tau$ . Due to the presence of hostile corrosive environment, the components undergo uniform corrosion on the inner surface which leads to wall thickness reduction and likely a catastrophic failure. Therefore, this chapter deals with estimation of wall thickness reduction of SS components due to uniform corrosion for assessment of remaining life of the components. If the component is having wall thickness reduction more than 50 % then, in general the component is not continued to operate in nuclear applications. Therefore, the study focuses estimation of thickness of components. The PEC instrument and optimal probe have been used for estimation of thickness reduction in an 8.0 mm thick stainless steel plate. The details of the plate with thickness reduction ( $t_r$ ) from 3.0 to 0.0 mm are shown in Figure 5.1.

The PEC instrument and optimal probe have been used for estimation of thickness reduction in an 8.0 mm thick stainless steel plate. The details of the plate with thickness reduction are shown in Figure 5.1.

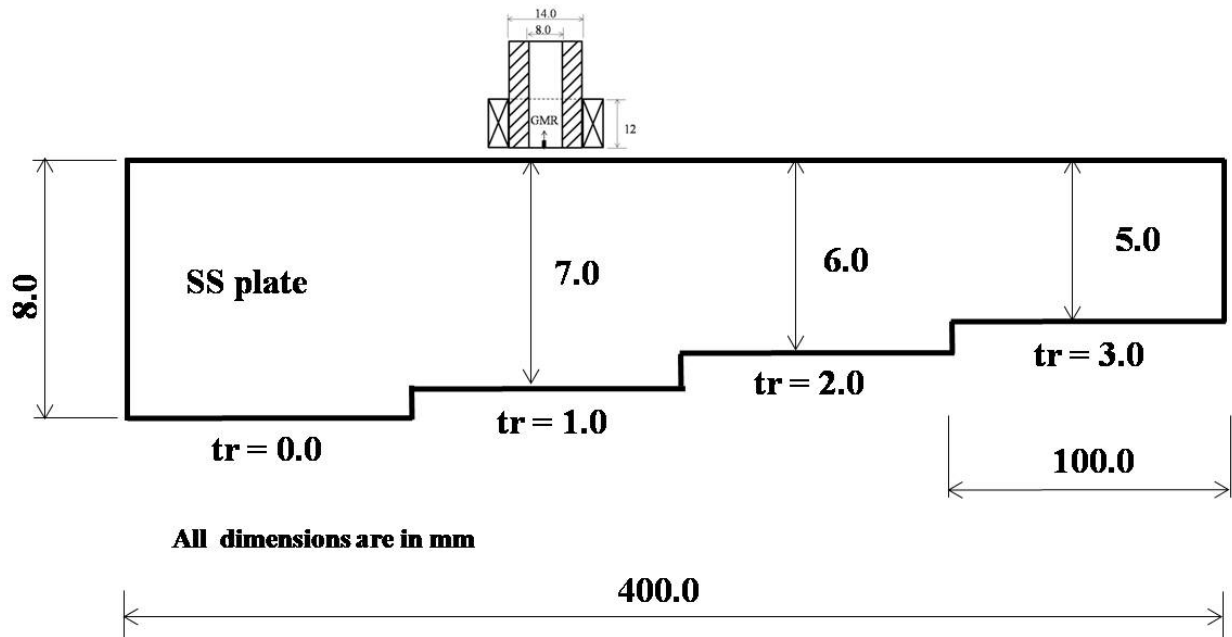


Figure 5.1. Simulated thickness reduction (tr) from 0.0 to 3.0 mm in an 8.0 mm thick SS plate.

The PEC probe is kept at the centre of each thickness region of test plate and the response signals are acquired. The experimental parameters are given in the Table 5.1. The PEC time-domain signals (absolute) obtained from the four thickness reduction are shown in Figure 5.2. It can be seen from the inset of Figure 5.2 that with decrease in thickness reduction of the plate, the response pulses are delayed due to phase lag of different frequency components and pulse broadening.

Table 5.1. Experimental test parameters

S. No.	Parameter	Value
1.0	Current	0.6 A
2.0	Pulse width	6.0 ms
3.0	PRF	100 Hz
4.0	$E_r$	1.0 ms
5.0	Lift-off	0.1 mm

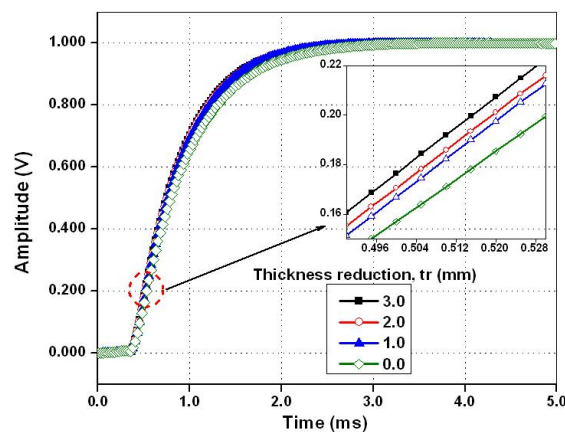


Figure 5.2. PEC signals obtained from different thickness reduction locations of the test plate.

Further, to estimate the thickness reduction of the component, the fit parameters  $V_r$  and  $\tau$  are determined by fitting the PEC signals to Equation 4.2 and the results are shown in Figure 5.3. It can be inferred from the Figure 5.3 that  $V_r$  and  $\tau$  increases with decrease in thickness reduction of the test plate, like in the case of subsurface flaws due to localised corrosion (refer Figure 4.2).

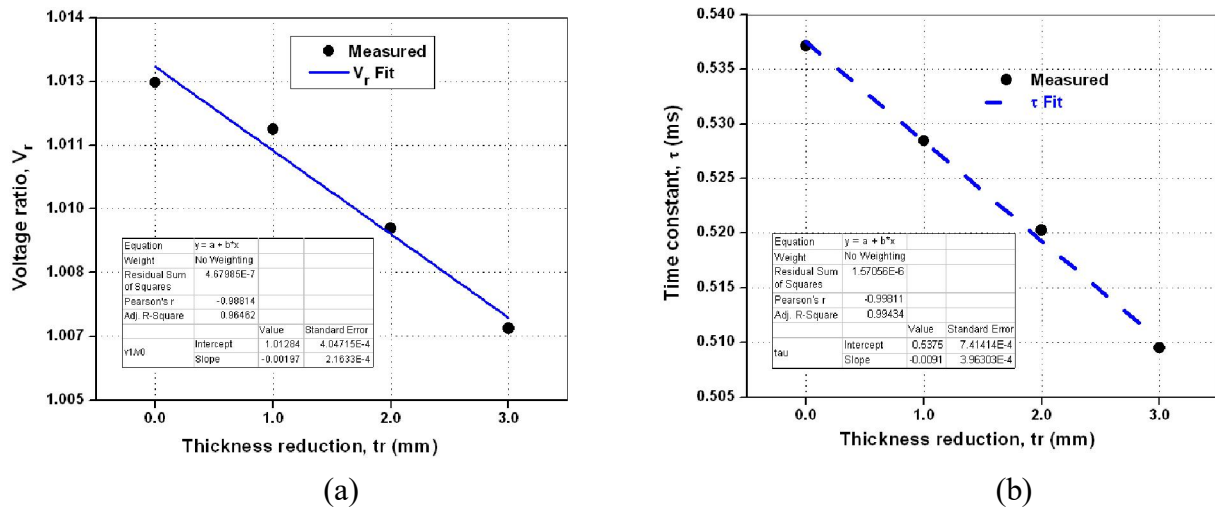


Figure 5.3. Variation of fit parameters (a) voltage ratio and (b) time constant with thickness.

The sensitivity of  $V_r$  and  $\tau$  are  $0.0019 \text{ mm}^{-1}$  and  $9.2 \text{ } \mu\text{s}/\text{mm}$  respectively as compared to  $0.0029 \text{ mm}^{-1}$  and  $1.43 \text{ } \mu\text{s}/\text{mm}$  respectively observed for subsurface flaws. The difference in sensitivity is due to the variation of volume loss in the test component. These results clearly demonstrate that  $V_r$  and  $\tau$  can be used for estimation of the wall thickness reduction of the components.

It is essential to study the influence of lift-off on estimation of thickness reduction because variation in lift-off causes change in electromagnetic coupling between the probe and the component leading to likely reduction in detection sensitivity. In order to study the effect of lift-off on  $V_r$  and  $\tau$ , experiments are carried out by varying lift-off ( $L$ ) on the test plate as shown in Figure 5.4. Here the thickness reduction of the plate is varied from 1.0 to 3.0 mm (thickness is from 7.0 to 5.0 mm) in an 8.0 mm thick SS plate and lift-off varied from 1.0 to 5.0 mm.

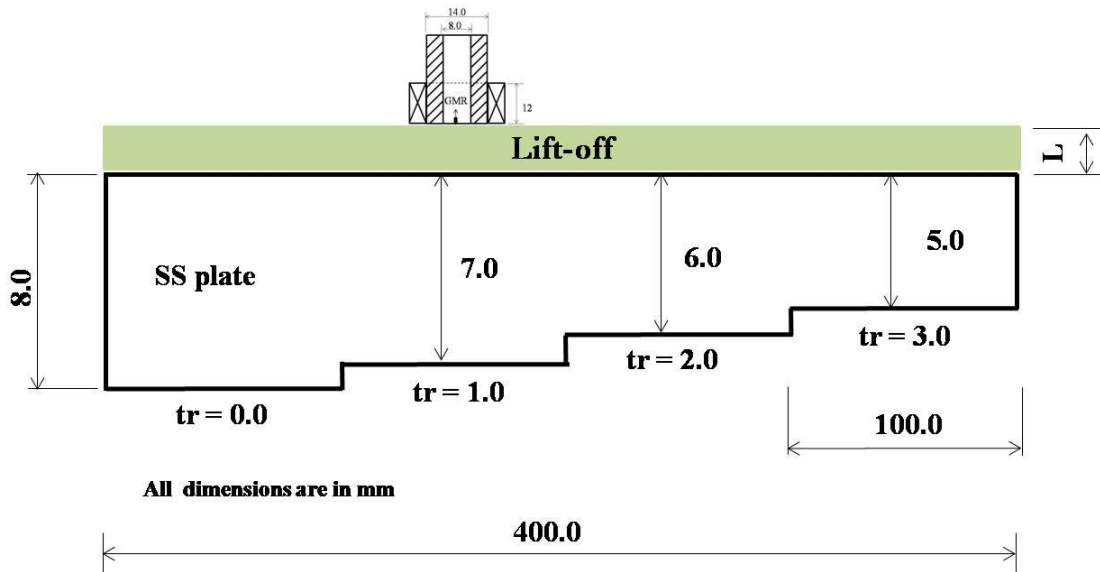


Figure 5.4. Simulated of the thickness reduction of the plate with lift-off (L).

Figure 5.5 shows the variation of  $V_r$  and  $\tau$  for different thickness reduction regions (0.0 mm to 3.0 mm) at varying lift-off (1.0 to 5.0 mm). As can be observed from Figure 5.5 (a), both  $V_r$  and  $\tau$  parameters are decrease with an increase in lift-off and increase with decrease in thickness reduction of the plate.

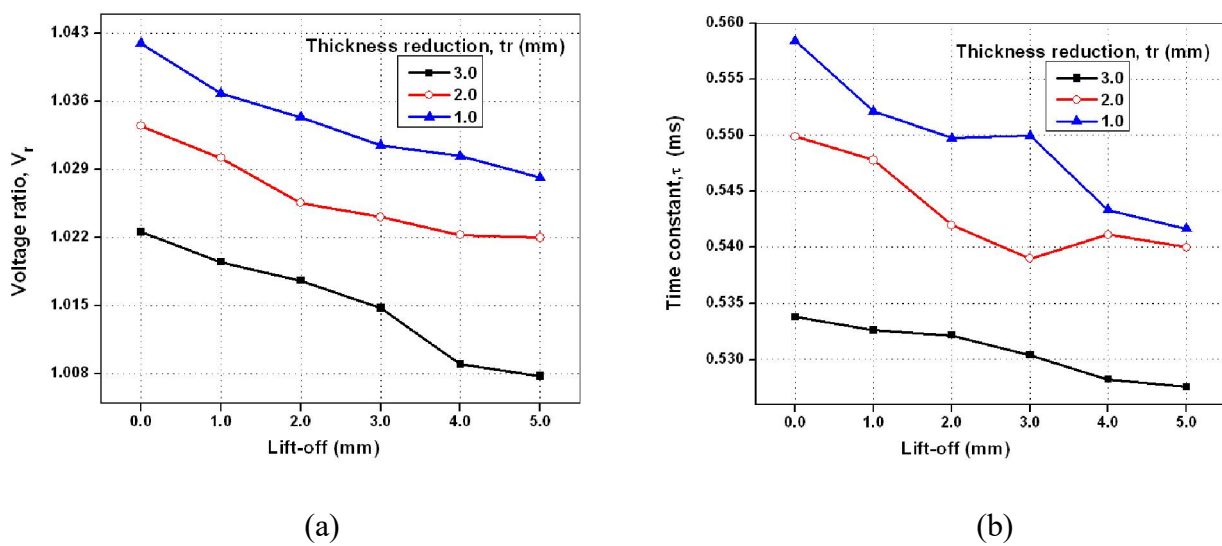


Figure 5.5. Variation of (a)  $V_r$  and (b)  $\tau$  with thickness at different lift-off.

These results reveal that thickness estimation is influenced by lift-off variations. The lift-off intersection (LOI) point is one of the time-domain parameter used to estimate thickness reduction independent of lift-off variation. However, this parameter cannot be extracted from the PEC signals obtained using GMR sensor as it measures the absolute field and not the rate of change. Computing the first order derivative is an option to overcome this problem as suggested by Tian *et.al.*[74]. However, this technique also suffers from limitations due to intrinsic noise present in the PEC signals resulting in non-unique LOI point [86,34]. Hence, there is a necessity to develop a new technique for accurate estimation of thickness reduction of components in the presence of lift-off variations.

As discussed earlier in Section 1.3, a pulse contains a continuum of frequencies; as a result electromagnetic response from a range of depths due to several frequencies can be obtained at once. The individual frequency components in a pulse are influenced differently in a test component with varying thickness due to the *skin-effect*. Especially, the low frequency components are selectively attenuated due to higher depth of penetration. This would cause minor variations in the time-domain parameters like the rise time or time-to-peak. The conventional time-domain parameters are not efficient to correlate well with thickness as they are influenced by many parameters. In this context, it would be beneficial to analyse the PEC signals in frequency-domain to perceive the changes in individual frequency components of the pulse with variation in thickness as well as lift-off.

### **5.3 Wavelet based technique proposed**

Fourier transform is the most widely used technique to analyze signals in frequency domain. However, it provides only frequency components present in the signal and the time information is not available. Lacks of temporal capability of Fourier transform can be overcome by windowed short time Fourier transform (STFT). However, the STFT has problem in selection of

window size i.e. narrow window give good time resolution, but poor frequency resolution and vice versa. Other alternative is wavelet transform technique.

Wavelet transform technique has gained a widespread use in numerous applications in NDT [92,93] and speech recognition etc.[94]. The fundamental idea behind the wavelet transform is to exploit both time and scale (i.e. frequency) aspects simultaneously. Therefore, both gross and fine features of a signal are obtained. The continuous wavelet transform (CWT) of a time domain signal  $x(t)$  is defined as:

$$X_w(s, b) = \frac{1}{\sqrt{s}} \int_{-\infty}^{\infty} x(t) \psi^* \left( \frac{t-b}{s} \right) dt \quad 5.1$$

where

$\psi(t)$  is the mother wavelet which is continuous in both time and frequency domains,

$b$  is the translation factor that depends on time and

$s$  is the scale factor which is a function of frequency.

From the mother wavelet daughter wavelets are derived by varying the scaling factor ( $s$ ). Therefore, the frequency bandwidths of daughter wavelets are different from one another. The CWT coefficients  $X_w(s, b)$  are obtained by cross-correlation of  $x(t)$  with different daughter wavelets. From equation (5.1), for every  $b$  and  $s$  values, there is a wavelet coefficient representing how much a daughter wavelet is similar to the function at time,  $t$ . It must be noted here that high scaling factors would extract low frequency components whereas low scaling factors would extract high frequency components[95].

The interesting aspect of wavelet transform is that it offers good time resolution for high frequency components. This aspect would be advantageous to observe the selective attenuation of certain frequency components due to *skin effect*. With the above mentioned features of the

CWT technique, it has been chosen for analysing PEC signals in time-frequency domain. Among the family of wavelets the Mexican hat showed better correlation with the PEC signals and hence, chosen as the mother wavelet.

The flow chart of the CWT based technique is shown in Figure 5.6. Here the reference signal ( $R(t)$ ) is obtained by keeping the PEC probe in air. Test signals ( $T(t)$ ) are obtained from a plate at constant thickness reduction with variable lift-off. PEC difference (input) signals are obtained by subtracting the test signals from that of the reference signal. CWT is applied to the input signals to obtain wavelet coefficients which represent the percentage of energy at each time-scale values. From the time-scale matrix, the frequency parameter is extracted based on the maximum coefficient value. The frequency at which the coefficient value is maximum is called the peak frequency ( $F_p$ ). A calibration graph between  $F_p$  and thickness reduction in plate is obtained at different lift-off and  $F_p$  is used for estimation of thickness reduction in components.

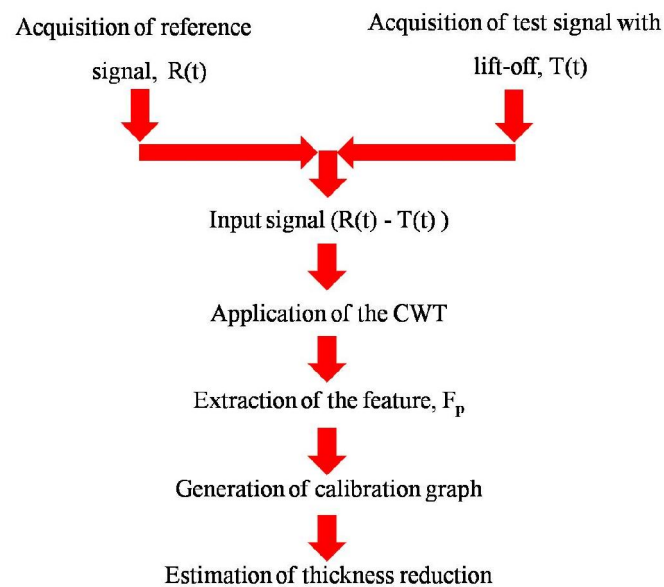


Figure 5.6. Flow chart of the proposed CWT based technique.

## 5.4 Performance evaluation of the proposed technique

Experiments are carried out to validate the performance of the proposed technique. Figure 5.7 shows the CWT spectrogram for PEC signals for three lift-off values viz., 1.0, 3.0 and 5.0 mm on a 6.0 mm thick SS plate. As can be observed from the results, the maximum intensity of the plot decreases with increase in lift-off and its location moves along the time axis. However, there is no shift in the location of the peak in the frequency axis. This result establishes that the peak-frequency parameter is independent of lift-off.

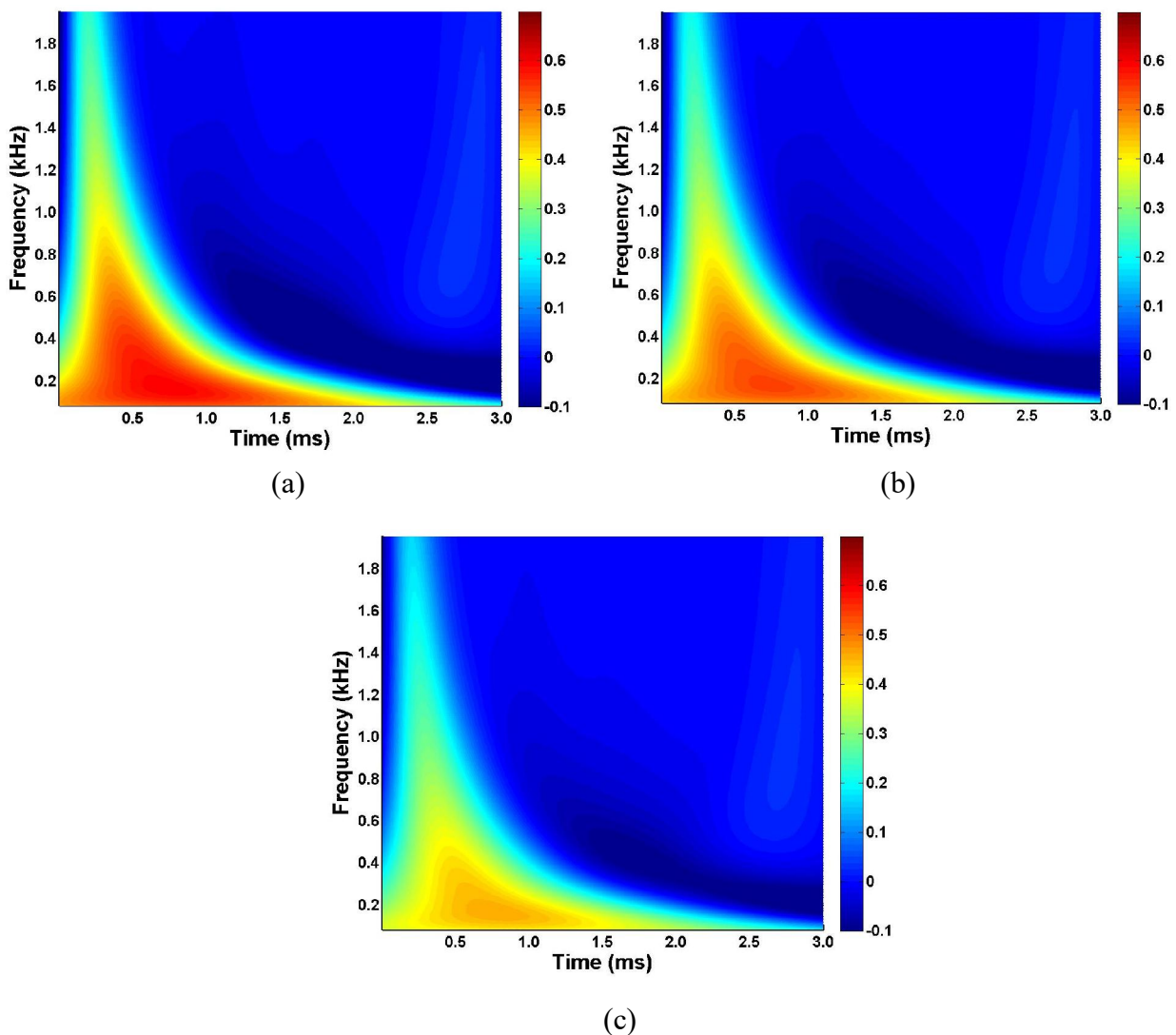


Figure 5.7. CWT of PEC signals from a 6.0 mm thick plate at lift-off of (a) 1.0 mm (b) 3.0 mm and (c) 5.0 mm.

Further, the thickness reduction of the test plate is varied from 1.0 mm to 3.0 mm at a constant lift-off of 3.0 mm. The CWT spectrograms of three thickness reduction (tr) i.e. 1.0, 2.0 and 3.0 mm is shown in Figure 5.8. It is observed that the intensity value decreases with an increase in thickness reduction of the plate and also its location shifts along the time axis with an increase in frequency. Therefore, from the Figure 5.7 and Figure 5.8 the proposed parameter  $F_p$  is not influenced by the lift-off variations (1.0 to 5.0 mm) and it increases with an increase in thickness reduction (1.0 to 3.0 mm) of the SS plate.

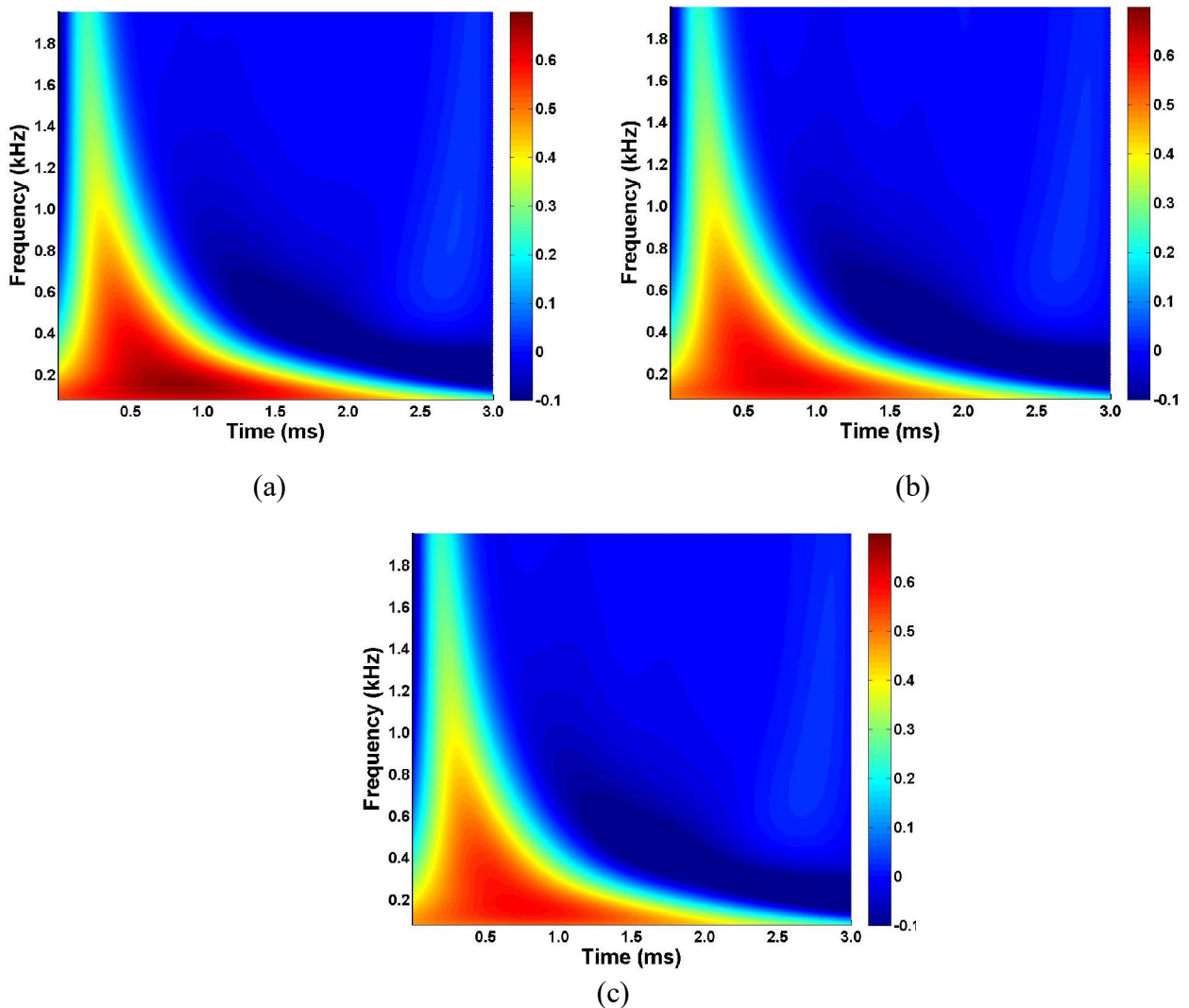


Figure 5.8. CWT of PEC signals for a thickness reduction of (a) 1.0 mm (b) 2.0 mm and (c) 3.0 mm at a constant lift-off of 3.0 mm.

These observations are in-line with that reported by Yin *et al.* [96]. They observed the existences of a peak frequency as the imaginary part of the inductance is zero for the limiting cases of frequency ( $f$ ) = 0 and  $\infty$ . The reason for this behavior is attributed the selective attenuation of certain frequency components of the pulse due to the *skin-effect*. Interestingly  $F_p$  and the imaginary part of the inductance of the probe do not change when the probe is placed on a non-magnetic metallic plate which is covered with non-magnetic and non-conductive materials i.e. lift-off and increases with increase in thickness reduction of the test component. Thus,  $F_p$  is promising parameter to estimate thickness of SS components in the presence of lift-off variations.

Figure 5.9 shows the variation of  $F_p$  with respect to lift-off (1.0 to 5.0 mm) for thickness of the plate ranging from 5.0 mm to 7.0 mm. It is inferred from Figure 5.9 (a) that the  $F_p$  value is independent of lift-off and decreases with increase in the thickness of the plate from 5.0 to 7.0 mm. Results clearly reveal that the peak frequency parameter is not influenced by lift-off and it is decreases with increase in thickness of the plate. Figure 5.9(b) shows the results corresponding variation of  $F_p$  with thickness to a lift-off values of 3.0 mm and 5.0 mm.

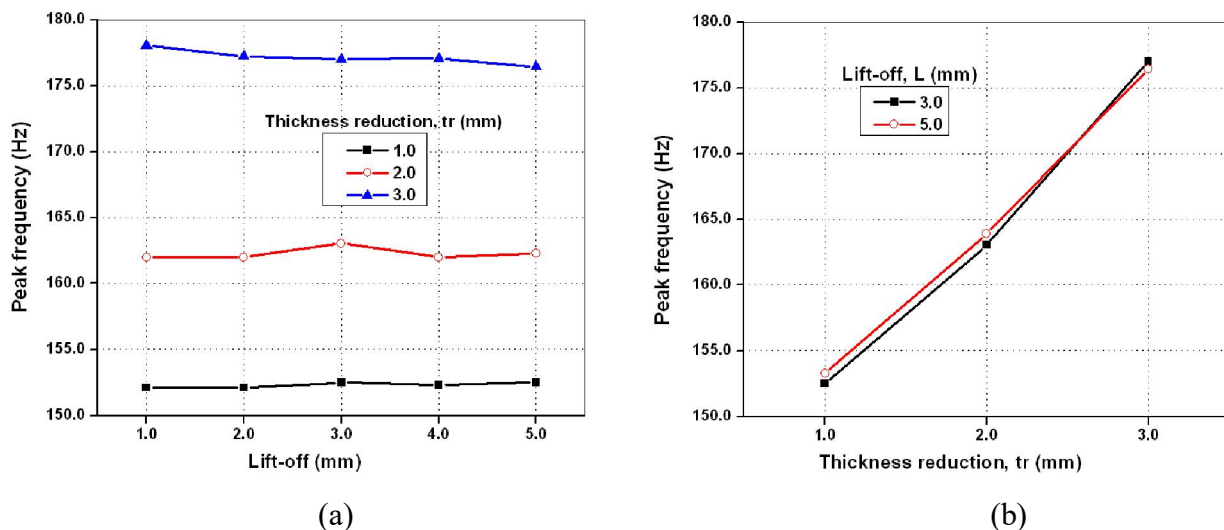


Figure 5.9. CWT results for (a)  $F_p$  vs. lift-off for different thickness and (b)  $F_p$  vs. thickness for two different lift-offs.

A linear relationship exists with thickness reduction and the peak frequency parameter. Figure 5.9(b) can be used as calibration graph and for estimating thickness reduction in an installed SS component. The sensitivity of the  $F_p$  is 13 Hz/mm for thickness reduction of 1.0 to 3.0 mm in the component. Therefore, the  $F_p$  derived by the CWT technique is showed enough sensitivity for estimating thickness reduction of the component in the presence of varying lift-off.

### 5.5 Comparison the proposed parameters

The performance of the three new parameters proposed in this thesis i.e.  $V_r$ ,  $\tau$  and  $F_p$  are compared. For this, PEC signal are obtained from a constant thickness region of 6.0 mm and at different lift-offs of 1.0 to 5.0 mm. Table 5.2 shows the results.

Table 5.2. Comparison of the parameters at constant thickness (6.0 mm) for different lift-off

Lift-off (mm)	$V_r$	$\tau$ (ms)	$F_p$ (Hz)	Estimated thickness (mm)
1.0	1.033	0.5499	162.337	5.973
2.0	1.030	0.5478	162.337	5.973
3.0	1.025	0.5419	163.185	6.044
4.0	1.024	0.5411	162.337	5.973
5.0	1.022	0.5389	163.185	6.044

The fit parameters  $V_r$  and  $\tau$  are changing with change in lift-off. However, the variation of  $F_p$  is negligible with respect to lift-off as compared with other parameters. Therefore,  $F_p$  can be used for accurate estimation of thickness of the components in the presence of lift-off variations up to 5.0 mm. This chapter focuses only on detection of flaws due to uniform independent of lift-

off variations. The technique can also be applicable for detection of flaws. However, the parameter  $F_p$  is not changing linearly with subsurface flaw depth. A stepping behavior is observed. To understand this behavior further detailed study is required.

The technique in Chapter 4 is used for detection of flaws due to localised corrosion. The proposed technique in Chapter 4 can also be applicable for estimation thickness reduction only. However, lift-off is a parameter which will affect PEC time domain signal parameters. Hence, for accurate estimation of thickness reduction of the component independent of lift-off variation the parameters  $V_r$  and  $\tau$  are not suitable. To understand this behavior further, detailed study is required.

## 5.6 Summary

Lift-off influences accurate estimation of thickness reduction of components due to uniform corrosion. To reduce the influence of lift-off on PEC time-domain parameters for accurate estimation of thickness reduction, studies have been carried and the following observations have been made.

- ✓ The fit parameters viz.,  $V_r$  and  $\tau$  can be effectively used for estimating thickness under constant lift-off conditions. However, they are limited to conditions when the lift-off varies with position.
- ✓ The novel peak frequency ( $F_p$ ) parameter derived from the CWT spectrograms of PEC signals are useful for accurate estimation of thickness reduction of the components even in the presence of lift-off variations.
- ✓ The parameter  $F_p$  has been found to be less influenced by lift-off variations and correlate well with the thickness reduction.

- ✓ Experimental results demonstrate that  $F_p$  is able to estimate the thickness reduction in thick SS components even in the presence of lift-off up to 5.0 mm.

# 6

## Conclusion and future work

---

The thesis has focused studies on the development of a PEC system that includes a PEC instrument, optimal send-receive type probe configuration and techniques for detection of flaws that occur due to localised corrosion as well as uniform corrosion in thick AISI stainless steel components. Through extensive FE simulations and experimental studies in SS plates having machined flaws, the thesis has demonstrated the possible approaches for detection of flaws due to localised corrosion and wall thickness reduction due to uniform corrosion in thick stainless steel components. The major conclusions drawn from these studies are:

### 6.1 Conclusions

- ✓ The pulsed eddy current instrument designed and developed has shown the capability to deliver a variable current (in the range from 0.2 A to 7.0 A) based on MOSFET switching logic and a variable high gain (up to 60.0 dB) receiver unit has been designed and developed along with a variable cut-off frequency low-pass filter and a high dynamic range data acquisition unit.
- ✓ Based on the finite element model predictions and experimental studies, a send-receive type PEC probe having an outer diameter of 20.0 mm and a height of 12.0 mm with a GMR sensor at the center measuring z-component ( $B_{zc}$ ) is found optimal for detection of localized flaws located up to 7.0 mm below the surface.
- ✓ A new technique has been proposed based on the application of modified inductor current equation to the PEC signals from a GMR sensor.

Two novel flaw parameters viz. voltage ratio,  $V_r$  and time constant,  $\tau$  have been proposed, for the first time.  $V_r$  and  $\tau$  have been found to increase with increase in subsurface flaws while they decrease for surface flaws. These parameters have been found to superior to the traditional PEC signal parameters viz. peak amplitude ( $V_p$ ) and time-to-peak ( $T_p$ ). A plot of  $V_r$  and  $\tau$  enables classification of surface flaws and subsurface flaws. The parameters  $V_r$  and  $\tau$  have shown a sensitivity of  $0.0029 \text{ mm}^{-1}$  and  $1.43 \text{ } \mu\text{s}/\text{mm}$  respectively for detection of subsurface flaws whereas  $0.0016 \text{ mm}^{-1}$  and  $0.652 \text{ } \mu\text{s}/\text{mm}$  for surface flaws. The advantage of the proposed technique is that it doesn't require either a reference signal for subtraction or signal processing techniques for detection of flaws.

- ✓ Excitation rise time ( $E_r$ ) optimisation studies have been carried out for the first time. Results revealed that the detection sensitivity for subsurface flaws is highest for  $E_r$  at 1.0ms. The enhanced sensitivity for flaw detection is due to fact that the availability of low frequency components in the excitation pulse to interact with flaws located at deeper locations.
- ✓ A novel parameter called peak frequency  $F_p$  derived from continuous wavelet transform (CWT) spectrogram to PEC signals has been proposed, for the first time, in PEC technique for estimation of thickness reduction in SS components due to uniform corrosion in the presence of lift-off variations. Results clearly establish that the parameter is able to estimate thickness reduction of the component range from 5.0 to 7.0 mm in the presence of lift-off up to 5.0 mm. This parameter is found to be superior to PEC parameters viz.  $V_p$ ,  $T_p$  and LOI.

The techniques presented in this thesis demonstrate that a synergistic combination of PEC instrument, optimal probe configuration and new signal parameters are essential for detection and classification of flaws located up to 7.0 mm below the surface in 8.0 mm thick austenitic stainless steel components. The studies establish a possible way to assess the structural integrity of nuclear waste storage tanks made of austenitic stainless steels.

## 6.2 Future works

The studies carried out and the results obtained in this thesis have contributed significantly to enhancement on pulsed eddy current systems, especially for detection of flaws that occur due to localised corrosion and uniform corrosion in thick stainless steel components. The developed PEC instrument, probe, and techniques have demonstrated the capability to detect and classify flaws located up to 7.0 mm below the surface. It is worth exploring the instrument and probe development for detection of corrosion in the second and third layer of aircraft multilayer structures.

Further, research needs to be carried out to improve the performance of the PEC system. For example the excitation unit in PEC instrument works on constant voltage mode. The induced voltage in the pickup sensor may change with varying lift-off and heating losses in the excitation coil. It may be beneficial to design an excitation unit with a constant current source to obtain meaningful results with less errors and better repeatability.

In this thesis, the optimal probe diameter is found to be 20.0 mm for an AISI 304L stainless steel plate of 8.0 mm thickness. For other thicknesses and conductivity of components, optimal diameter and height is expected to change. Hence, it may be beneficial to investigate further and

establish a relationship among probe dimensions, component thickness, conductivity and permeability of the component for better applicability of the ferrite core send-receive type PEC probe for various applications.

In the present study, flaw depth and location are only considered for checking the performance of the optimal probe configuration, its dimensions and the PEC instrument. However, width and length of the flaws are also expected to affect probe optimisation and detection sensitivity. Hence, it may be worth to carry out more model based studies and experiments.

The parameters  $V_r$  and  $\tau$  are used for detection and classification of flaws due to localised corrosion. However, studies need to be focused on detection of embedded flaws in the components using these parameters. The excitation rise time of the pulse ( $E_r$ ) is optimised for an 8.0 mm thick SS component. It may be beneficial to optimise  $E_r$  for other conductive materials based on the thickness and conductivity.

The novel parameter i.e. peak frequency ( $F_p$ ) is used for estimation of thickness reduction of the component due to uniform corrosion in the presence of lift-off variations. However, it is essential to attempt detection of flaws due to localised corrosion.

For optimisation of the probe configuration, a 2D axisymmetric FE model is used as execution times are larger. These model predictions are sufficient to optimise excitation coil diameter and sensor location. But the model does not consider the flaw orientation and localised flaws which are likely to influence the PEC results significantly in real situation. Hence, use of 3D finite element models will be beneficial to study the influence of localised and directional oriented flaws.

In this study surface curvature of the storage vessels is approximated to a planar geometry due to the large diameter of the component ( $\sim 10.0$  m). It will be useful to test the PEC probes on actual components and design suitable curved front face to minimise the electromagnetic coupling issues.

In order to enhance the information obtained from the component and to improve the inspection efficiency, the use of array of sensors could be investigated in future. The research can also lead to application of concepts such as data fusion of sensors data in an integrated manner to generate flaw information in a comprehensive manner. Potentially this will reduce the inspection time and costs.

Adopting image fusion techniques that superimpose different magnetic fields i.e.  $B_z$  and  $B_r$  around the probe may enhance the detection sensitivity of flaws that are inclined to surface.

PEC technique is a potential electromagnetic tool for assessing the material integrity by multiple frequencies at one go. Remote field is a well suited technique for NDT of ferromagnetic tubes. Pulsed remote field eddy current (PRFEC) technique maybe attractive for quantitative characterization of flaws in ferromagnetic tubes.

---

## References

- [1] Don E. Bray and Roderic K. Stanley, *Nondestructive evaluation: a tool for design.*: CRC Press Inc., 1989.
- [2] Charles J. Hellier, *Handbook of nondestructive evaluation.*: McGrawHill, 2001.
- [3] B. P. C. Rao, *Practical eddy current testing.*: Alpha Science Int'l Ltd, 2007.
- [4] P.J. Shull, *Nondestructive evaluation: theory, techniques and applications.*: New York: Marcel Dekkar Inc., 2002.
- [5] M.R. Clark, D.M. McCann, and M.C. Forde, "Application of infrared thermography to the non-destructive testing of concrete and masonry bridges," *NDT&E Inter.*, vol. 36, pp. 265-275, 2003.
- [6] O.P. Moore and S. Udpa, *Nondestructive Testing Handbook, Vol. 5 – Electromagnetic Testing 3rd ed.*, Columbus, OH: ASNT Edition, ed., 2004.
- [7] Ali Sophian, Gui Yun Tian, David Taylor, and John Rudlin, "Design of a pulsed eddy current sensor for detection of defects in aircraft lap-joints," *Sensor. Acuat.A-Phys.*, vol. 101, no. 1, pp. 92-98, 2002.
- [8] H. L. Libby, *Introduction to Electromagnetic Nondestructive Test Methods.*: New York John Wiley-: Interscience, 1971.
- [9] H. Hoshikawa, R. M. Li, and N. Ida, "Finite element analysis of eddy current surface probes," *Review of Progress in Quantitative Nondestructive Evaluation*, vol. 3A, pp. 675-682, 1984.
- [10] B. Sasi, B. P. C. Rao, S. Thirunavukkarasu, T. Jayakumar, and Baldev Raj, "Eddy Current-Giant Magneto-Resistive (GMR) Sensor for Nondestructive Detection of Deep-surface Defects," in *12th National seminar on Physics and Technology of Sensors*, Mumbai, 2007, pp. 273-275.
- [11] B.A. Lepine, J.S.R. Giguere, D.S. Forsyth, J.M.S. Dubois, and A. Chahbaz, "Applying PEC NDT to the aircraft hidden corrosion problem," in *5th NASA/FAA/DoD Conf. Aging Aircraft*, Orlando, 2001.
- [12] John C. Moulder, Jay A. Bieber, W.W. Ward Iii, and James H. Rose, "Scanned pulsed eddy current instrument for nondestructive inspection of aging aircraft," in *International Society for Optics and Photonics*, 1996, pp. 2-13.
- [13] R.A. Smith and G.R. Hugo, "Transient eddy current NDE for ageing aircraft-capabilities and limitations," *Insight: Non-Destructive Testing and Condition Monitoring*, vol. 43, no. 1, pp. 14-25, 2001.
- [14] Robert A. Smith and Geoffrey R. Hugo, "Deep corrosion and crack detection in aging aircraft using transient eddy current NDE," , 2001.

- [15] A. Lopes Ribeiro and H. Geirinhas Ramos, "Inductive probe for flaw detection in non-magnetic metallic plates using eddy currents," in *Instrum. Meas. Technol.*, 2008, pp. 1447-1451.
- [16] P.Y. Joubert, E. Voure'h, Alan Tassin, and Yohan Le Diraison, "Source separation techniques applied to the detection of subsurface defects in the eddy current NDT of aeronautical lap-joints," *NDT&E. Int.*, vol. 43, no. 7, pp. 606-614, 2010.
- [17] C. J. Renken, "The use of a personal computer to extract information from pulsed eddy current tests," *Mater. Eval.*, vol. 59, no. 3, pp. 356-360, 2001.
- [18] Young-Kil Shin, Dong-Myung Choi, Young-Joo Kim, and Seung-Seok Lee, "Signal characteristics of differential-pulsed eddy current sensors in the evaluation of plate thickness," *NDT&E. Int.*, vol. 42, no. 3, pp. 215--221, 2009.
- [19] W.E. Deeds and C.V. Dodd, "Determination of multiple properties with multiple eddy-current measurements," *Int. Adv. Nondestr. Test.*, vol. 8, 1981.
- [20] Thierry Clauzon, Frederic Thollon, and Alain NicolaS, "Flaws characterization with pulsed eddy currents NDT," *IEEE. Trans. Magn.*, vol. 35, no. 3, pp. 1873-1876, 1999.
- [21] L.M. Vallese, "Diffusion of pulsed currents in conductors," *J. Appl. Phys.*, vol. 25, pp. 225-228, 1954.
- [22] Ilham Zainal Abidin, Catalin Mandache, Gui Yun Tian, and Maxim Morozov, "Pulsed eddy current testing with variable duty cycle on rivet joints," *NDT&E. Int.*, vol. 42, no. 7, pp. 599-605., 2009.
- [23] D.L. Waidelich, "Measurement of coating thicknesses by use of pulsed eddy currents," *Mater. Eval*, vol. 14, pp. 14-16, 1956.
- [24] G. Witting, H.M. Thomas, and D. Maser, "Developments and investigations for the application of the pulsed eddy current technique, New Procedures in Nonde structive Testing," , 1983, pp. 479-488.
- [25] Allen Sather, "Investigation in to the depth of PEC penetration, Eddy current characterization of materials and structures," ASTM STP, pp. 374-386 , 1981.
- [26] B. Allen, N. Ida, and W. Lord, "Finite element modeling of pulse eddy current NDT phenomena," *IEEE. Trans. Magn.*, vol. 21, no. 6, pp. 2250-2253, 1985.
- [27] M. Luloff, J. Morelli, and T.W. Krause, "Finite Element Modelling of Conventional and Pulsed Eddy Current Probes for CANDU® Fuel Channel Inspection," in *Comsol*, Boston, 2014, pp. 1-5.
- [28] R.A. Smith, D. Harrison, and J. Skramstad, "Enhanced detection of deep corrosion using transient eddy currents," in *7th Joint DoD/FAA/NASA Conference on Aging Aircraft*, New Orleans, 2003.
- [29] Gui Yun Tian and Ali Sophian, "Study of magnetic sensors for pulsed eddy current techniques," *Insight-Non-Destructive Testing and Condition Monitoring*, vol. 47, no. 5, pp. 277-279, 2005.
- [30] MB Kishore et al., "Detection of Deep Subsurface Cracks in Thick Stainless Steel Plate," *J. Magn.*, vol. 20, no. 3, pp. 312-316, 2015.

- [31] B Sasi, BPC Rao, S Thirunavukkarasu, T Jayakumar, and Baldev Raj, "Eddy current giant magnetoresistive (GMR) sensor for non-destructive detection of deep-surface defects," in *Phys. Technol. Sensors*, vol. 1, Mumbai, 2007, pp. 273-275.
- [32] Milan Smetana, Tatiana Strapacova, and Ladislav Janousek, "Pulsed excitation in eddy current non-destructive testing of conductive materials," *adv. Electr. Electron. Eng.*, vol. 7, no. 1-2, p. 326, 2008.
- [33] Tianlu Chen, Gui Yun Tian, Ali Sophian, and Pei Wen Que, "Feature extraction and selection for defect classification of pulsed eddy current NDT," *NDT&E. Int.*, vol. 41, no. 6, pp. 467-476, 2008.
- [34] Yunze He et al., "Pulsed eddy current technique for defect detection in aircraft riveted structures," *NDT&E. Int.*, vol. 43, no. 2, pp. 176-181, 2010.
- [35] Maxim Morozov, Gui Yun Tian, and Philip J. Withers, "The pulsed eddy current response to applied loading of various aluminium alloys," *NDT&E. Int.*, vol. 43, no. 6, pp. 493-500, 2010.
- [36] Ali Sophian, Gui Yun Tian, David Taylor, and John Rudlin, "A feature extraction technique based on principal component analysis for pulsed Eddy current NDT," *NDT&E. Int.*, vol. 36, no. 1, pp. 37-41, 2003.
- [37] Bruno Lebrun, Yves Jayet, and Jean-Claude Baboux, "Pulsed eddy current signal analysis: application to the experimental detection and characterization of deep flaws in highly conductive materials," *NDT&E. Int.*, vol. 30, no. 3, pp. 163-170, 1997.
- [38] J.C. Moulder and J.A. Bieber, "Pulsed eddy-current measurements of corrosion and cracking in aging aircraft," in *Cambridge Univ Press*, vol. 503, 1997, p. 263.
- [39] Thierry Clauzon, Frdric Thollon, and Alain Nicolas, "Flaws characterization with pulsed eddy currents NDT," *IEEE. Trans. Magn.*, vol. 35, no. 3, pp. 1873-1876, 1999.
- [40] Deqiang Zhou et al., "The investigation on the optimal design of rectangular PECT probes for evaluation of defects in conductive structures," *Int. J. Appl. Electromagnet Mech.*, vol. 42, no. 2, pp. 313-326, 2013.
- [41] R.A. Smith and G.R. Hugo, "Detection of deep corrosion and cracks in ageing aircraft using transient eddy-current NDE," in *40th annual BINDT conference*, 2001.
- [42] D.L. Waidelich, "Coating thickness measurements using pulsed eddy currents," in *proc. Nat. Electronics. Conf.*, 1995, pp. 500-507.
- [43] D.L. Waidelich, "Pulsed eddy currents gage plating thickness," *Nondestr. Test.*, vol. 14, pp. 14-16, 1956.
- [44] Gui Yun Tian and Ali Sophian, "Reduction of lift-off effects for pulsed eddy current NDT," *NDT&E. Int.*, vol. 38, no. 4, pp. 319-324, 2005.
- [45] Yunze He et al., "Defect classification based on rectangular pulsed eddy current sensor in different directions," *Sensor. Acuat.A-Phys.*, vol. 157, no. 1, pp. 26-31, 2010.
- [46] D. Roy, R. Chakroborty, and BK. Kaushik, "Comparative study of E-shaped coil and evolution of new methodology for crack detection using eddy current testing," *Insight-Non-Destructive Testing and Condition Monitoring*, vol. 55, no. 10, pp. 553-557, 2013.

- [47] R.E. Beissner, M.J. Sablik, K.J. Krzywosz, and J.E. Doherty, "Optimization of Pulsed Eddy Current Probes," in *Review of Progress in Quantitative Nondestructive Evaluation.*: Springer, 1983, pp. 1159-1172.
- [48] Young-Kil Shin and Dong-Myung Choi, "Design of a shielded reflection type pulsed eddy current probe for the evaluation of thickness," *J. Korean. Soc. Nondestr. Test*, vol. 27, no. 5, pp. 398-408, 2007.
- [49] D.G. Park, C.S. Angani, G.D. Kim, C.G. Kim, and Y.M. Cheong, "Evaluation of pulsed eddy current response and detection of the thickness variation in the stainless steel," *IEEE. Trans. Magn.*, vol. 45, no. 10, pp. 3893-3896, 2009.
- [50] B.A. Lepine, J.S.R. Giguere, D.S. Forsyth, A. Chahbaz, and J.M.S. Dubois, "Interpretation of pulsed eddy current signals for locating and quantifying metal loss in thin skin lap splices," in *AIP. Conf.*, vol. 615, 2002, pp. 415-422.
- [51] P. Palanisamy and K.M. Lakin, "Development of EC inspection technique for sleeved engine disk bolt holes," *Review of Progress in Quantitative Nondestructive Evaluation*, vol. 2A, pp. 205-223, 1983.
- [52] G. Panaitov, H.J. Krause, and Y. Zhang, "Pulsed eddy current transient technique with HTS SQUID magnetometer for non-destructive evaluation," *Physica C: Superconductivity*, vol. 372, pp. 278-281, 2002.
- [53] C.S. Angani et al., "The pulsed eddy current differential probe to detect a thickness variation in an insulated stainless steel," *J. Nondestr. Eval.*, vol. 29, no. 4, pp. 248-252, 2010.
- [54] A. Habibalahi and M. S. Safizadeh, "Pulsed eddy current and ultrasonic data fusion applied to stress measurement," *Meas. Sci. Technol.*, vol. 25, no. 5, pp. 1-10.
- [55] A. Habibalahi and M.S. Safizadeh, "Application of Pulsed eddy current technique to stress and residual stress measurement," *Int. J. Appl. Electromagnet Mech*, vol. 7, no. 1, pp. 67-74, 2014.
- [56] C.V. Dodd, D.W. Koerner, W.E. Deeds, and C.A. Pickett, "Pulsed eddy-current inspection of thin-walled stainless steel tubing," Oak Ridge National Lab., TN (USA), Tech. rep. 1987.
- [57] Zhiyuan Xu, Xinjun Wu, Chen Huang, and Hai ke, "Analysis of excitation current parameters in pulsed eddy current testing for ferromagnetic metallic materials," *Int. J. Appl. Electromagnet Mech*, vol. 39, no. 1, pp. 213-219, 2012.
- [58] S.K. Burke, G.R. Hugo, and D.J. Harrison, "Transient eddy-current NDE for hidden corrosion in multilayer structures," in *Review of progress in quantitative nondestructive evaluation.*: Springer, 1998, pp. 307-314.
- [59] Yunze He et al., "Steel corrosion characterization using pulsed eddy current systems," *IEEE Sens.*, vol. 12, no. 6, pp. 2113-2120, 2012.
- [60] Jay A. Bieber, Sunil K. Shaligram, James H. Rose, and John C. Moulder, "Time-gating of pulsed eddy current signals for defect characterization and discrimination in aircraft lap-joints," , 1997, pp. 1915-1921.
- [61] John C Moulder, Sunil K Shaligram, Jay A Bieber, and James H Rose, Pulsed eddy current inspections and the calibration and display of inspection results, #mar#~14 2000, US Patent

6,037,768.

- [62] M.A. Robers and R. Scottini, "Pulsed eddy current in corrosion detection," , 2002.
- [63] Yunze He et al., "Defect edge identification with rectangular pulsed eddy current sensor based on transient response signals," *NDT&E. Int.*, vol. 43, no. 5, pp. 409-415, 2010.
- [64] H. Hoshikawa, K. Koyama, and M. Maeda, "A New Eddy Current Surface Probe for Short Flaws with Minimal Lift-Off Noise," in *AIP. Conf.*, 2003, pp. 413-418.
- [65] Li Shu, Huang Songling, and Zhao Wei, "Development of differential probes in pulsed eddy current testing for noise suppression," *Sensor. Acuat.A-Phys.*, vol. 135, no. 2, pp. 675-679, 2007.
- [66] C.S. Angani et al., "Pulsed eddy current differential probe to detect the defects in a stainless steel pipe," *J. Appl. Phys.*, vol. 109, no. 7, pp. 1-3, 2011.
- [67] Shejuan Xie, Zhenmao Chen, Toshiyuki Takagi, and Tetsuya Uchimoto, "Efficient numerical solver for simulation of pulsed eddy-current testing signals," *IEEE. Trans. Magn.*, vol. 47, no. 11, pp. 4582-4591, 2011.
- [68] Yunze He et al., "Pulsed eddy current technique for defect detection in aircraft riveted structures," *NDT&E. Int.*, vol. 43, no. 2, pp. 176-181, 2010.
- [69] Mengchun Pan, Yunze He, Guiyun Tian, Dixiang Chen, and Feilu Luo, "PEC frequency band selection for locating defects in two-layer aircraft structures with air gap variations," *IEEE. Trans. Instrum. Meas.*, vol. 62, no. 10, pp. 2849-2856, 2013.
- [70] Saleh Hosseini and Aouni A. Lakis, "Application of time-frequency analysis for automatic hidden corrosion detection in a multilayer aluminum structure using pulsed eddy current," *NDT&E. Int.*, vol. 47, pp. 70-79, 2012.
- [71] Qi Zhang, Tian-lu Chen, Guang Yang, and Li Liu, "Time and Frequency Domain Feature Fusion for Defect Classification Based on Pulsed Eddy Current NDT," *Res. Nondestr. Eval.*, vol. 23, no. 3, pp. 171-182, 2012.
- [72] S. Giguere, B.A. Lepine, and J. M.S. Dubois, "Pulsed eddy current technology: Characterizing material loss with gap and lift-off variations," *J. Res. Nondestr. Eval.*, vol. 13, no. 3, pp. 119-129, 2001.
- [73] L. Shu, H. Songling, Z. Wei, and Y. Peng, "Improved immunity to lift-off effect in pulsed eddy current testing with two-stage differential probes," *Russ. J. Nondestr. Test.*, vol. 44, no. 2, pp. 138-144, 2008.
- [74] Tian Gui Yun, Yong Li, and Catalin Mandache, "Study of lift-off invariance for pulsed eddy-current signals," *IEEE. Trans. Magn.*, vol. 45, no. 1, pp. 184-191, 2009.
- [75] Mengbao Fan et al., "Pulsed eddy current thickness measurement using phase features immune to liftoff effect," *NDT&E. Int.*, vol. 86, no. 1, pp. 123-131, 2017.
- [76] B. A. Lepine, B. P. Wallace, D. S. Forsyth, and A. Wyglinski, "Pulsed eddy current method developments for hidden corrosion detection in aircraft structures," in *in Canadian Society for NDT, Defence & Civil Institute of Environmental Medicine*, Toronto , 1988.
- [77] Jia Guan and Yu Yating, "Investigation of signal features of pulsed eddy current testing

technique by experiments," *Insight-Non-Destructive Testing and Condition Monitoring*, vol. 55, no. 9, pp. 487-491, 2013.

- [78] N. IDA, *Numerical modelling for electromagnetic Nondestructive Evaluation.*: Springer Science & Business Media, 1994.
- [79] Jin-Ming Jian, *The finite element method in electromagnetic.* New York: John Wiley & Sons, Inc, 2002.
- [80] M.V.K. Chari and S.J. salon, *Numerical methods in electromagnetism.*: Academic Press, 2000.
- [81] Zhou Deqiang, Tian Gui Yun, and Li Yong, "Simulation based on optimisation of pulsed eddy current probe design," *Nondestr. Test. Eval*, vol. 25, no. 3, pp. 219-230, 2010.
- [82] Yang Binfeng, Zhang Hui, Kang Zhibin, and Wang Xiaofeng, "Investigation of pulsed eddy current probes for detection of defects in riveted structures," *Nondestr. Test. Eval*, vol. 28, no. 3, pp. 278-290, 2013.
- [83] Desimoni E and Brunetti B, "About Estimating the Limit of Detection by the Signal to Noise Approach," *Pharm Anal Acta*, vol. 6, no. 3, pp. 1-4, 2015.
- [84] Yunze He, Feilu Luo, Mengchun Pan, Feibing Weng, Xiangchao Hu, Junzhe Gao, and Bo Liu, "Pulsed eddy current technique for defect detection in aircraft riveted structures," *NDT&E. Int.*, vol. 43, no. 2, pp. 176-181, 2010.
- [85] Heydari Payam and Massoud Pedram, "Analysis of jitter due to power-supply noise in phase-locked loops," in *Custom Integrated Circuits* , 2000, pp. 443-446.
- [86] Mengbao Fan, Binghua Cao, Tian Gui yun, Bo Ye, and Wei Li, "Thickness measurement using liftoff point of intersection in pulsed eddy current responses for elimination of liftoff effect," *Sensor. Acuat.A-Phys.*, vol. 251, pp. 66-74, 2016.
- [87] F. Fu and J.R. Bowler, "Transient eddy-current driver pickup probe response due to a conductive plate," *IEEE. Trans. Magn.*, vol. 42, no. 8, pp. 2029-2037., 2006.
- [88] Deqiang Zhou, Gui Yun Tian and Yong Li, "Simulation based on optimisation of pulsed eddy current probe design," *Nondestr. Test. Eval*, vol. 25, no. 3, pp. 219-230, 2010.
- [89] Gui Yun Tian and Ali Sophian, "Defect classification using a new feature for pulsed eddy current sensors," *NDT&E Int.*, vol. 38, pp. 77-82, 2005.
- [90] H.J. Krause and M.V. Kreutzbruck., "Recent developments in SQUID NDE," *Physica C: Superconductivity*, vol. 368, no. 1, pp. 70-79, 2002.
- [91] Trevo.J. Cadeau and Thomas W. Krause., "Pulsed Eddy Current Probe Design Based on Transient Circuit Analysis," in *Review of progress in quantitative nondestructive evaluation*, 2009, pp. 327-334.
- [92] Li, Xiaoli, Shiu Kit Tso, and Jun Wang, "Real-time tool condition monitoring using wavelet transforms and fuzzy techniques," *IEEE Transactions on Systems, Man, and Cybernetics, Part C*, vol. 30, no. 3, pp. 352-357, 2000.
- [93] Yen, G. Gary, and K.C. Lin, "Wavelet packet feature extraction for vibration monitoring," *IEEE Trans. Ind. Electron.*, vol. 47, no. 3, pp. 650-667, 2000.

- [94] Sarikaya, Ruhi, and John H L Hansen, "High resolution speech feature parametrization for monophone-based stressed speech recognition," *IEEE Signal Process Lett.*, vol. 7, no. 7, pp. 182-185, 2000.
- [95] C. Sidney Burrus, A. Ramesh Gopinath, and Haitoo Guo, *Introduction to wavelets and wavelet transform primer*. New Jersey: Prentice Hall, 1988.
- [96] W. Yin and A.J. Peyton, "Thickness measurement of non-magnetic plates using multi-frequency eddy current sensors," *NDT&E. Int.*, vol. 40, no. 1, pp. 43-48, 2007.

